



**US Army Corps
of Engineers**
Waterways Experiment
Station

Technical Report ITL-96-8
August 1996

Computer-Aided Structural Engineering (CASE) Project

Hyperbolic Stress-Strain Parameters for Structured/Cemented Silts

by *Timothy D. Stark, Kenneth R. Daly,*
University of Illinois at Urbana-Champaign

Robert M. Ebeling, WES

DTIC QUALITY IMPROVED 4

DTIC QUALITY IMPROVED 4

Approved For Public Release; Distribution Is Unlimited

19960930 072

Prepared for Headquarters, U.S. Army Corps of Engineers

DISCLAIMER NOTICE



THIS DOCUMENT IS BEST QUALITY AVAILABLE. THE COPY FURNISHED TO DTIC CONTAINED A SIGNIFICANT NUMBER OF PAGES WHICH DO NOT REPRODUCE LEGIBLY.

The contents of this report are not to be used for advertising, publication, or promotional purposes. Citation of trade names does not constitute an official endorsement or approval of the use of such commercial products.



PRINTED ON RECYCLED PAPER

Hyperbolic Stress-Strain Parameters for Structured/Cemented Silts

by Timothy D. Stark, Kenneth R. Daly

Department of Civil Engineering
University of Illinois at Urbana-Champaign
Urbana, IL 61801

Robert M. Ebeling

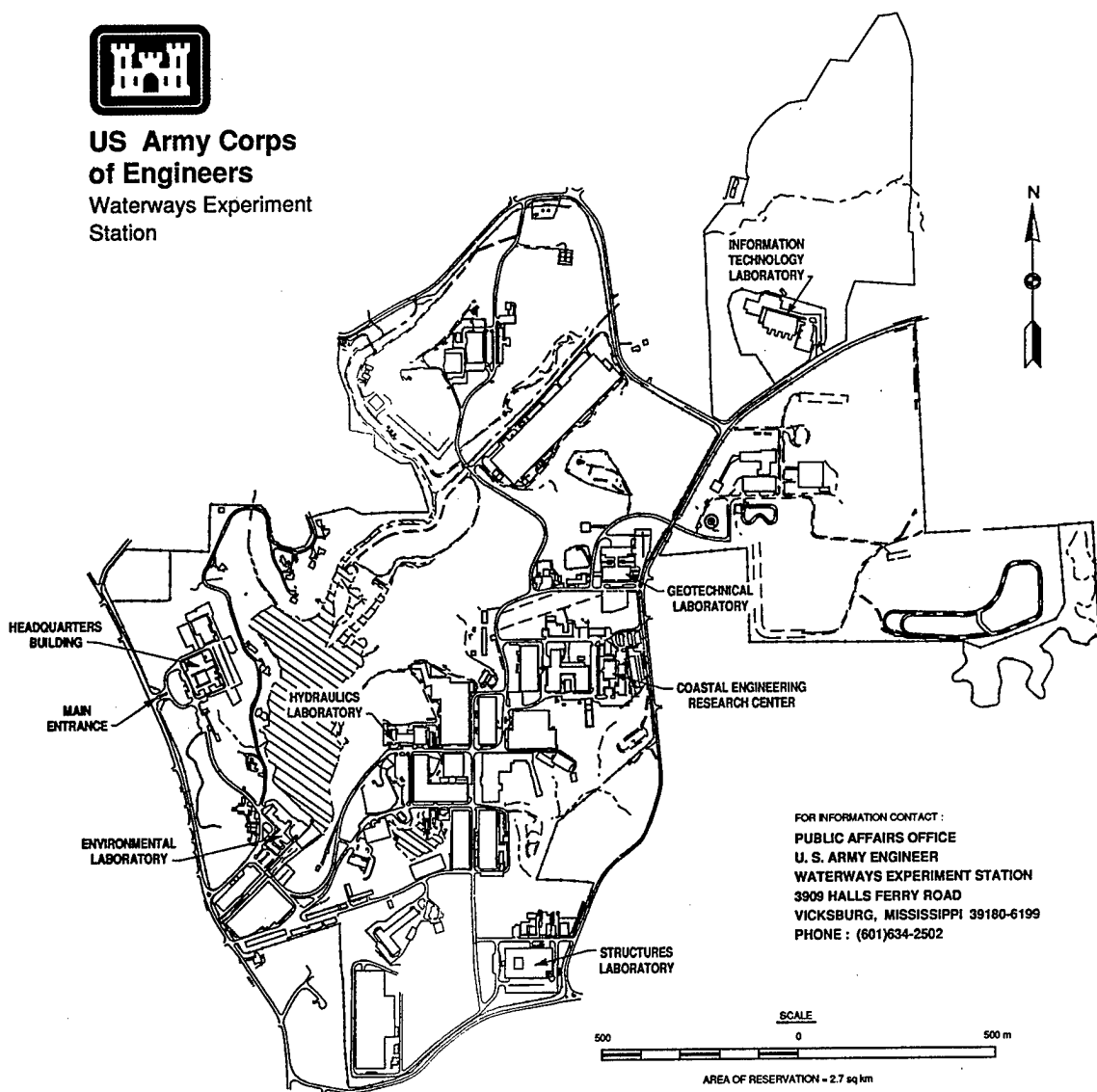
U.S. Army Corps of Engineers
Waterways Experiment Station
3909 Halls Ferry Road
Vicksburg, MS 39180-6199

Final report

Approved for public release; distribution is unlimited



**US Army Corps
of Engineers**
Waterways Experiment
Station



FOR INFORMATION CONTACT :
PUBLIC AFFAIRS OFFICE
U. S. ARMY ENGINEER
WATERWAYS EXPERIMENT STATION
3909 HALLS FERRY ROAD
VICKSBURG, MISSISSIPPI 39180-6199
PHONE : (601)634-2502

Waterways Experiment Station Cataloging-in-Publication Data

Stark, Timothy D.

Hyperbolic stress-strain parameters for structured/cemented silts / by Timothy D. Stark, Kenneth R. Daly, Robert M. Ebeling ; prepared for U.S. Army Corps of Engineers.

136 p. : ill. ; 28 cm. -- (Technical report ; ITL-96-8)

Includes bibliographic references.

1. Silt. 2. Finite element method. 3. Soil-structure interaction. 4. Differential equations, Hyperbolic. I. Daly, Kenneth R. II. Ebeling, Robert M., 1954- III. United States. Army. Corps of Engineers. IV. U.S. Army Engineer Waterways Experiment Station. V. Information Technology Laboratory (U.S. Army Engineer Waterways Experiment Station) VI. Computer-aided Structural Engineering Project. VII. Title. VIII. Series: Technical report (U.S. Army Engineer Waterways Experiment Station) ; ITL-96-8.
TA7 W34 no.ITL-96-8

Contents

List of Figures.....	v
List of Tables.....	ix
Preface.....	xi
Conversion Factors, Non-SI to SI Units of Measurement	xiii
1--Introduction	1
Background.....	1
Purpose and Scope	2
2--Hyperbolic Stress-Strain Model	5
Stiffness Parameters.....	5
Volume Change Parameters	8
Unload/Reload Parameters.....	9
Nonlinear Stress-Strain Response of Soil Using SOILSTRUCT	10
3--Results of Previous Research Using Silt	13
Background.....	13
Silt Origin	13
Original Research Objectives and Results	15
4--Laboratory Testing Program Using Structured/Cemented Silt.....	23
Background.....	23
Silt Origin	23
Silt Sampling and Index Properties	27
5--Oedometer Testing	31
Background.....	31
Effect of Structure/Cementation on Compressibility	31
Effect of Inundation on Compressibility	36
6--Triaxial Compression Test Procedures	43
Preparation of Structured/Cemented Triaxial Specimens	43
Triaxial Compression Tests on Partially Saturated Specimens.....	44
Triaxial Compression Tests on Saturated Specimens.....	45
7--ICD Triaxial Tests on Partially Saturated Specimens	47
Structured/Cemented Silt Specimens	47
Reconstituted Silt Specimens	49
Drained Hyperbolic Stress-Strain Parameters	55
Anisotropy of Structured/Cemented Silt	62
Initial Stiffness from Hyperbolic Stress-Strain Model	62

8--ICD Triaxial Tests on Saturated Specimens	73
Laboratory Saturation of Silt Specimens	73
Hydrostatic Saturation of Structured/Cemented Silt Specimens	73
Hydrostatic Saturation of Reconstituted Specimens	76
Drained Hyperbolic Stress-Strain Parameters of Saturated Silt.....	79
Anisotropy of Saturated Structured/Cemented Silt	80
Hyperbolic Volume Change Parameters	80
9--ICD Unload/Reload Triaxial Tests on Partially Saturated Specimens	83
Unload/Reload Parameters.....	83
10--Summary	93
References	97
Appendix A: Results of ICD Triaxial Compression Tests on Partially Saturated Structured/Cemented Silt	A1
Appendix B: Results of ICD Triaxial Compression Tests on Partially Saturated Reconstituted Silt.....	B1
Appendix C: Results of ICD Triaxial Compression Tests on Hydrostatically Saturated Structured/Cemented Silt	C1
Appendix D: Results of ICD Triaxial Compression Tests on Hydrostatically Saturated Reconstituted Silt.....	D1

SF 298

List of Figures

Figure 1. Hyperbolic representation of a stress-strain curve (from Duncan, et al 1980)	6
Figure 2. Unloading-reloading modulus (from Duncan, et al 1980) ..	10
Figure 3. Location map of silt borrow area.....	14
Figure 4. Scanning electron microscope photograph of naturally occurring silt (magnification equals 1000 times).....	25
Figure 5. Two silt particles cemented together in the right center of ... the photograph (magnification equals 1500 times).....	25
Figure 6. Closeup view of cementation joining two silt particles (magnification equals 5000 times)	26
Figure 7. Plan and closeup views of Natural Cementation (Magnification equals 1500 times)	26
Figure 8. Gradation of kaolinite-silt mixtures and structured/cemented silt.....	29
Figure 9. Comparison of results of oedometer tests on structured/cemented and reconstituted silt.....	32
Figure 10. Void ratio-effective stress relationships for structured/cemented and reconstituted silt.....	33
Figure 11. Effect of inundation in the recompression range (2400 psf) on the compressibility of structured/cemented silt.....	37
Figure 12. Effect of inundation in the recompression range (2400 psf) on the void ratio-effective stress relationship of structured/cemented silt.....	38
Figure 13. Effect of inundation in the virgin compression range (23,000 psf) on the compressibility of structured/cemented silt.....	39
Figure 14. Effect of inundation in the virgin compression zone (23,000 psf) on the void ratio-effective stress relationship of structured/cemented silt.....	40
Figure 15. Stress-strain relationships from ICD triaxial compression tests on partially saturated structured/cemented silt	48
Figure 16. Stress-strain relationships from ICD triaxial compression tests on partially saturated reconstituted silt	50

Figure 17. ICD triaxial compression tests on partially saturated structured/cemented and reconstituted silt at an effective confining pressure of 1000 psf	51
Figure 18. ICD triaxial compression tests on partially saturated structured/cemented and reconstituted silt at an effective confining pressure of 2160 psf	52
Figure 19. ICD triaxial compression tests on partially saturated structured/cemented and reconstituted silt at an effective confining pressure of 5760 psf	53
Figure 20. ICD triaxial compression tests on partially saturated structured/cemented and reconstituted silt at an effective confining pressure of 11,520 psf	54
Figure 21. Comparison of measured and hyperbolic stress-strain relationships of partially saturated structured/cemented silt at an effective confining pressure of 1000 psf	56
Figure 22. Comparison of measured and hyperbolic stress-strain relationships of partially saturated structured/cemented silt at an effective confining pressure of 2160 psf	57
Figure 23. Comparison of measured and hyperbolic stress-strain relationships of partially saturated structured/cemented silt at an effective confining pressure of 5760 psf	58
Figure 24. Comparison of measured and hyperbolic stress-strain relationships of partially saturated structured/cemented silt at an effective confining pressure of 11,520 psf	59
Figure 25. Comparison of measured and hyperbolic stress-strain relationships of partially saturated reconstituted silt at an effective confining pressure of 1000 psf	63
Figure 26. Comparison of measured and hyperbolic stress-strain relationships of partially saturated reconstituted silt at an effective confining pressure of 2160 psf	64
Figure 27. Comparison of measured and hyperbolic stress-strain relationships of partially saturated reconstituted silt at an effective confining pressure of 5760 psf	65
Figure 28. Comparison of measured and hyperbolic stress-strain relationships of partially saturated reconstituted silt at an effective confining pressure of 11,520 psf	66
Figure 29. Variation in initial tangent modulus for partially saturated structured/cemented silt and reconstituted silt	70

Figure 30. Variation in tangent modulus at an axial strain of 0.5 percent for partially saturated structured/cemented and reconstituted silt	71
Figure 31. Stress-strain relationships from ICD triaxial compression tests on hydrostatically saturated structured/cemented Silt .	74
Figure 32. Stress-strain relationships from ICD triaxial compression tests on hydrostatically saturated reconstituted silt	77
Figure 33. Results of ICD Triaxial Unload/Reload Test on Partially saturated structured/cemented silt at an effective confining pressure of 1000 psf	84
Figure 34. Results of ICD triaxial unload/reload test on partially saturated structured/cemented silt at an effective confining pressure of 2160 psf	85
Figure 35. Results of ICD triaxial unload/reload test on partially saturated structured/cemented silt at an effective confining pressure of 5760 psf	86
Figure 36. Results of ICD triaxial unload/reload test on partially saturated structured/cemented silt at an effective confining pressure of 11,520 psf	87
Figure 37. Comparison of results of partially saturated unload/reload and conventional ICD triaxial compression tests at an effective confining pressure of 1000 psf	90
Figure 38. Comparison of results of partially saturated unload/reload and conventional ICD triaxial compression tests at an effective confining pressure of 2160 psf	91
Figure A1. Results of ICD triaxial compression tests on partially saturated structured/cemented silt at an effective confining pressure of 1000 psf	A2
Figure A2. Results of ICD triaxial compression tests on partially saturated structured/cemented silt at an effective confining pressure of 2160 psf.....	A3
Figure A3. Results of ICD triaxial compression tests on partially saturated structured/cemented silt at an effective confining pressure of 5760 psf.....	A4
Figure A4. Results of ICD triaxial compression tests on partially saturated structured/cemented silt at an effective confining pressure of 11,520 psf	A5
Figure B1. Results of ICD triaxial compression tests on partially saturated reconstituted silt at an effective confining pressure of 1000 psf.....	B2

Figure B2. Results of ICD triaxial compression tests on partially saturated reconstituted silt at an effective confining pressure of 2160 psf.....	B3
Figure B3. Results of ICD triaxial compression tests on partially saturated reconstituted silt at an effective confining pressure of 5760 psf.....	B4
Figure B4. Results of ICD triaxial compression tests on partially saturated reconstituted silt at an effective confining pressure of 11,520 psf	B5
Figure C-1. . Results of ICD triaxial compression tests on hydrostatically saturated structured/cemented silt at an effective confining pressure of 1000 psf.....	C2
Figure C-2. . Results of ICD triaxial compression tests on hydrostatically saturated structured/cemented silt at an effective confining pressure of 2160 psf.....	C3
Figure C-3. . Results of ICD triaxial compression tests on hydrostatically saturated structured/cemented silt at an effective confining pressure of 5760 psf.....	C4
Figure C-4. . Results of ICD triaxial compression tests on hydrostatically saturated structured/cemented silt at an effective confining pressure of 11,520 psf	C5
Figure D-1. . Results of ICD triaxial compression tests on hydrostatically saturated reconstituted silt at an effective confining pressure of 1000 psf.....	D2
Figure D-2. . Results of ICD triaxial compression tests on hydrostatically saturated reconstituted silt at an effective confining pressure of 5760 psf	D3
Figure D-3. . Results of ICD triaxial compression tests on hydrostatically saturated reconstituted silt at an effective confining pressure of 11,520 psf	D4

List of Tables

Table 1.	Summary of Hyperbolic Stress-Strain Parameters (from Duncan et al. 1978)	3
Table 2.	Effective Stress Mohr-Coulomb Shear Strength Parameters for Kaolinite-Silt Mixtures from Consolidated-Drained Triaxial Compression Tests	17
Table 3.	Effective Stress Hyperbolic Stress-Strain Parameters for Kaolinite-Silt Mixtures from Consolidated-Drained Triaxial Compression Tests.....	18
Table 4.	Total and Effective Stress Mohr-Coulomb Shear Strength Parameters for Kaolinite-Silt Mixtures from Consolidated-Undrained Triaxial Compression Tests	19
Table 5.	Total Stress Hyperbolic Stress-Strain Parameters for Kaolinite-Silt Mixtures from Consolidated-Undrained Triaxial Tests.....	20
Table 6.	Effective Stress Mohr-Coulomb Shear Strength Parameters for Montmorillonite-Silt Mixtures from Consolidated-Drained Triaxial Compression Tests	21
Table 7.	Effective Stress Hyperbolic Stress-Strain Parameters for Montmorillonite-Silt Mixtures from Consolidated-Drained Triaxial Compression Tests	22
Table 8.	Compressibility Parameters of Natural and Reconstituted Silt	34
Table 9.	Effective Stress Mohr-Coulomb Shear Strength Parameters and Hyperbolic Stress-Stain Parameters for Partially Saturated Structured/Cemented and Reconstituted Silt	60
Table 10.	Initial Stiffness from Hyperbolic Stress-Strain Model for Structured/Cemented Silt	68
Table 11.	Initial Stiffness from Hyperbolic Stress-Strain Model for Reconstituted Silt	69
Table 12.	Effective Stress Mohr-Coulomb Shear Strength Parameters and Hyperbolic Stress-Stain Parameters for Laboratory Saturated Structured/Cemented and Reconstituted Silt	78

Table 13. Effective Stress Mohr-Coulomb Shear Strength Parameters and Hyperbolic Volume Change Parameters for Laboratory Saturated Structured/Cemented and Reconstituted Silt 82

Preface

This report describes the research completed under the project titled "Soil-Structure Interaction Parameters For Structured Silts." The main objective of this research was to characterize the drained stress-strain behavior of naturally occurring structured/cemented silts. The results of this research were also used to develop recommendations for drained hyperbolic stress-strain and Mohr-Coulomb shear strength parameters for use in soil-structure interaction analyses involving structured/cemented silts. This research utilized oedometer and isotropically consolidated-drained triaxial compression tests on structured/cemented and reconstituted specimens to evaluate the importance of the structure/cementation on the stress-strain behavior and anisotropy of silts. Triaxial compression tests were conducted on structured/cemented and reconstituted specimens at the natural degree of saturation and after laboratory saturation to investigate the effect of saturation on the drained stress-strain behavior of silts. In addition, unload/reload triaxial compression tests were conducted to estimate the unload/reload modulus and the effect of unloading/reloading on the degradation of the structure/cementation of silt.

This report was prepared by Dr. Timothy D. Stark, Associate Professor of Civil Engineering at the University of Illinois at Urbana-Champaign, and Mr. Kenneth R. Daly, Graduate Research Assistant at the University of Illinois at Urbana-Champaign. The research was conducted at the University of Illinois at Urbana-Champaign under Contract No. DACW39-94-M-6534 with the U.S. Army Engineer Waterways Experiment Station (WES). Mr. Kenneth R. Daly, Mr. Mohammad A. Aljouni, and Mr. Massimo Maniaci, Graduate Research Assistants at the University of Illinois at Urbana-Champaign, performed the laboratory tests described in this report under the supervision of Dr. Stark. Dr. Robert M. Ebeling, Research Civil Engineer, Computer-Aided Engineering Division (CAED), Information Technology Laboratory (ITL), WES, supervised and monitored the research. Dr. Ebeling provided technical guidance and review on the project under the general supervision of Mr. H. Wayne Jones, Chief, CAED, and Dr. N. Radhakrishnan, Director, ITL.

At the time of publication of this report, Director of WES was Dr. Robert W. Whalin. Commander was COL Bruce K. Howard, EN.

The contents of this report are not to be used for advertising, publication, or promotional purposes. Citation of trade names does not constitute an official endorsement or approval for the use of such commercial products.

Conversion Factors, Non-SI to SI Units of Measurement

Non-SI units of measurement used in this report can be converted to SI units as follows:

Multiply	By	To Obtain
acre-feet	1,233.489	cubic meters
cubic feet per second	0.02831685	cubic meters per second
cubic yards	0.7645549	cubic meters
cubic feet	0.2831685	cubic meters
square feet	0.092903	square meters
square inches	6.4516	square meters
feet	0.3048	meters
inches	2.54	centimeters
miles	1.609347	kilometers
nautical miles	1.852	kilometers
pounds (mass)	0.4535924	kilograms
pounds (mass) per cubic foot	16.01846	kilograms per cubic meter
pounds (force) per square foot	0.04788	kilopascals
tons (force) per square foot	95.76	kilopascals

I Introduction

Background

The finite element method provides a powerful technique for the analysis of stresses and movements in earth masses, and it has been applied to a variety of soil-structure interaction problems. The results of soil stress-deformation analyses are controlled by the stress-strain characteristics of the soil being modeled. Modeling the stress-strain characteristics of soils is extremely complex because the behavior of soil is nonlinear, inelastic, and highly dependent on the magnitude of the stresses in the soil.

The hyperbolic stress-strain relationships developed by Duncan and Chang (1970) provide a simple model that encompasses the most important characteristics of soil stress-strain behavior using data from conventional laboratory tests. Due to its simplicity, applicability to drained and undrained problems, and the availability of a data base of hyperbolic stress-strain parameters, the hyperbolic stress-strain model is frequently used in soil-structure interaction problems (Ebeling et al. 1992b; Kuppusamy et al. 1994). The model has been successfully applied to embankment dams (Duncan et al. 1982), open excavations (Chang 1969), retaining walls (Duncan et al. 1990; Ebeling et al. 1990; Ebeling et al. 1992a), braced excavations (Mana and Clough 1981), lock and dam structures (Clough and Duncan 1969; Ebeling et al. 1993), and a variety of soil-structure interaction problems (Ebeling 1990), such as compaction-induced earth pressures (Seed and Duncan 1986).

The data base of drained and undrained hyperbolic parameters for approximately 135 different soils was assembled by Duncan et al. (1978 and 1980) and has been extremely useful for:

- a. Judging the reliability of parameter values determined from laboratory test data.
- b. Determining the effects of various factors that influence the values of the parameters.
- c. Estimating values of the parameters when insufficient data are available for their determination.

The soil types included in the data base range from clays to gravels. However, hyperbolic parameters and shear strength parameters for silts and clayey silts have not been adequately defined in the data base or the professional literature. As a result, the summary table presented by Duncan et al. (1978) (see Table 1) does not include hyperbolic or shear strength parameters for silts or clayey silts.

Purpose and Scope

Due to the limited information available on the drained hyperbolic and shear strength parameters of silts, the main objectives of this research are to:

- a.* Investigate the effects of natural structure/cementation on the drained stress-strain behavior of a naturally occurring structured silt deposit.
- b.* Characterize the drained stress-strain behavior of natural structured/cemented silt.
- c.* Determine the appropriate drained hyperbolic stress-strain and Mohr-Coulomb strength parameters for natural structured/cemented silt.
- d.* Apply the research objectives described above to reconstituted samples of the naturally occurring silt. A comparison of the test results on reconstituted and structured/cemented silt specimens will quantify the effect of structure/cementation on the stress-strain behavior and shear strength of silts.
- e.* Determine the effect of laboratory saturation on the drained stress-strain behavior of silts.
- f.* Investigate the effect of unloading/reloading on the degradation of the structure/cementation of naturally occurring silt.
- g.* Estimate the anisotropy of the structure/cementation by conducting tests on cemented specimens trimmed 90 degrees from the field orientation.

Table 1

Summary of Hyperbolic Stress-Strain Parameters (from Duncan et al. 1978)

Unified Soil Classification	RC Stand. AASHTO %	γ_m^1 k/ft ³	$\phi_0(\Delta\phi)$ deg	c k/ft ²	K	n	R_f	K_b	m
GW,GP SW&SP	105	0.150	42(9)	0	600	0.4	0.7	175	0.2
	100	0.145	39(7)	0	450	0.4	0.7	125	0.2
	95	0.140	36(5)	0	300	0.4	0.7	75	0.2
	90	0.135	33(3)	0	200	0.4	0.7	50	0.2
SM	100	0.135	36(8)	0	600	0.25	0.7	450	0.0
	95	0.130	34(6)	0	450	0.25	0.7	350	0.0
	90	0.125	32(4)	0	300	0.25	0.7	250	0.0
	85	0.120	30(2)	0	150	0.25	0.7	150	0.0
SM-SC	100	0.135	33(0)	0.5	400	0.6	0.7	200	0.5
	95	0.130	33(0)	0.5	200	0.6	0.7	100	0.5
	90	0.125	33(0)	0.3	150	0.6	0.7	75	0.5
	85	0.120	33(0)	0.2	100	0.6	0.7	50	0.5
CL	100	0.135	30(0)	0.4	150	0.45	0.7	140	0.2
	95	0.130	30(0)	0.3	120	0.45	0.7	110	0.2
	90	0.125	30(0)	0.2	90	0.45	0.7	80	0.2
	85	0.120	30(0)	0.1	60	0.45	0.7	50	0.2

¹ A table of factors for converting non-SI units of measurement to SI is presented on page xiii.

The resulting information on the behavior of structured/cemented silt was used to develop a data base of drained hyperbolic stress-strain and Mohr-Coulomb strength parameters for structured/cemented silt.

2 Hyperbolic Stress-Strain Model

Stiffness Parameters

Duncan et al. (1980) provides an extensive derivation of the hyperbolic stress-strain model and a detailed procedure for determining the values of the hyperbolic stress-strain parameters from conventional triaxial tests. As a result, only the major features of the stress-strain model will be described in this introduction in order to define the various hyperbolic stress-strain parameters.

The hyperbolic model represents the nonlinear stress-strain curve of soils using a hyperbola as shown in Figure 1. Transforming the hyperbolic equation results in a linear relationship between $\varepsilon/(\sigma'_1 - \sigma'_3)$ and ε , where ε is the axial strain and $(\sigma'_1 - \sigma'_3)$ is the effective deviator stress. The stress-dependent stress-strain behavior of soil is represented by varying the initial tangent modulus, E_i , and the ultimate deviator stress, $(\sigma'_1 - \sigma'_3)_{ult}$, with the effective confining pressure, σ'_3 . Figure 1 shows that the ultimate deviator stress is the asymptotic value of the deviator stress and is related to the compressive strength of the soil. The variation of the initial tangent modulus with confining pressure is represented by an empirical equation proposed by Janbu (1963):

$$E_i = Kp_a \left(\frac{\sigma'_3}{p_a} \right)^n \quad (1)$$

where K is the modulus number, n is the modulus exponent, and p_a is the atmospheric pressure in the same units as σ'_3 and E_i (e.g., 2116.2 psf or 101.3 kPa).

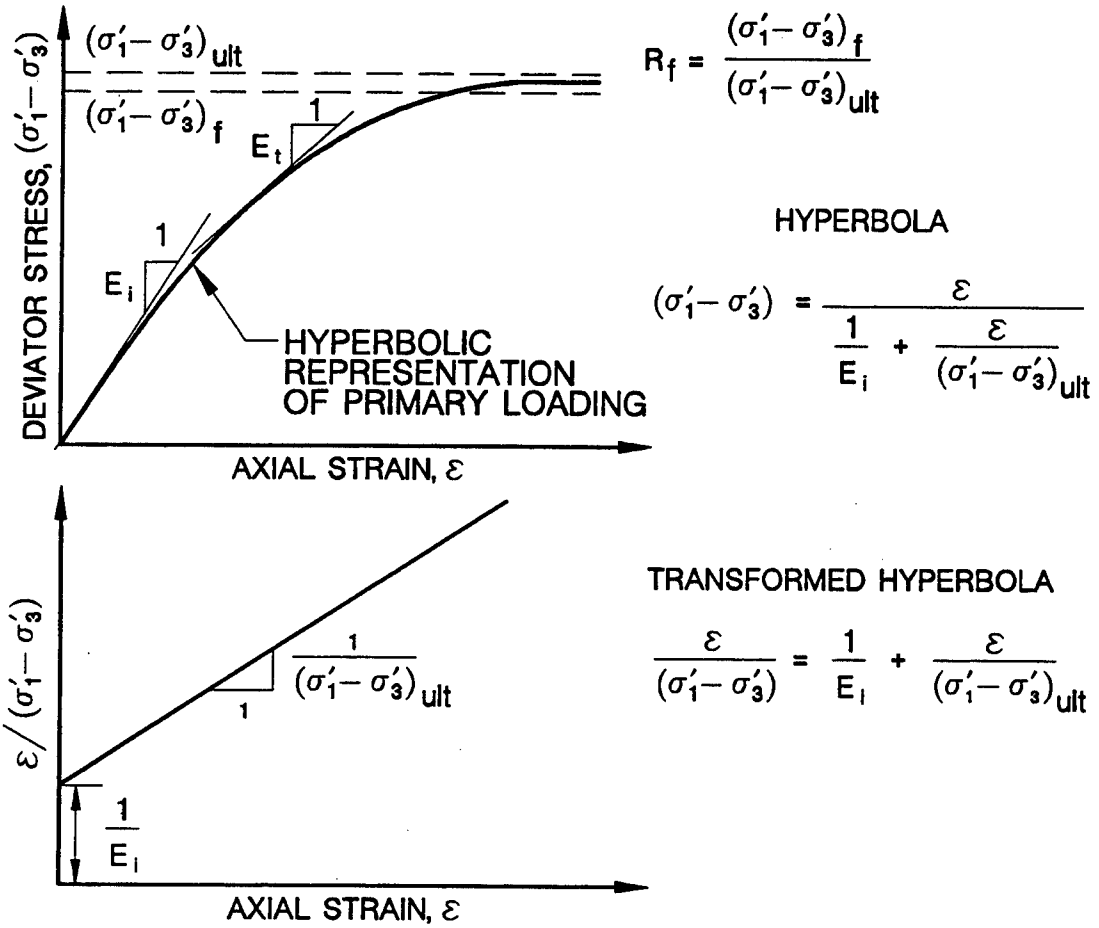


Figure 1. Hyperbolic representation of a stress-strain curve (from Duncan et al. 1980)

The variation of E_i with σ'_3 is linear when the logarithms of (E_i/p_a) and (σ'_3/p_a) are plotted against each other. The modulus number equals (E_i/p_a) when σ'_3/p_a equals unity and n is the slope of the resulting line.

The variation of ultimate deviator stress with σ'_3 is accounted for by relating $(\sigma'_1 - \sigma'_3)_{ult}$ to the stress difference at failure, $(\sigma'_1 - \sigma'_3)_f$, and using the Mohr-Coulomb strength equation to relate $(\sigma'_1 - \sigma'_3)_f$ to σ'_3 . The criterion used to define $(\sigma'_1 - \sigma'_3)_f$ is usually the maximum deviator stress. However, the criterion that results in the best approximation of the actual stress-strain curve should be used. The values of $(\sigma'_1 - \sigma'_3)_{ult}$ and $(\sigma'_1 - \sigma'_3)_f$ are related by:

$$(\sigma'_1 - \sigma'_3)_f = R_f * (\sigma'_1 - \sigma'_3)_{ult} \quad (2)$$

in which R_f is the failure ratio as shown in Figure 1. The value of R_f is always less than or equal to unity and varies from 0.5 to 0.9 for most soils. The variation of $(\sigma'_1 - \sigma'_3)_f$ with σ'_3 can be expressed as follows using the Mohr-Coulomb strength equation:

$$(\sigma'_1 - \sigma'_3)_f = \frac{(2c' \cos \phi' + 2\sigma'_3 \sin \phi')}{(1 - \sin \phi')} \quad (3)$$

in which c' and ϕ' are the effective stress Mohr-Coulomb cohesion intercept and friction angle, respectively.

By differentiating the equation of the hyperbola shown in Figure 1 with respect to the axial strain and substituting the expression into Equations (1), (2), and (3), an expression for the tangent modulus, E_t , can be obtained:

$$E_t = K p_a \left(\frac{\sigma'_3}{p_a} \right)^n \left[1 - \frac{R_f (1 - \sin \phi') (\sigma'_1 - \sigma'_3)}{(2c' \cos \phi' + 2\sigma'_3 \sin \phi')} \right]^2 \quad (4)$$

This equation can be used to calculate the value of E_t for any stress condition if the hyperbolic parameters K , n , and R_f and the Mohr-Coulomb shear strength parameters, c' and ϕ' , are known. Alternatively, Equation (4) may be presented as:

$$E_t = E_i (1 - S_L * R_f)^2 \quad (5)$$

where the mobilized shear strength is equal to the stress level, S_L ,

$$S_L = \frac{(\sigma'_1 - \sigma'_3)}{(\sigma'_1 - \sigma'_3)_f} \quad (6)$$

Volume Change Parameters

The hyperbolic stress-strain model accounts for the nonlinear volume change behavior of soils by assuming that the bulk modulus is independent of stress level, $(\sigma'_1 - \sigma'_3)$, and that it varies with confining pressure. The variation of bulk modulus, B , with confining pressure is approximated by the following equation:

$$B = K_b p_a \left(\frac{\sigma'_3}{p_a} \right)^m \quad (7)$$

where K_b is the bulk modulus number and m is the bulk modulus exponent. The variation of B is linear when the logarithm of (B/p_a) and the logarithm (σ'_3/p_a) are plotted against each other. The bulk modulus number equals (B/p_a) when (σ'_3/p_a) equals unity and m is the slope of the resulting line.

Unload/Reload Parameters

If a triaxial specimen is unloaded at some stage during a test, the stress-strain relationship followed during unloading is steeper than the curve followed during primary loading, as shown in Figure 2. If the specimen is subsequently reloaded, the stress-strain relationship followed is also steeper than the primary loading relationship and is quite similar to the unloading relationship. Thus, the soil behavior is inelastic because the strains occurring during primary loading are only partially recoverable upon unloading. On subsequent reloading there is always some hysteresis, but it is usually accurate to approximate the behavior during unloading and reloading as linear and elastic. As a result, the same value of unloading-reloading modulus, E_{ur} , is used for both unloading and reloading. E_{ur} is related to the confining pressure by the following equation:

$$E_{ur} = K_{ur} p_a \left(\frac{\sigma'_3}{p_a} \right)^n \quad (8)$$

In this equation, K_{ur} is the unloading-reloading modulus number. K_{ur} is always greater than K (for primary loading). K_{ur} may be 20 percent greater than K for stiff soils such as dense sands. For soft soils such as loose sands, K_{ur} may be three times greater than K . If the zones undergoing unloading and/or reloading are not large and do not have a dominant effect on the results of the analysis, assuming a value of K_{ur} within the range of 1.2 to 3 times the modulus number is probably sufficiently accurate. The value of n is similar for primary loading and unloading, and in the hyperbolic model it is assumed to be the same.

In summary, the nonlinear stress-strain relationship is approximated by a series of straight lines using an incremental stress analysis. The value of the tangent modulus at any stress is determined twice using Eq. (4) during each increment. The unloading-reloading stress-strain curve is assumed to be linear and elastic and thus represented by one modulus, E_{ur} , expressed by Eq. (8). In the calculations, the stress condition is determined to be unloading or reloading by comparing the stress level before and after the load increment.

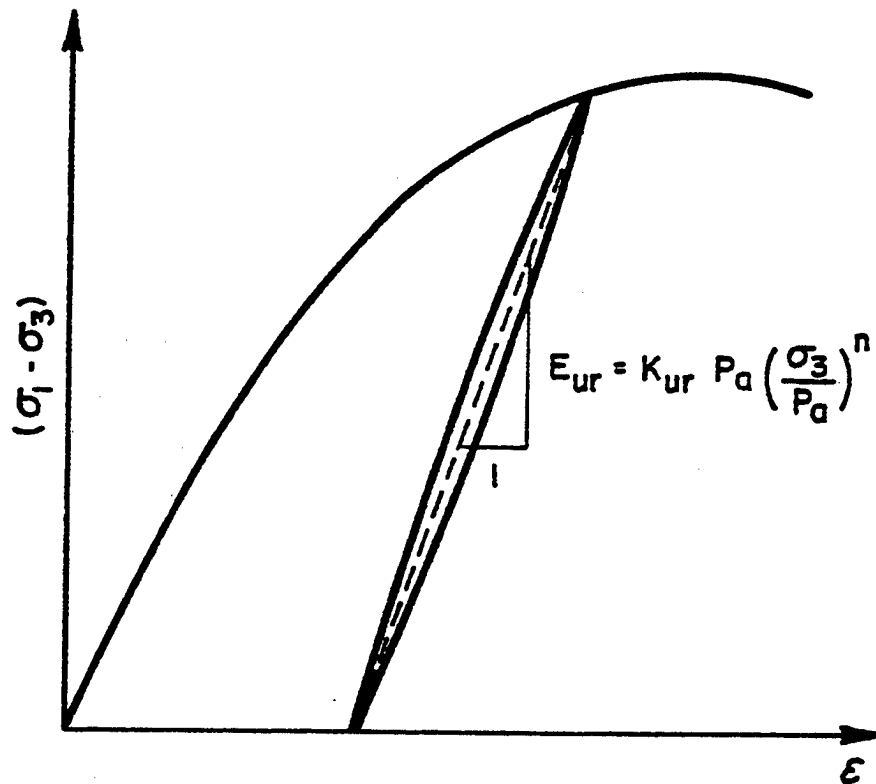


Figure 2. Unloading-Reloading Modulus
(from Duncan et al. 1980)

Nonlinear Stress-Strain Response of Soil Using SOILSTRUCT

The constitutive relationship used for all two-dimensional finite elements in SOILSTRUCT (Ebeling et al. 1992b) is Hooke's law. SOILSTRUCT uses an incremental, equivalent linear method of analysis to model nonlinear material behavior. In this type of analysis, incremental changes in stresses are related to the incremental strains through a linear relationship. This relationship is defined for each element by two engineering constants, Young's modulus and the bulk modulus.

A plane strain, isotropic drained or undrained stress-strain model is incorporated within SOILSTRUCT. The computer program uses a nonlinear

stress-dependent hyperbolic curve to represent the relationship between stress-strain response during primary loading of the soil (Figure 1) and a linear stress-strain response during unloading or reloading of the soil (Figure 2). The unload-reload stress-strain response is applicable when the current (deviator) stress state is less than that which has been applied previously. Otherwise, the primary loading stress-strain curve is appropriate.

The nonlinear soil response to loading is modeled by performing a series of analyses in which each load is applied incrementally, with the total change in stress computed at the center of each soil element being equal to the sum of the incremental changes in stress over all of the load steps (Ebeling et al. 1992b). In general, the greater the curvature of the stress-strain relationship or the greater the magnitude of the applied load, the greater the number of load steps required to accurately model the nonlinear soil response. This may be achieved in two ways using SOILSTRUCT: either the total load approach using a greater number of incremental loadings, or the substep approach. Under the substep approach during the course of each load case analysis, the load vector may be applied in a series of increments.

Application of each loading in the finite element analysis results in a change in stress within each of the soil elements. In addition to the change in stress, there is a corresponding change in stiffness. Since each incremental analysis is performed assuming equivalent linear element response, SOILSTRUCT updates the value of the elastic moduli assigned to each soil element using Equation (4) during primary loading or Equation (8) during unloading and reloading. The bulk modulus is computed for each soil element using Equation (7). To account for the change in stiffness that occurs during the application of a load increment, each incremental load calculation may be repeated using the iteration option. When the iteration option is invoked, the load vector is reapplied with a revised value for the element stiffness. The value assigned for the stiffness of the soil element reflects the average of the stress state developing at the end of the previous load case, or substep, and that which develops during the current iteration. However, when only one iteration is specified, the modulus values are calculated using the stresses developing at the end of the previous load increment. Upon completion of the last iteration for each load case or substep,

the arrays tabulating the values of the total nodal point displacements and total element stresses are updated with the computed incremental values.

3 Results of Previous Research Using Silt

Background

The research described herein is a continuation of two previous research projects with the Information Technology Laboratory at WES. The first project evaluated the hyperbolic stress-strain parameters of reconstituted silt-clay mixtures. The results of this study are described by Stark et al. (1991). A technical paper summarizing the drained and undrained stress-strain behavior and hyperbolic parameters of normally consolidated silt-clay mixtures was published in the February, 1994, issue of the *Journal of Geotechnical Engineering* published by the American Society of Civil Engineers (Stark et al. 1994). The second project evaluated the anisotropy of naturally occurring structured/cemented silt. Anisotropy was evaluated by conducting tests on structured/cemented specimens trimmed 90 degrees from the field orientation. The results of the study are described by Stark et al. (1995).

Silt Origin

The silt tested during the first phase of the study was excavated from a 40-ft-high bluff composed of Mississippi loess at the WES. The location of the bluff is shown on the information map of WES in Figure 3. The undisturbed loess is highly structured/cemented, which allows the 40-ft-high bluff to maintain a nearly vertical face. Because the loess was excavated from the bluff using a pick and shovel, the natural structure/cementation of the soil was destroyed during sampling. Confining pressures of 5 to 16 tsf were used to consolidate the reconstituted silt-clay mixtures to ensure that the specimens were normally consolidated prior to shear. The specimens were reconstituted by mixing various percentages of kaolinite and montmorillonite with the purified silt. The natural silt was purified using a sedimentation process to remove the naturally occurring clay size particles. Therefore, the quantity and composition of the

clay-silt mixtures could be accurately determined. The specimens were saturated prior to shear using back pressure saturation techniques.

Original Research Objectives and Results

The main objective of the original (1991) research program was to characterize the drained and undrained stress-strain behavior of normally consolidated silts and clayey silts. To achieve this objective, extensive drained and undrained triaxial tests were conducted on silt mixtures with varying clay contents. The percentages of clay used in the silt mixtures were 0, 10, 30, and 50. Manufactured kaolinite and montmorillonite were mixed with the silt to determine the effect of clay mineralogy on the stress-strain behavior of silt. The effect of density or unit weight on the stress-strain behavior was investigated by compacting the triaxial specimens at Standard Proctor relative compactions of 85, 90, 95, and 100 percent. The main conclusions regarding the behavior of normally consolidated silts and clayey-silts are summarized below (Stark et al. 1991):

The shear behavior of silt is controlled by the percentage of clay and the clay mineral in the soil. At low clay contents, the silt exhibits shear characteristics similar to a sand, and at high clay contents, the shear behavior is similar to that of a clay. The transition point from sand to clay behavior is a function of the clay mineralogy and was found to be between 10 and 30 percent for the kaolinite-silt mixtures and at or near 10 percent for the montmorillonite-silt mixtures.

The effect of density or unit weight on the shear strength and stress-strain parameters decreased as the clay content increased. At a low clay content (0 and 10 percent), increasing the Standard Proctor relative compaction from 85 to 100 percent resulted in a substantial increase in the shear strength and hyperbolic stress-strain parameters. However, at high clay contents (30 and 50 percent), there was only a small increase in the shear strength and hyperbolic stress-strain parameters when the relative compaction increased from 85 to 100 percent. Therefore, there appears to be little benefit, in terms of shear strength and stiffness, of specifying a field relative compaction greater than 90 percent if

the clay content is greater than or equal to 30 percent. However, the test results suggest that the volumetric strain may be reduced by 25 percent if the relative compaction is greater than 90 percent.

At low (0 and 10 percent) clay contents, the kaolinite-silt mixtures exhibited dilation even though the test specimens were normally consolidated. At high (30 and 50 percent) clay contents, the volume change behavior was contractive. Conversely, the montmorillonite-silt mixtures all exhibited a contractive volume change behavior. Therefore, the volume change behavior during shear is a function of the clay content and the clay mineralogy.

Effective confining pressures greater than 8 to 10 tsf were usually required to obtain a normally consolidated condition.

Total stress and effective stress Mohr-Coulomb strength parameters can be estimated for normally consolidated silts and clayey silts using the in situ water content and unit weight and the data base described herein. The effective stress friction angle for the kaolinite-silt mixtures ranged from 40 to 25 degrees and from 40 to 14 degrees for the montmorillonite-silt mixtures. The effective stress cohesion was measured to be zero for all of the mixtures. This also indicates that the test specimens were in a normally consolidated condition.

Clay mineralogy, as well as percentage of clay, controls the shear behavior of a silt deposit. The more active the clay mineral, the lower the modulus and shear strength of the silt. In addition, increasing the activity reduces the percentage of clay required to reach the transition point between sand and clay shear behavior.

Tables 2 through 7 can be used to estimate the drained and undrained shear strength and hyperbolic stress-strain parameters of normally consolidated silts and clayey silts using the in situ water content and dry unit weight.

Table 2
 Effective Stress Mohr-Coulomb Shear Strength Parameters for Kaolinite-Silt Mixtures from Consolidated-Drained Triaxial Compression Tests

% Clay	Standard Proctor Relative Compaction (%)	Average of Initial Dry Unit Weight (pcf)	Average of Initial Water Content (%)	Range of Effective Confining Pressure (tsf)	Effective Stress Cohesion (psf)	Effective Stress Friction Angle (degrees)
0 Kao	100	98	27	11.7 - 18.2	0	40
0 Kao	95	97	27	7.9 - 18.0	0	37
0 Kao	90	96	28	8.0 - 16.6	0	35
0 Kao	85	NA	NA	NA	NA	NA
10 Kao	100	104	23	9.8 - 17.0	0	37
10 Kao	95	103	23	11.7 - 17.4	0	35
10 Kao	90	103	23	3.1 - 15.4	0	34
10 Kao	85	102	24	3.1 - 14.5	0	33
30 Kao	100	115	17	10.2 - 17.6	0	33
30 Kao	95	115	17	8.3 - 15.5	0	31
30 Kao	90	114	17	4.1 - 15.8	0	30
30 Kao	85	114	18	3.1 - 17.3	0	29
50 Kao	100	111	18	9.2 - 17.4	0	28
50 Kao	95	109	19	8.2 - 15.4	0	27
50 Kao	90	108	20	4.1 - 13.3	0	26
50 Kao	85	107	21	3.7 - 13.4	0	25

NOTES:
 1.) Kao = Kaolinite
 2.) NA = Not available

Table 3
Effective Stress Hyperbolic Stress-Strain Parameters for Kaolinite-Silt Mixtures from Consolidated-Drained Triaxial Compression Tests

% Clay	Standard Proctor Relative Compaction (%)	Average of Initial Dry Unit Weight (pcf)	Average of Initial Water Content (%)	Range of Effective Confining Pressure (tsf)	Effective Stress Friction Angle (degrees)	Effective Stress Cohesion (psf)	Modulus Number K	Modulus Exponent n	Bulk Modulus Number Kb	Bulk Modulus Exponent m	Failure Ratio Rf
0 Kao	100	98	27	11.7 - 18.2	40	0	270	1.0	115	1.0	0.75
0 Kao	95	97	27	7.9 - 18.0	37	0	150	1.0	65	1.0	0.70
0 Kao	90	96	28	8.0 - 16.6	35	0	120	1.0	50	1.0	0.65
0 Kao	85	NA	NA	NA	NA	NA	NA	NA	NA	NA	NA
10 Kao	100	104	23	9.8 - 17.0	37	0	240	1.0	85	1.0	0.85
10 Kao	95	103	23	11.7 - 17.4	35	0	125	1.0	55	1.0	0.80
10 Kao	90	103	23	3.1 - 15.4	34	0	100	1.0	40	1.0	0.75
10 Kao	85	102	24	3.1 - 14.5	33	0	75	1.0	30	1.0	0.70
30 Kao	100	115	17	10.2 - 17.6	33	0	105	1.0	35	1.0	0.80
30 Kao	95	115	17	8.3 - 15.5	31	0	70	1.0	30	1.0	0.75
30 Kao	90	114	17	4.1 - 15.8	30	0	65	1.0	25	1.0	0.70
30 Kao	85	114	18	3.1 - 17.3	29	0	60	1.0	20	1.0	0.65
50 Kao	100	111	18	9.2 - 17.4	28	0	65	1.0	30	1.0	0.75
50 Kao	95	109	19	8.2 - 15.4	27	0	60	1.0	25	1.0	0.70
50 Kao	90	108	20	4.1 - 13.3	26	0	55	1.0	20	1.0	0.65
50 Kao	85	107	21	3.7 - 13.4	25	0	50	1.0	15	1.0	0.60

NOTES:
 1.) Kao = Kaolinite
 2.) NA = Not available

Table 4
Total and Effective Stress Mohr-Coulomb Shear Strength Parameters for Kaolinite-Silt Mixtures from Consolidated-Undrained Triaxial Compression Tests

% Clay	Standard Proctor Relative Compaction (%)	Average of Initial Dry Unit Weight (pcf)	Average of Initial Water Content (%)	Range of Effective Confining Pressure (tsf)	Total Stress Cohesion (psf)	Total Stress Friction Angle (degrees)
0 Kao	100	97	27	11.3 - 16.4	0	19
0 Kao	95	95	28	6.1 - 16.6	0	18
0 Kao	90	94	29	8.7 - 16.6	0	16
0 Kao	85	NA	NA	NA	NA	NA
10 Kao	100	106	22	13.8 - 16.9	0	18
10 Kao	95	103	23	10.3 - 16.3	0	17
10 Kao	90	102	24	5.2 - 16.9	0	16
10 Kao	85	100	25	4.2 - 17.3	0	15
30 Kao	100	113	18	9.2 - 15.4	0	16
30 Kao	95	110	20	3.1 - 12.8	0	15
30 Kao	90	108	21	4.1 - 15.9	0	13
30 Kao	85	107	22	3.1 - 13.4	0	12
50 Kao	100	104	22	6.7 - 14.4	0	15
50 Kao	95	103	23	7.2 - 15.4	0	14
50 Kao	90	102	24	7.6 - 13.3	0	13
50 Kao	85	101	25	3.7 - 13.4	0	12

NOTES:
 1.) Kao = Kaolinite
 2.) NA = Not available

Table 5
Total Stress Hyperbolic Stress-Strain Parameters for Kaolinite-Silt Mixtures from Consolidated-Undrained Triaxial Compression Tests

% Clay	Standard Proctor Relative Compaction (%)	Average of Initial Dry Unit Weight (pcf)	Average of Initial Water Content (%)	Range of Effective Confining Pressure (tsf)	Total Stress Cohesion (psf)	Total Stress Friction Angle (degrees)	Modulus Number K	Modulus Exponent n	Failure Ratio Rf
0 Kao	100	97	27	11.3 - 16.4	0	19	450	1.0	0.65
0 Kao	95	95	28	6.1 - 16.6	0	18	400	1.0	0.60
0 Kao	90	94	29	8.7 - 16.6	0	16	350	1.0	0.55
0 Kao	85	NA	NA	NA	NA	NA	NA	NA	NA
10 Kao	100	106	22	13.8 - 16.9	0	18	425	1.0	0.45
10 Kao	95	103	23	10.3 - 16.3	0	17	375	1.0	0.55
10 Kao	90	102	24	5.2 - 16.9	0	16	350	1.0	0.60
10 Kao	85	100	25	4.2 - 17.3	0	15	300	1.0	0.70
30 Kao	100	113	18	9.2 - 15.4	0	16	400	1.0	0.90
30 Kao	95	110	20	3.1 - 12.8	0	15	350	1.0	0.90
30 Kao	90	108	21	4.1 - 15.9	0	13	325	1.0	0.95
30 Kao	85	107	22	3.1 - 13.4	0	12	270	1.0	0.95
50 Kao	100	104	22	6.7 - 14.4	0	15	250	1.0	0.80
50 Kao	95	103	23	7.2 - 15.4	0	14	240	1.0	0.85
50 Kao	90	102	24	7.6 - 13.3	0	13	230	1.0	0.90
50 Kao	85	101	25	3.7 - 13.4	0	12	210	1.0	0.90

NOTES:

- 1.) Kao = Kaolinite
- 2.) NA = Not available

Table 6
 Effective Stress Mohr-Coulomb Shear Strength Parameters for Montmorillonite-Silt Mixtures
 from Consolidated-Drained Triaxial Compression Tests

% Clay	Standard Proctor Relative Compaction (%)	Average of Initial Dry Unit Weight (pcf)	Average of Initial Water Content (%)	Range of Effective Confining Pressure (tsf)	Effective Stress Cohesion (psf)	Effective Stress Friction Angle (degrees)
0 Mont	100	98	27	2.1 - 17.1	0	40
10 Mont	100	102	24	11.3 - 16.9	0	35
30 Mont	100	100	26	10.3 - 16.9	0	20
50 Mont	100	94	30	8.8 - 15.5	0	14

NOTES:
 1.) Mont = montmorillonite

Table 7
Effective Stress Hyperbolic Stress-Strain Parameters for Montmorillonite-Silt Mixtures from Consolidated-Drained Triaxial Compression Tests

% Clay	Standard Proctor Relative Compaction (%)	Average of Initial Dry Unit Weight (pcf)	Average of Initial Water Content (%)	Range of Effective Confining Pressure (tsf)	Effective Stress Friction Angle (degrees)	Effective Stress Cohesion (psf)	K	Modulus Number Exponent n	Bulk Modulus Number Exponent m	Bulk Modulus Exponent m	Failure Ratio Rf
0 Mont	100	98	27	2.1 - 17.1	40	0	270	1.0	115	1.0	0.75
10 Mont	100	102	24	11.3 - 16.9	35	0	90	1.0	50	1.0	0.75
30 Mont	100	100	26	10.3 - 16.9	20	0	55	1.0	20	1.0	0.75
50 Mont	100	94	30	8.7 - 15.5	14	0	35	1.0	15	1.0	0.75

NOTES:

1.) Mont = montmorillonite

4 Laboratory Testing Program Using Structured/Cemented Silt

Background

The main objective of the previous and current research was to characterize the drained stress-strain behavior of naturally occurring structured/cemented silt. To achieve this objective, extensive oedometer and drained triaxial compression tests were conducted on undisturbed silt. The tests were conducted using specimens trimmed in their field orientation and 90 degrees from the field orientation. Both sets of tests were conducted on undisturbed structured/cemented silt from the same location.

Silt Origin

A bluff containing Mississippi loess was located at WES (Figure 3). This is the same bluff from which the silt used in the previous research was excavated. The bluff stands at a nearly vertical slope as do many of the loess slopes in the Vicksburg area. This fact does not correspond with the hyperbolic stress-strain parameters and effective stress friction angles that were estimated from the triaxial compression tests on the reconstituted, normally consolidated silt-clay mixtures. Therefore, the natural structure/cementation of the loess appears to result in a significantly higher shear strength and stiffness. During the sampling and reconstituting of the silt in the previous (1991) study, all of the structure/cementation was destroyed. Therefore, the shear strength and hyperbolic stress-strain parameters estimated using reconstituted specimens are likely to be lower than the in situ parameters, as indicated by the presence of a nearly vertical bluff. As a result, the main objective of this research is to investigate the effect

of structure/cementation on the shear behavior and stiffness as characterized in terms of the hyperbolic stress-strain parameters of naturally occurring structured/cemented silt.

The Mississippi loess belt is approximately 70 to 120 miles wide, extending eastward from the bluffs along the Mississippi River. Generally, the loess is less than 10 feet thick except at the bluffs where it is up to 100 feet thick. The bluff at WES where the loess samples were obtained is approximately 40 feet high.

The Mississippi loess deposits were created by westerly winds carrying fine particles from the Mississippi River alluvial valley to its eastern uplands where it was deposited. This deposition occurred during the late Pleistocene and early Recent times.

Mississippi loess contains mainly silt and clay size particles. Scanning electron microscope analyses reveal that the silt particles are subangular to subrounded (Figure 4). The loess is a highly structured and/or cemented material. Figure 5 is a scanning electron microscope photograph that illustrates the cemented/structured nature of the silt. Figure 6 presents a closeup of the bonding or cementation between two silt particles. Finally, Figure 7 presents plan and closeup views of the natural cementation. It is interesting to note that the cementation forms two columns with a meniscus-like hole in the center. The cementing agents in the loess are predominantly carbonates, iron salts, and clays in various combinations (Krinitzsky and Turnbull 1967). It is assumed that the carbonates were present at the time the sediment was first deposited. Local migration of the carbonates probably occurred by means of groundwater or capillary movements. This migration resulted in the concretions and tubules that were found in the loess. Iron cementation is minor and largely indeterminate, since it is usually a much less constituent than the carbonate and clay (Krinitzsky and Turnbull 1967). The clay particles are evenly distributed among the silt grains forming jackets or husks around the silt particles, and thus holding them together. Another important aspect of the bonding attributed to the clay is the binding force resulting from capillary attraction of soil moisture. As a result, the capillary and clay bonding effects may vary appreciably with changes in moisture content in the loess.

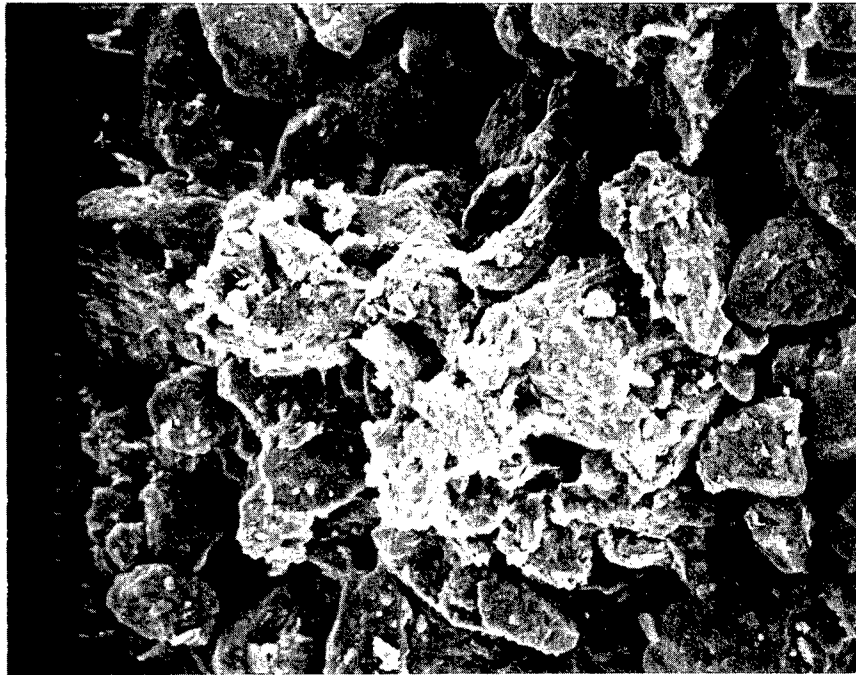


Figure 4. Scanning Electron Microscope Photograph of Naturally Occurring Silt (Magnification equals 1000 times)

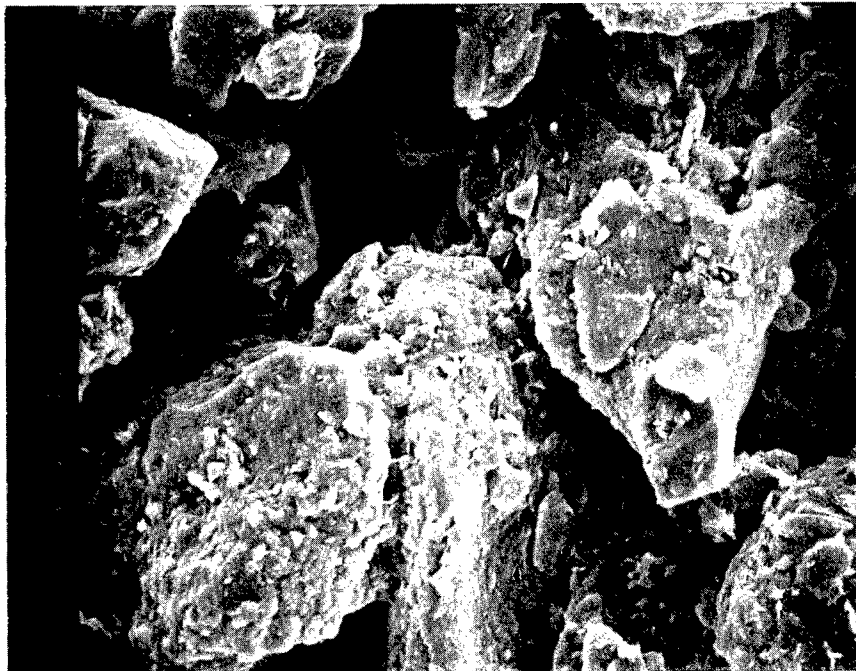


Figure 5. Two Silt Particles Cemented Together in the Right Center of the Photograph (Magnification equals 1500 times)

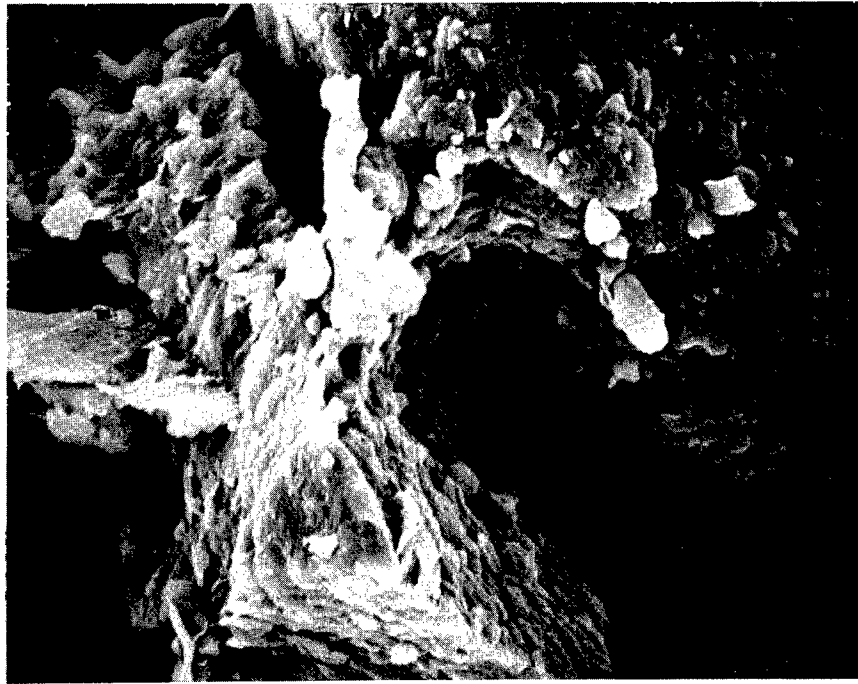


Figure 6. Closeup View of Cementation Joining Two Silt Particles
(Magnification equals 5000 times)



Figure 7. Plan and Closeup View of Natural Cementation
(Magnification equals 1500 times)

Oedometer and triaxial compression test results will indicate that the carbonate bonding is resistant to distilled water and provides a stronger bond than the clay/capillary bonds. This was concluded because laboratory saturated specimens exhibited similar shear strength and compressibility behavior as specimens tested at the natural water content. Laboratory saturation removed or reduced the capillary and clay bonds. Thus, the remaining bonding should be attributed to the carbonates. Carbonates are not soluble in distilled water but could be soluble when inundated with site-specific liquids. As a result, site-specific testing should be conducted to investigate the permanence of the carbonate bonding.

Silt Sampling and Index Properties

In August, 1991, Dr. Timothy D. Stark of the University of Illinois at Urbana-Champaign and Dr. Robert M. Ebeling of WES hand excavated two undisturbed block samples of the loess. The blocks were excavated adjacent to each other and therefore probably consist of similar material. The blocks are approximately 1.5- by 1.5- by 1.5-ft and were taken to the University of Illinois where they were waxed and stored in a moist room. As a result, these blocks provide an excellent source of structured/cemented silt. One block was used for tests on specimens trimmed in the natural direction, and the other was used to obtain specimens trimmed 90 degrees from the field direction.

Hydrometer analyses revealed that the clay content of the light-brown loess is approximately 10 to 12 percent. The percentage of clay is defined as the material finer than 0.002 mm. Approximately 2 to 3 percent of the loess is fine sand, shells, and organics particles which do not pass the U.S. Standard Sieve No. 200 sieve. The grain size distribution of the structured/cemented silt is labeled S/C in Figure 4. The grain size distributions for the previous research project (Stark et al. 1994) involving reconstituted silt-clay mixtures are labeled 0 percent clay, 10 percent Kaolinite, 30 percent Kaolinite, and 50 percent Kaolinite are also shown in Figure 8. The liquid limit, plastic limit, and plasticity index of the naturally occurring structured/cemented silt are 30,

nonplastic, and nonplastic, respectively. The silt classifies as a low plasticity silt (ML) according to the Unified Soil Classification System. The natural water content and total unit weight of the undisturbed silt are 19.9 percent and 113.9 pcf, respectively. The initial void ratio and degree of saturation of the undisturbed silt are 0.793 and 68.3 percent, respectively. The specific gravity of solids of the silt was measured to be 2.71.

Clay mineralogy tests were conducted on the silt by Professor Stephen P. Altaner of the Geology Department at the University of Illinois at Urbana-Champaign. X-ray diffraction tests were conducted using air-dried and glycol treated specimens. The bulk sample contains quartz (38 percent), potassium-feldspar (3 percent), plagioclase feldspar (11 percent), carbonates (33 percent), and clay minerals (15 percent). The carbonates consist of calcite (4 percent) and dolomite (29 percent). These percentages are in agreement with the following values reported by Lutton (1969) for loess in the Vicksburg area: quartz (55 percent), feldspar (15 percent), carbonates (15 percent), and clay minerals (15 percent). The clay minerals (materials smaller than 0.002 mm) detected in the University of Illinois tests consist of smectite, illite, and kaolinite. The percentages of each clay mineral, based on the material finer than 0.002 mm, are smectite (90 percent), illite (9 percent), and kaolinite (1 percent). X-ray diffraction tests on air-dried material indicate that the predominant cation in the smectite mineral is calcium.

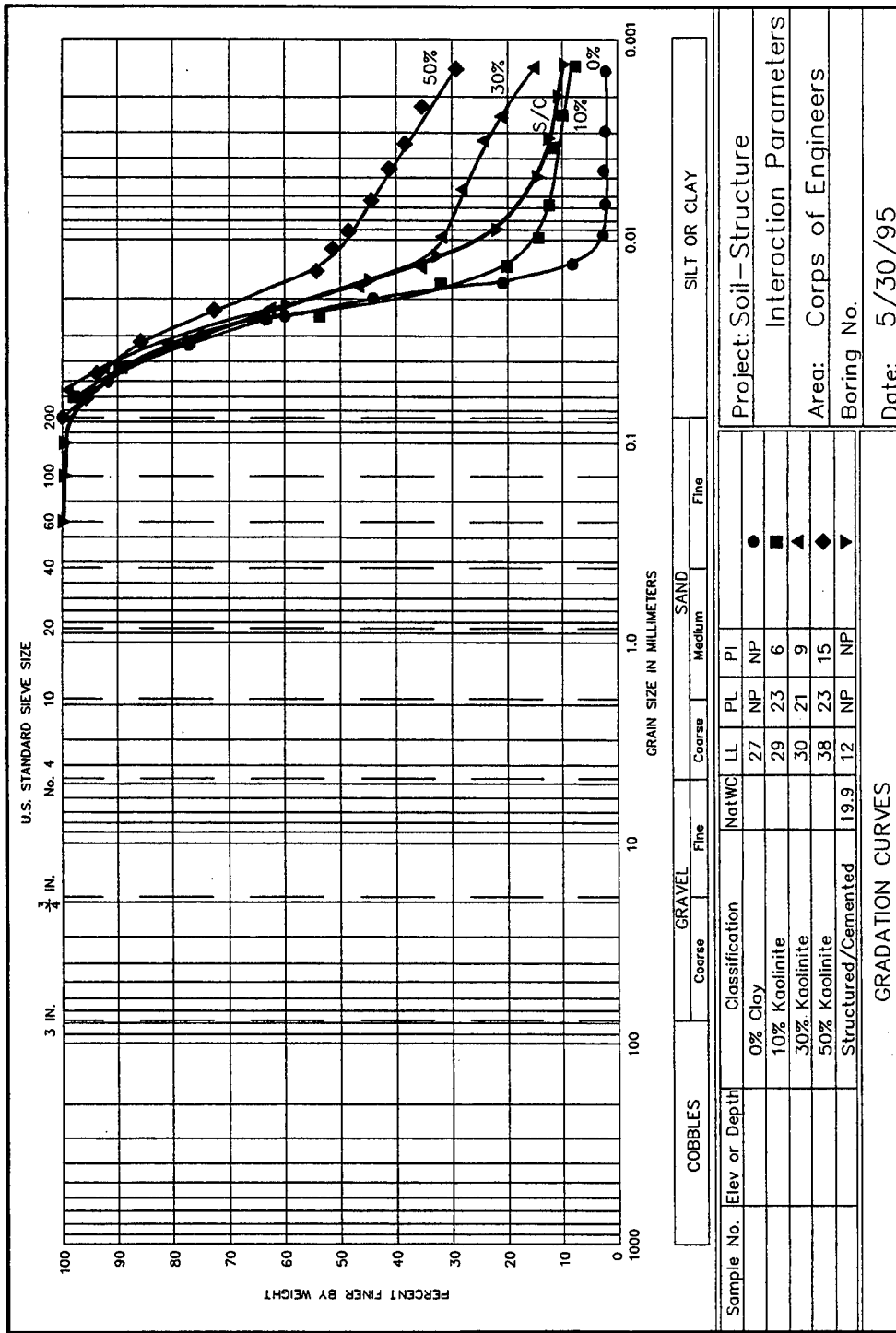


Figure 8. Gradation of kaolinite-silt mixtures and structured/cemented silt.

5 Oedometer Testing

Background

The main objective of this study is to characterize the drained shear strength and stress-strain behavior of naturally occurring structured/cemented silts. Oedometer tests were initially conducted to provide an important insight to the triaxial shear behavior. For example, the effective preconsolidation pressure and the effect of inundation can be determined from oedometer tests. This information provides a significant insight to the shear behavior of structured/cemented silts. As a result, oedometer testing was conducted prior to the triaxial compression testing to gain an insight to the shear behavior and quality of the structured/cemented silt samples.

Effect of Structure/Cementation on Compressibility

Figure 9 presents a comparison of results of oedometer tests on structured/cemented and reconstituted silt specimens. The structured/cemented silt was obtained by trimming the specimen directly from an undisturbed block into a rigid oedometer ring. The undisturbed specimen was not submerged prior to or during the oedometer test, and thus was partially saturated. The one-dimensional oedometer test was performed in accordance with ASTM (1993) Standard D2435-80. Figure 9 shows that the structured/cemented specimen yielded an effective preconsolidation pressure of approximately 20,000 psf. The modified compression and modified recompression indices, obtained from the axial strain-effective stress relationships, are estimated to be 0.132 and 0.01, respectively. Figure 10 presents the void ratio-effective stress relationships for the oedometer test on structured/cemented silt shown in Figure 9, which is presented in terms of axial strain. The compression and recompression indices, obtained from the void ratio-effective stress relationships, are estimated to be 0.26 and 0.017, respectively, and are presented in Table 8.

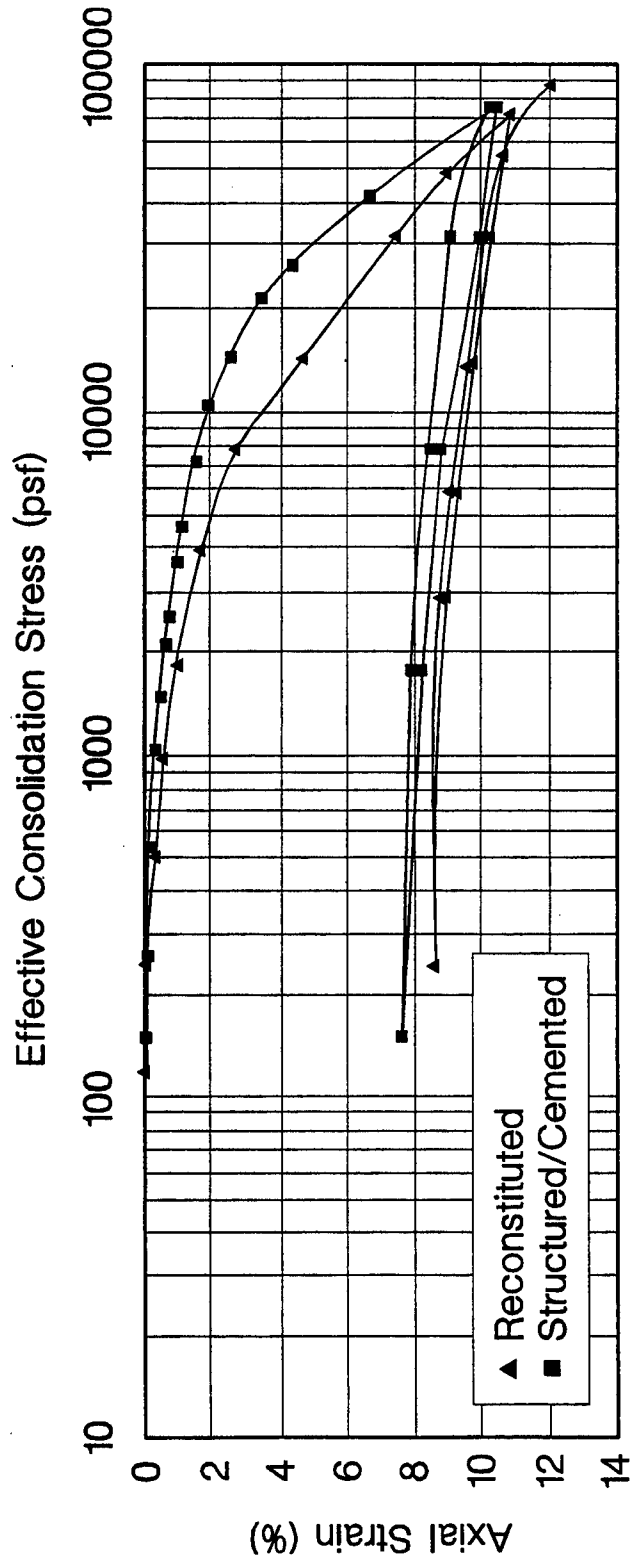


Figure 9. Comparison of results of oedometer tests on structured/ cemented and reconstituted silt.

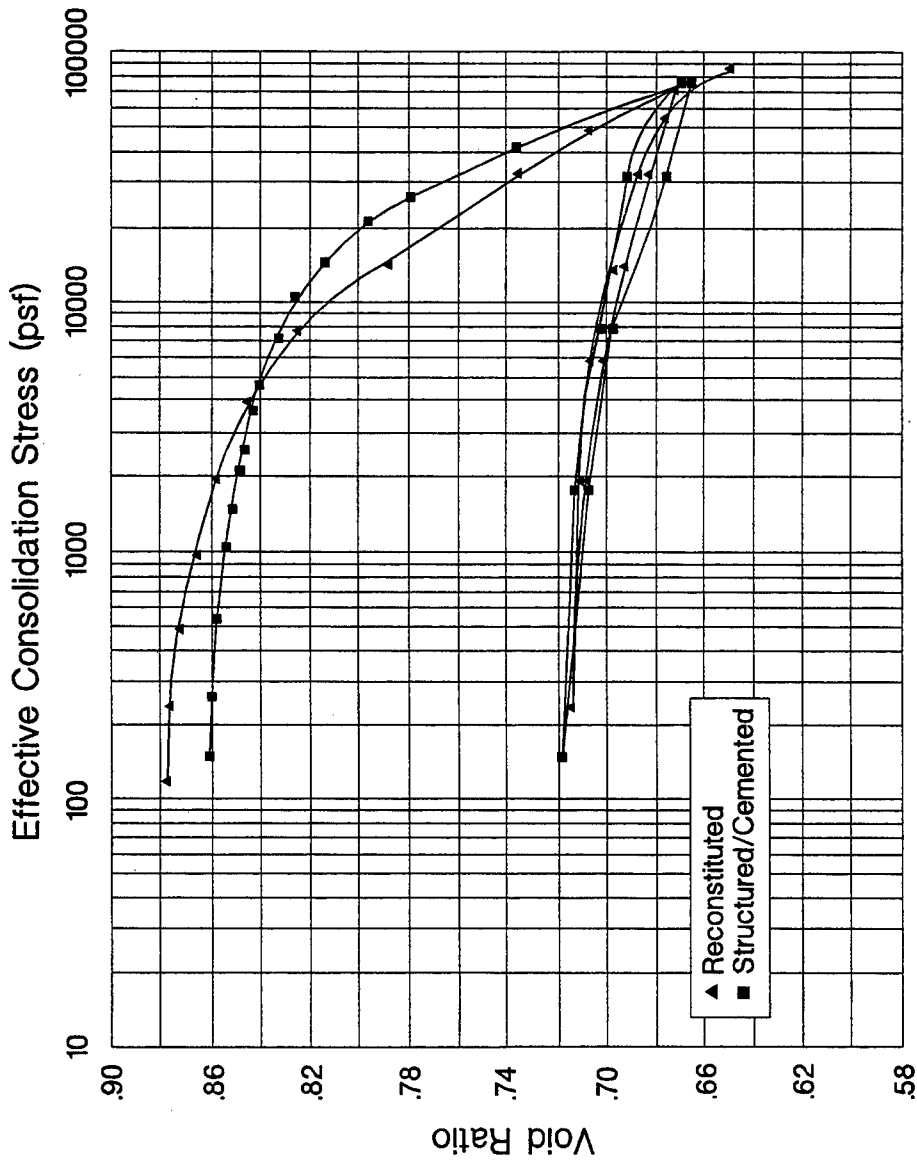


Figure 10. Void ratio-effective stress relationship for structured/cemented and reconstituted silt

Table 8
Compressibility Parameters of Structured/Cemented and Reconstituted Silt

Specimen Type	Maximum Preconsolidation Pressure (psf)	Compression Index	Recompression Index	Modified Compression Index	Modified Recompression Index
Partially Saturated					
Structured/Cemented (Field Direction)	20,000	0.26	0.017	0.132	0.01
Structured/Cemented (90 Degrees From Field Direction)	10,000	0.18	0.022	0.115	0.02
Reconstituted	8,000	0.16	0.026	0.11	0.018
Laboratory Inundated					
Structured/Cemented (Recompression Range Inundation)	15,000	0.176	0.016	0.093	0.009
Structured/Cemented (Compression Range Inundation)	15,000	0.3	0.016	0.156	0.008

NOTES:

- 1.) Compression and recompression indices obtained from void ratio-effective stress relationships
- 2.) Modified compression and recompression indices obtained from axial strain-effective stress relationships

Figure 9 also presents the results of an oedometer test on a reconstituted specimen. The reconstituted specimen was obtained by compacting the remolded silt in a fixed oedometer ring. The remolded silt was obtained by crushing the structured/cemented specimen after completion of the oedometer test described in the previous paragraph. The silt was crushed using a mortar and pestle. The remolded silt was mixed with distilled water to obtain the natural water content. The silt was compacted directly into a rigid oedometer ring at the natural water content of 19.9 percent and total unit weight of 113.9 pcf. A spatula was used to compact the silt so that the silt was not overcompacted and thus not preconsolidated. The silt was compacted in two lifts. The appropriate amount of soil was weighed and compacted to obtain the natural total unit weight. The top of the first lift was scarified before the next lift was placed to ensure an adequate bond between lifts. The one-dimensional oedometer test was performed in accordance with ASTM (1993) Standard D2435-80.

Figure 9 shows that the reconstituted specimen is more compressible than the structured/cemented specimen. The effective preconsolidation pressure is approximately 8000 psf, which is significantly less than the structured/cemented value of about 20,000 psf. The modified compression and modified recompression indices for the reconstituted silt, obtained from the axial strain-effective stress relationships, are approximately 0.11 and 0.018, respectively. Figure 10 presents the void ratio-effective stress relationships for the oedometer test on reconstituted silt shown in Figure 9, which is presented in terms of axial strain. The compression and recompression indices, obtained from the void ratio-effective stress relationships, are estimated to be 0.16 and 0.026, respectively.

In summary, the structure/cementation of the natural silt results in a significantly higher preconsolidation pressure and, thus, a stiffer and less compressible material. The compression indices of both specimens are similar in magnitude.

Effect of Inundation on Compressibility

Four oedometer tests were conducted to estimate the effect of soaking or inundation on the stiffness and compressibility of structured/cemented silt. In the "dry" tests, the specimen was trimmed directly from an undisturbed block of silt into a rigid oedometer ring. The "dry" specimen was not inundated at any time and was tested according to ASTM (1993) Standard D2435-80. The "inundated" specimen was trimmed from the same undisturbed block near the location of the "dry" specimen. The "inundated" specimens were tested according to ASTM (1993) Standard D2435-80, except that the specimens were soaked at a vertical effective stress of 2400 psf (Figures 11 and 12) and 23000 psf (Figures 13 and 14). The specimens were inundated by filling the chamber surrounding the specimen container with distilled-deaired water. A vertical effective stress of 2400 psf corresponds to the recompression range of the silt, and a vertical effective stress of 23,000 psf exceeds the effective preconsolidation pressure of approximately 20,000 psf, thus corresponding to the virgin compression range.

Figure 11 shows that there is a negligible difference between the compressibility of the "dry" and "inundated" specimens when inundation occurs in the recompression range. Therefore, inundation of structured/cemented silt in the recompression range does not significantly increase compressibility or decrease the stiffness of the material. However, inundation in the virgin compression range (Figure 13 or 14) results in an increase in axial strain at a vertical effective stress of 23,000 psf. After inundation and an increase in vertical effective stress, the silt exhibited a similar stress-strain behavior as the "dry" specimen. Figures 12 and 14 present the void ratio-effective stress relationships for the oedometer tests shown in Figures 11 and 13, respectively.

In summary, inundation of structured/cemented silt in the recompression range does not significantly change the compressibility or stiffness. Therefore, it was concluded that inundation does not damage or dissolve the natural structure/cementation. However, soaking in the virgin compression range may cause an increase in axial strain or a decrease in void ratio. This has important

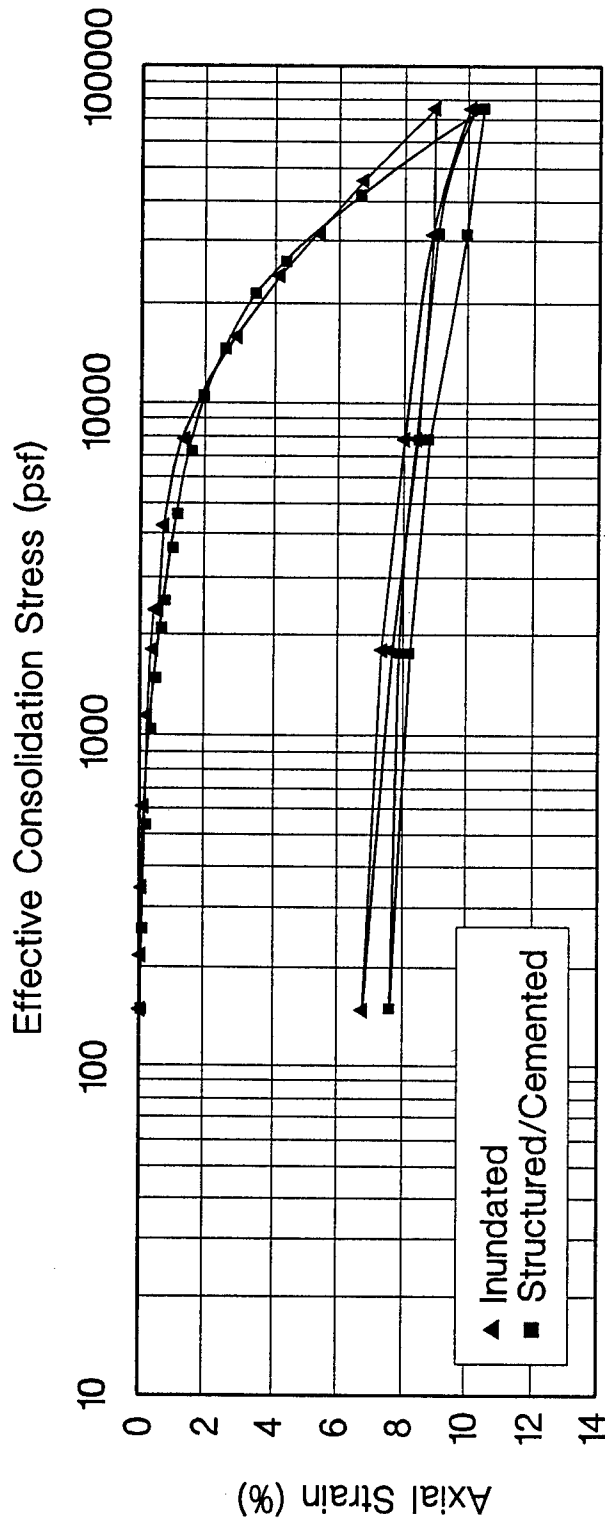


Figure 11. Effect of inundation in the recompression range (2400 psf) on the compressibility of structured/cemented silt.

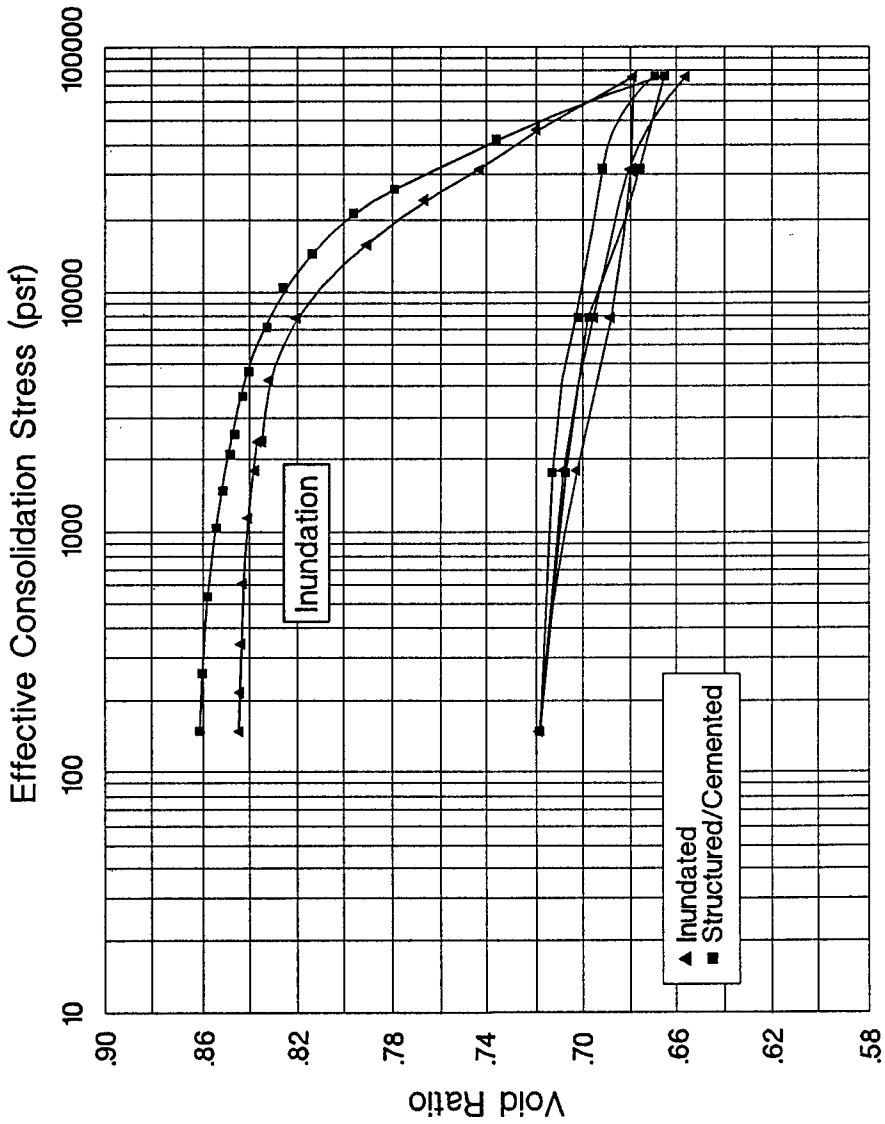


Figure 12. Effect of inundation in the recompression range (2400 psf) on the void ratio-effective stress relationship of structured/cemented silt.

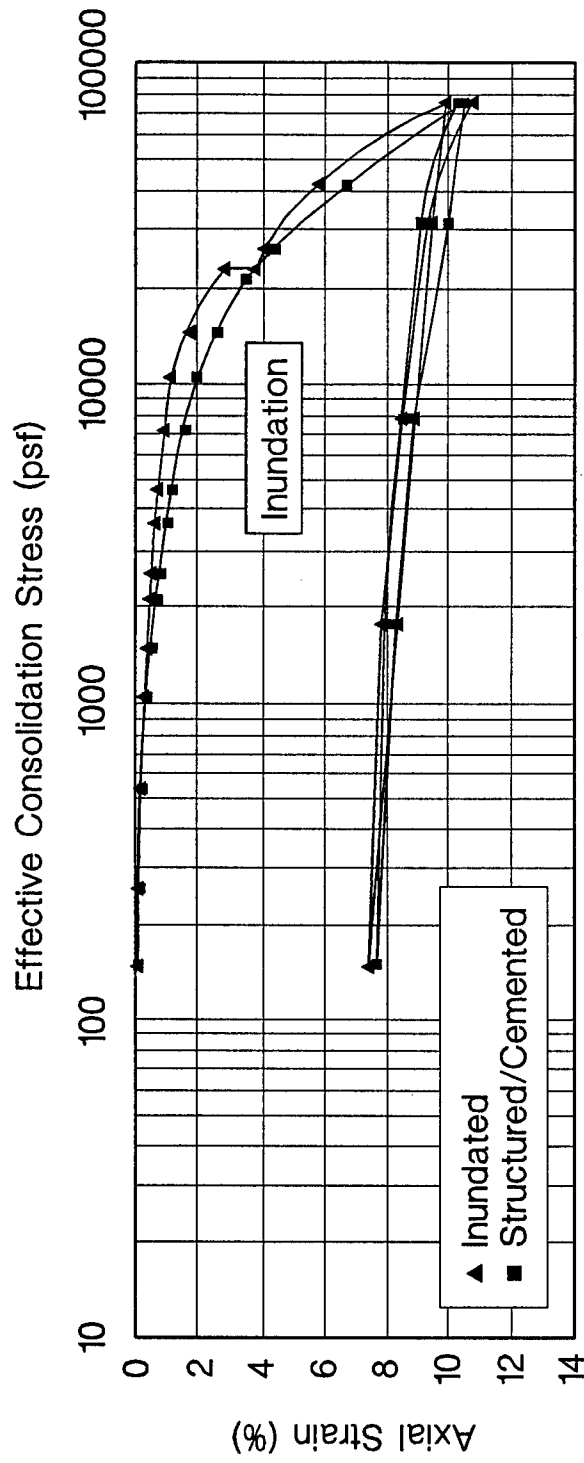


Figure 13. Effect of inundation in the virgin compression range (23,000 psf) on the compressibility of structured/cemented silt.

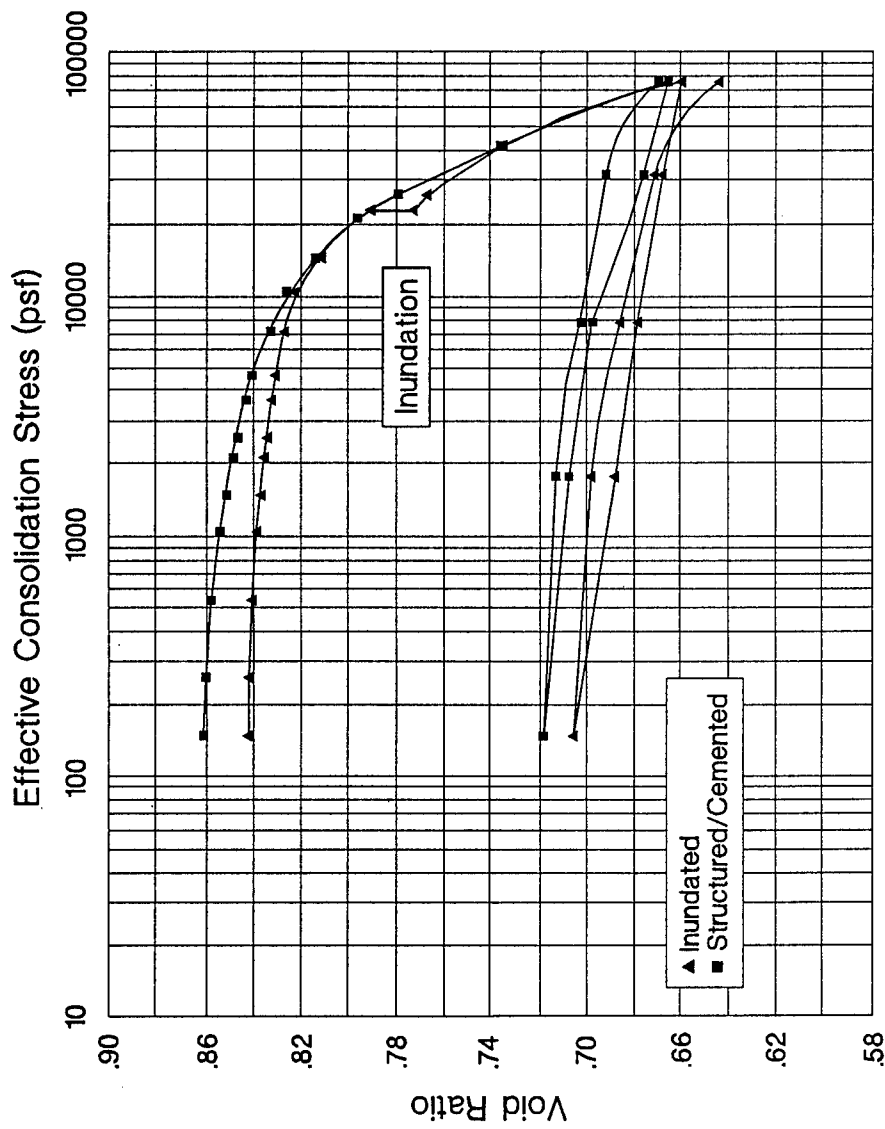


Figure 14. Effect of inundation in the virgin compression zone (23,000 psf) on the void ratio-effective stress relationship of structured/cemented silt.

implications for construction and inundation in structured/cemented silts.
Table 8 presents a summary of the compressibility parameters for the inundated structured/ cemented specimens.

6 Triaxial Compression Test Procedures

Preparation of Structured/Cemented Triaxial Specimens

The 1.5-in.-diam, 3.0-in.-long structured/cemented triaxial specimens were trimmed using a trimming lathe. One set of specimens was trimmed from a block sample oriented in the field direction, and the other set was trimmed from a block sample oriented 90 degrees from the field direction. A very fine wire saw and a surgical razor blade were used to trim the structured/cemented silt. A 3.0-in.-long miter box was used to obtain the final triaxial specimen after lathe trimming was completed. The water content and dry unit weight of each test specimen were determined from the trimmings before the specimen was inserted into the triaxial apparatus.

The 1.5-in.-diam, 3.0-in.-long reconstituted triaxial test specimens were fabricated using a mold. The remolded silt was obtained from the trimmings of the structured/cemented specimen compacted at the same effective confining pressure. Because the structured/cemented specimen trimming was conducted in a moisture room, the water content of the trimmings was similar to the natural water content of the silt. Therefore, no water had to be added to fabricate the reconstituted silt specimen. The remolded silt was compacted directly into a 1.5-in.-diam. stainless steel mold at the natural water content of 19.9 percent and total unit weight of 113.9 pcf. A spatula was used to compact the silt so that the silt was not overcompacted, and thus not preconsolidated. The silt was compacted in three lifts in a moisture room. The appropriate amount of soil was weighed and compacted to obtain the natural total unit weight. The top of each lift was scarified before the next lift was placed to ensure an adequate bond between lifts. A 3.0-in.-long miter box was used to obtain the final triaxial test specimen after reconstitution was completed. The

water content and dry unit weight of each reconstituted specimen were determined before the specimen was inserted into the triaxial apparatus.

Two triaxial cells with plexiglass containers were used for the testing. The triaxial apparatuses were designed and fabricated at the University of Illinois. The cells are connected to a volume change measurement device, which is read manually. The porous stones at the tops and bottoms of the test specimens were boiled for ten minutes before each test. Two membranes, i.e., prophylactics, were carefully rolled over each test specimen. To reduce the amount of air trapped in the system, the membranes were rolled over the test specimens and any wrinkles in either membrane were removed. Each membrane was secured with two O-rings at the top and bottom of each specimen.

To promote drainage in the isotropically consolidated-drained (S) triaxial tests, the specimens were wrapped in filter paper. Portions of the filter paper were cut out to reduce the strength of the filter paper as described by Bishop and Henkel (1962). (These slotted pieces of filter paper are sometimes referred to as Bishop's pajamas.) The appropriate strain rate for the isotropically consolidated-drained (S) triaxial compression tests was determined using the procedure described by Gibson and Henkel (1954) and the coefficient of consolidation measured during consolidation of each test specimen.

Triaxial Compression Tests on Partially Saturated Specimens

A series of isotropically consolidated-drained (ICD) triaxial compression tests was conducted on horizontally and vertically trimmed undisturbed specimens at the natural water content. The specimens were trimmed as previously described and tested at the natural water content. Therefore, water was not introduced to the specimen before, during, or after the tests. These tests were conducted at an axial displacement rate of 0.2 mm/minute, which corresponds to an axial strain rate of 1.7 percent/minute. The drainage valve to the specimen was closed during the consolidation and shear phases of the tests. Though the drainage valve to the specimens was closed, the tests were still considered drained

because the silt is highly permeable and the specimens were partially saturated. As a result, no volume change information was obtained from the triaxial tests on partially saturated specimens. A similar series of four ICD triaxial compression tests was conducted on reconstituted specimens to investigate the effect of structure/cementation on the stress-strain behavior of partially saturated silts.

In all of the triaxial compression tests conducted during this study, the cell pressure and back pressure were applied using a constant pressure system that utilizes mercury pots to generate pressure. This prevents any significant variations in the cell and back pressures caused by variations in a compressor or air pressure system. The deviator stress was applied using a Wykeham-Farrance constant rate of displacement loading frame. The isotropically consolidated-drained triaxial compression tests were performed in accordance with the U.S. Army Engineer Laboratory Soils Testing Manual (Office 1970).

Triaxial Compression Tests on Saturated Specimens

A series of ICD triaxial compression tests was conducted on horizontally and vertically trimmed structured/cemented specimens after the specimens had been saturated in the laboratory. The specimens were saturated to investigate the effect of laboratory saturation on the stress-strain behavior of structured/cemented silt. Distilled-deaired water was percolated through the specimen under a hydraulic head of 1 ft, or 62.4 psf, for a period of twenty-four hours. A confining pressure of 500 psf was applied to the specimen prior to the saturation/percolation process.

Percolation of water through the specimen resulted in degrees of saturation, measured after shearing, ranging from 90 to 99 percent using the hydraulic head of 1 ft. Black and Lee (1973) and Bishop and Henkel (1962) concluded that the desired degree of saturation should be greater than 90 percent for an ICD triaxial compression test. After completion of the saturation process, the desired consolidation pressure was applied. Upon equilibration, the specimen was sheared to an axial strain of 20 percent. Four and three ICD triaxial tests

were conducted on structured/cemented and reconstituted specimens, respectively, to investigate the effect of laboratory saturation on the behavior of silt.

The ICD triaxial compression tests on laboratory saturated specimens were conducted at an axial displacement rate of 0.02 mm/minute, which corresponds to an axial strain rate of 0.026 percent/minute. The drainage valve was open during the consolidation and shear phases of the tests. As a result, volume change information was obtained from the tests on laboratory saturated specimens.

7 ICD Triaxial Compression Tests on Partially Saturated Specimens

Structured/Cemented Silt Specimens

Four isotropically consolidated-drained (ICD) triaxial compression tests were conducted on partially saturated structured/cemented and reconstituted silt specimens. The specimens were not laboratory saturated, and thus were tested at the natural water content of approximately 17 percent. Shearing commenced after the specimens came to equilibrium under the applied effective confining pressure or consolidation stress. Since the natural or in situ degree of saturation is approximately 59 percent, no volumetric strain measurements were made during these tests. The test results illustrate the effect of structure/cementation and effective confining pressure on the drained stress-strain behavior of naturally occurring silts. Figure 15 presents the deviator stress-axial strain relationships from the ICD triaxial compression tests on partially saturated structured/cemented silt. Figure 15 shows that the effective confining pressure or consolidation stress (σ'_{3c}) ranged from 1000 to 11,520 psf.

Figure 15 also shows that the peak deviator stress and the deviator stress at an axial strain of approximately 20 percent increases with increasing effective confining pressure. The Mohr-Coulomb shear strength parameters were estimated for effective confining pressures ranging from 1000 to 11,520 psf using either the peak deviator stress or the deviator stress at an axial strain of 20 percent. The resulting effective stress cohesion and friction angle were 950 psf and 28 degrees, respectively.

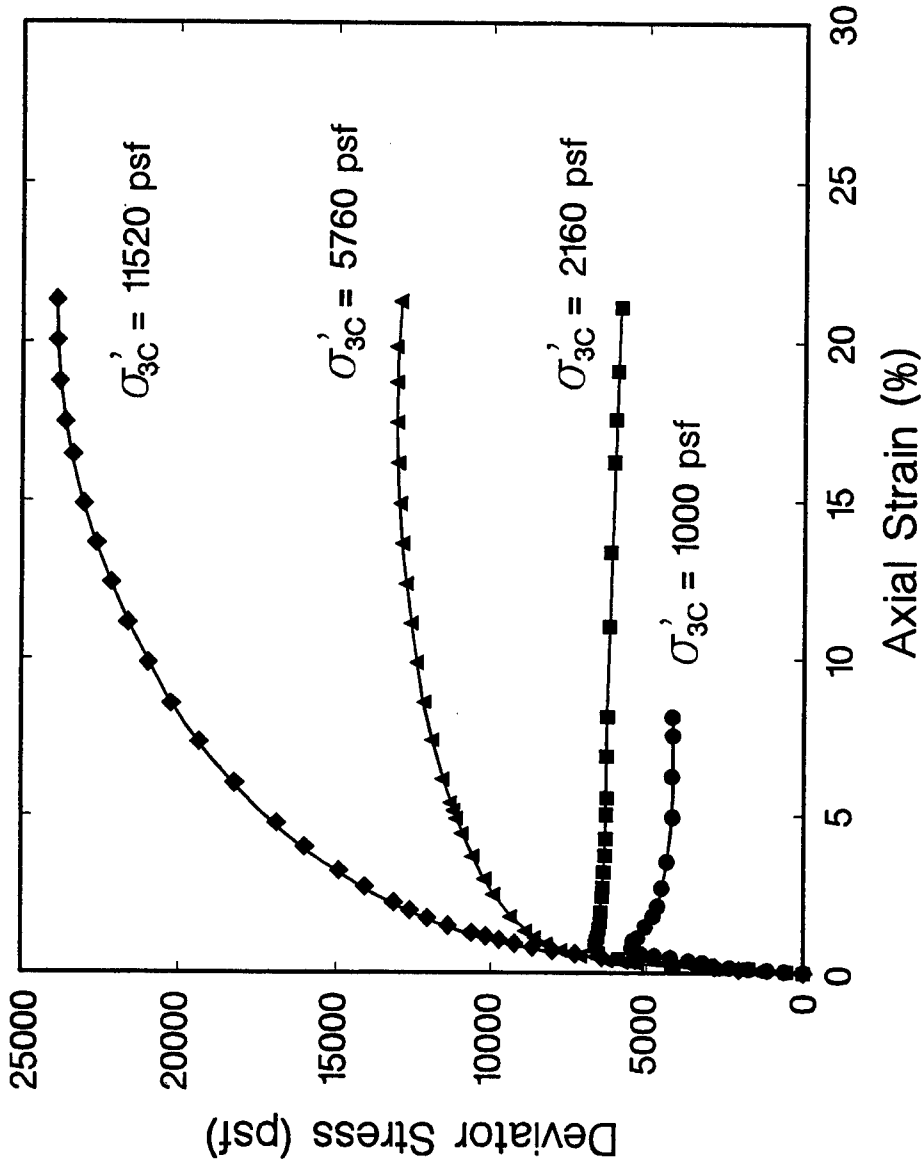


Figure 15. Stress-strain relationship from ICD triaxial compression tests on partially saturated structured/cemented silt.

Reconstituted Silt Specimens

Figure 16 presents the deviator stress-axial strain relationships from the four ICD triaxial compression tests on partially saturated, reconstituted specimens. Figure 16 shows that the deviator stress at an axial strain of approximately 20 percent increases with increasing effective confining pressure. The Mohr-Coulomb shear strength parameters were estimated using the deviator stress at an axial strain of 20 percent. The resulting effective stress cohesion and friction angle are 0 psf and 30 degrees, respectively. Therefore, the structure/cementation results in a higher value of effective stress cohesion and a lower value of friction angle than exhibited in the reconstituted specimens.

The tests on reconstituted specimens were conducted at the same effective confining pressures as the tests on the structured/cemented silt specimens. As a result, the ICD triaxial compression test results from Figures 15 and 16 are superimposed in Figures 17 through 20 for comparison purposes. Figures 17 and 18 present a comparison of the stress-strain relationships at effective confining pressures of 1000 and 2160 psf, respectively. At effective confining pressures of 1000 and 2160 psf, the stress-strain relationship of the structured/cemented silt exhibits a pronounced peak strength and a post-peak strength loss. In addition, the structured/cemented silts are significantly stiffer and stronger than the reconstituted silt. At a stress level between the confining pressures of 2160 and 5760 psf, the effects of structure/cementation diminish. This is evident from the stress-strain relationship in Figure 19 which no longer exhibits the post-peak behavior attributed to structure/cementation as shown in Figure 18. Thus, as the effective confining pressure increases (Figures 18 and 19), the effects of structure/cementation are destroyed and the difference in stiffness and maximum deviator stress decreases. Finally, at an effective confining pressure of 11,520 psf (Figure 20), the structured/cemented and reconstituted silt specimens exhibit similar stiffness and shear strength characteristics.

In summary, the effective confining pressure can break or overcome the structure/cementation of the undisturbed silt resulting in a reconstituted behavior. This transition from structured/cemented behavior to reconstituted behavior clearly has important implications for construction in naturally

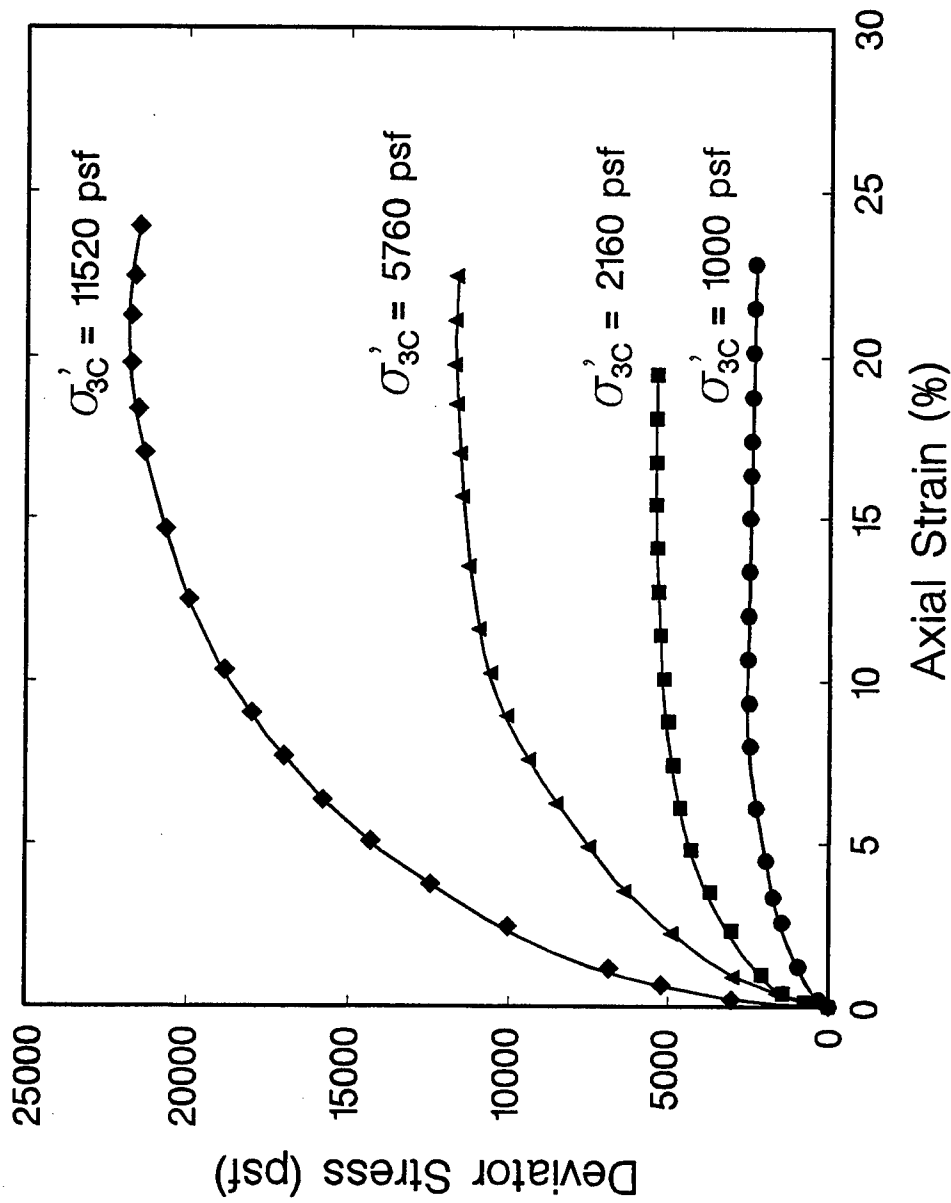


Figure 16. Stress-strain relationships from ICD triaxial compression tests on partially saturated reconstituted silt.

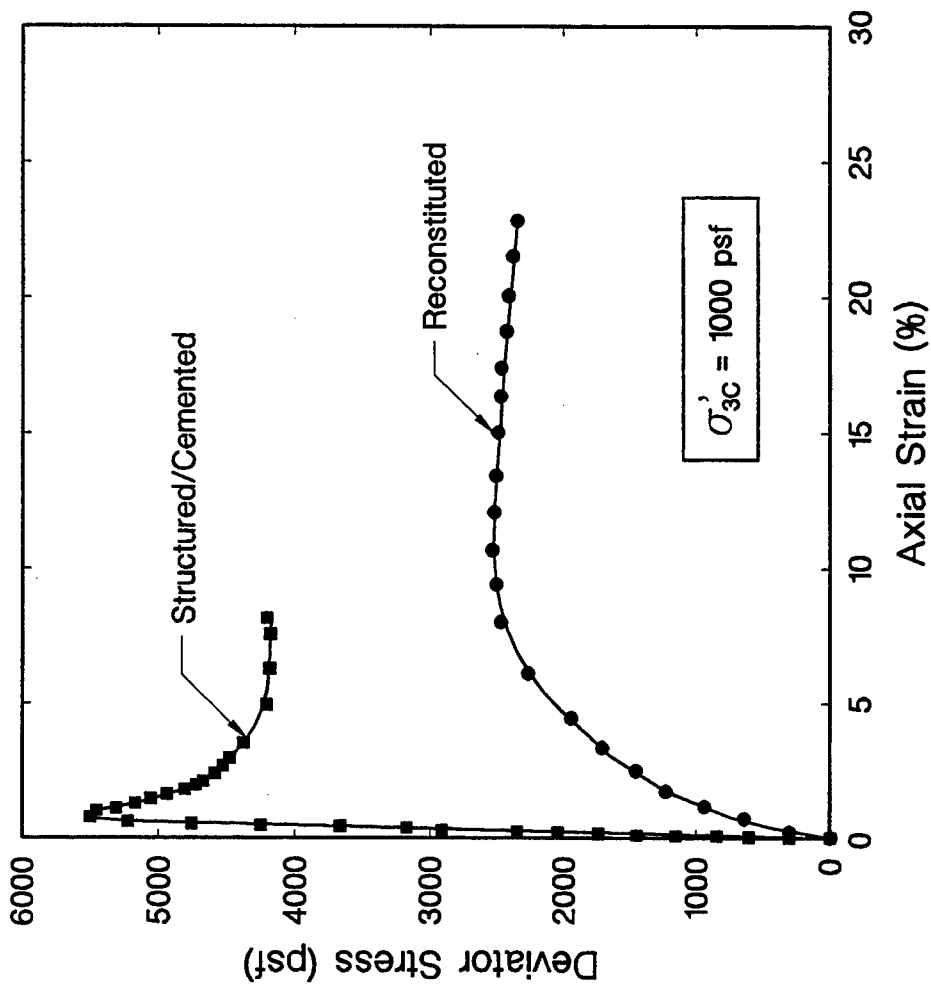


Figure 17. ICD triaxial compression tests on partially saturated structured/cemented and reconstituted silt at an effective confining pressure of 1000 psf.

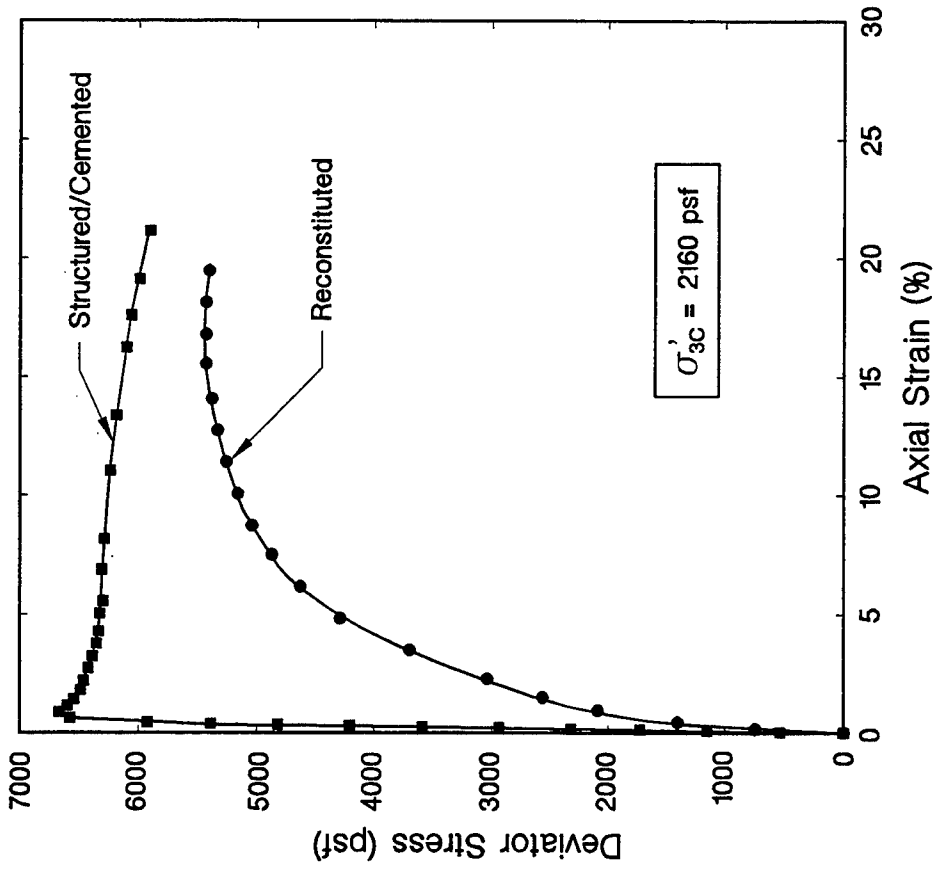


Figure 18. ICD triaxial compression tests on partially saturated structured/cemented and reconstituted silt at an effective confining pressure of 2160 psf.

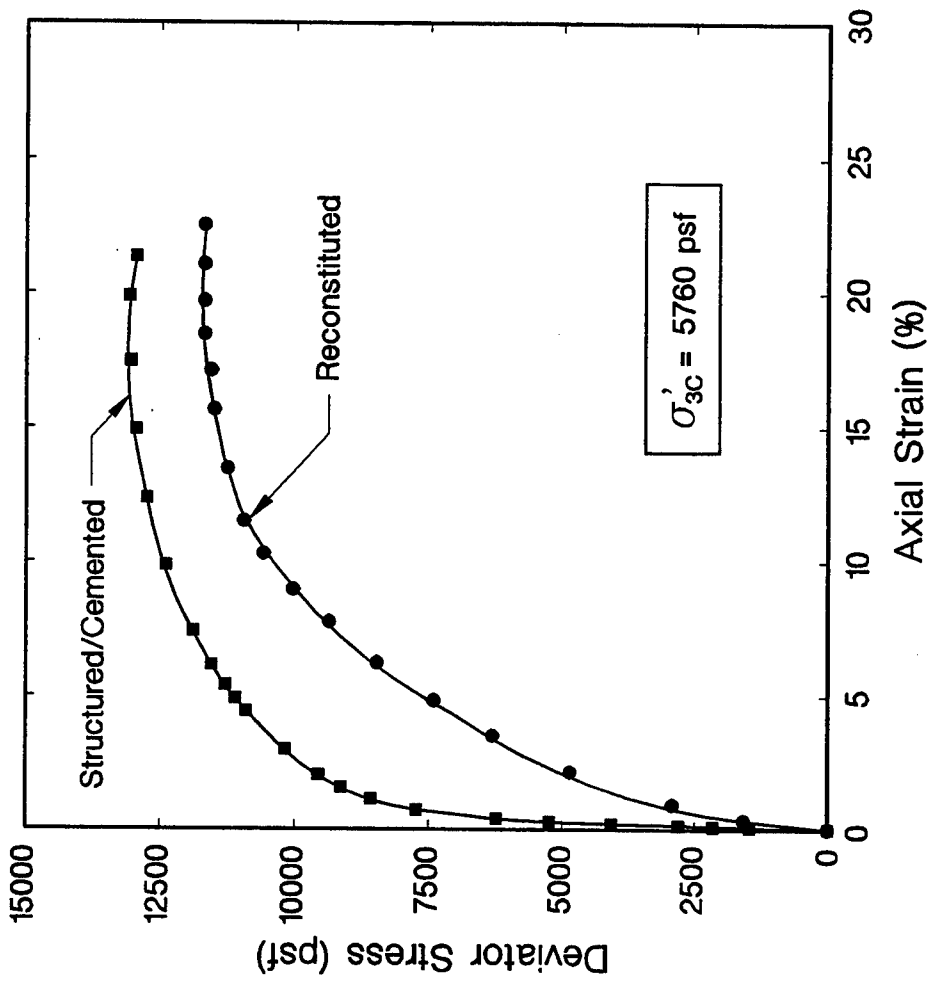


Figure 19. ICD triaxial compression tests on partially saturated structures/cemented and reconstituted silt at an effective confining pressure of 5760 psf.

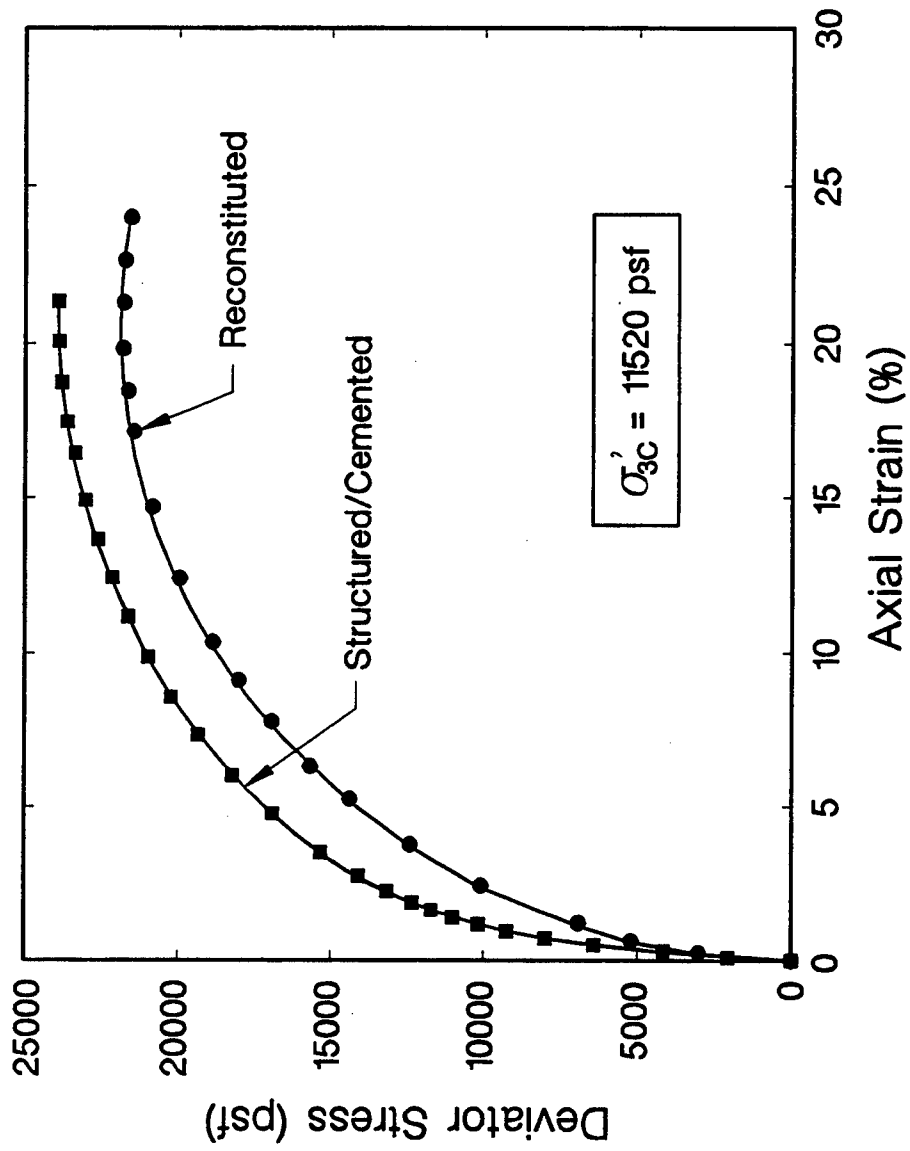


Figure 20. ICD triaxial compression tests on partially saturated structured/cemented and reconstituted silt at an effective confining pressure of 11,520 psf.

occurring silts. For example, if the proposed structure increases the applied stress to a value less than the effective preconsolidation pressure, the undisturbed silt will exhibit high shear strength and stiffness characteristics. If the applied stress exceeds the effective preconsolidation pressure, the undisturbed silt will exhibit shear strength and stiffness characteristics of a reconstituted silt. This may lead to significant settlement and/or stability problems.

Drained Hyperbolic Stress-Strain Parameters

The hyperbolic stress-strain parameters for the structured/cemented and reconstituted silt specimens were obtained using the previously reported Mohr-Coulomb shear strength parameters and the best geometric agreement between measured and hyperbolic stress-strain relationships. The geometric agreement was emphasized at axial strains of less than 5 percent to provide a reasonable estimate of the initial tangent modulus. The hyperbolic stress-strain parameters were obtained using the procedure recommended by Duncan et al. (1980) in which the deviator stresses at 70 and 95 percent of the maximum deviator stress are used to estimate the initial tangent modulus.

Figures 21 through 24 present the geometric agreement between the measured and hyperbolic stress-strain relationships for the structured/cemented silt specimens. The hyperbolic model provides a reasonable representation of the measured deviator stress-strain relationships. Figures 21 and 22 illustrate that the model is not capable of representing a post-peak behavior. Thus, at effective confining pressures too low to overcome the effects of structure/cementation, the model is applicable only to within 10 to 20 percent of peak values. Figures 23 and 24 show that at effective confining pressures great enough to overcome the effects of structure/cementation, the hyperbolic model provides an excellent representation of the measured deviator stress-strain relationship.

Table 9 presents the effective stress Mohr-Coulomb and hyperbolic stress-strain parameters for the partially saturated, structured/cemented silt. The table

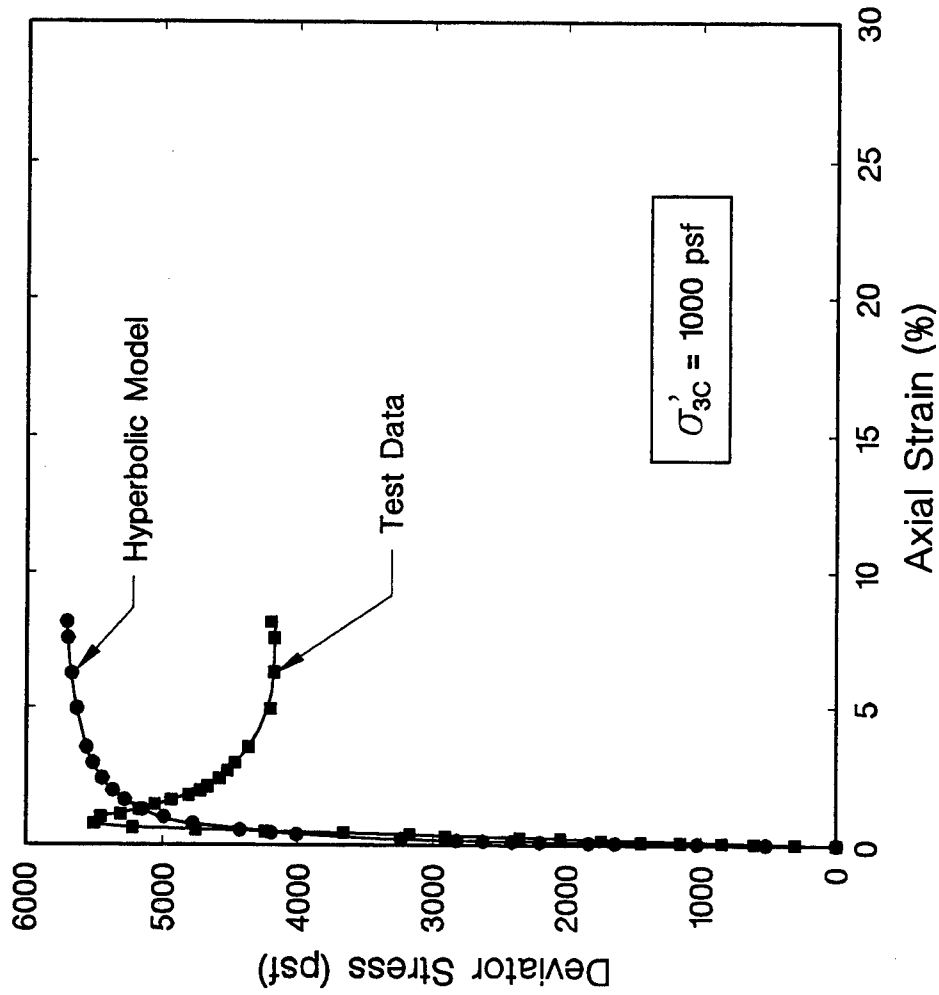


Figure 21. Comparison of measured and hyperbolic stress-strain relationships of partially saturated structured/cemented silt at an effective confining pressure of 1000 psf.

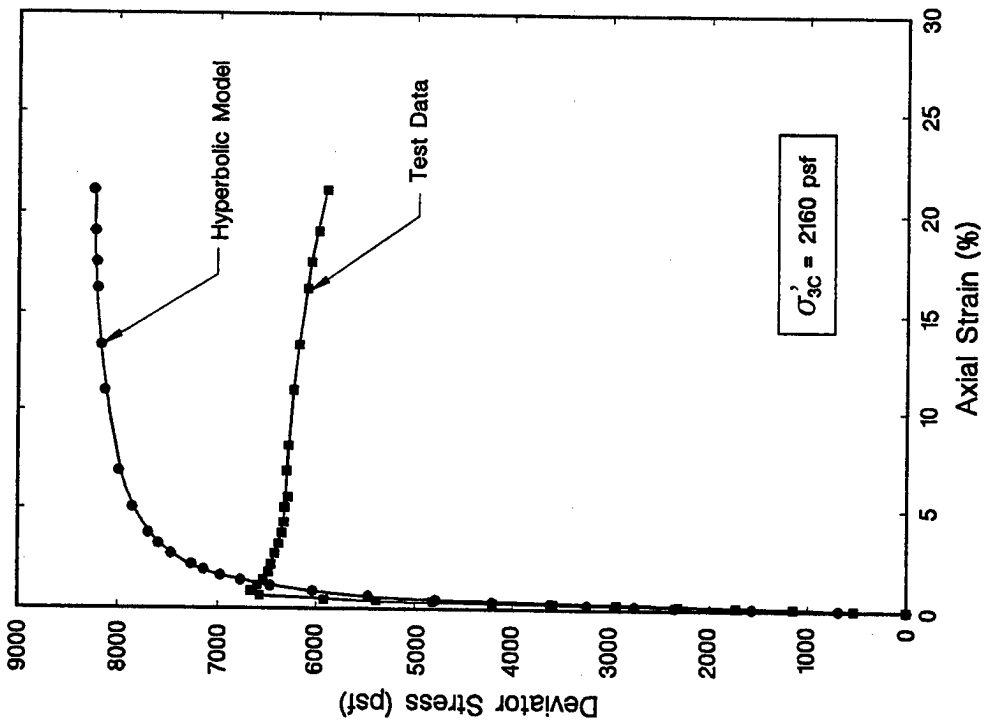


Figure 22. Comparison of measured and hyperbolic stress-strain relationships of partially saturated structured/cemented silt at an effective confining pressure of 2160 psf.

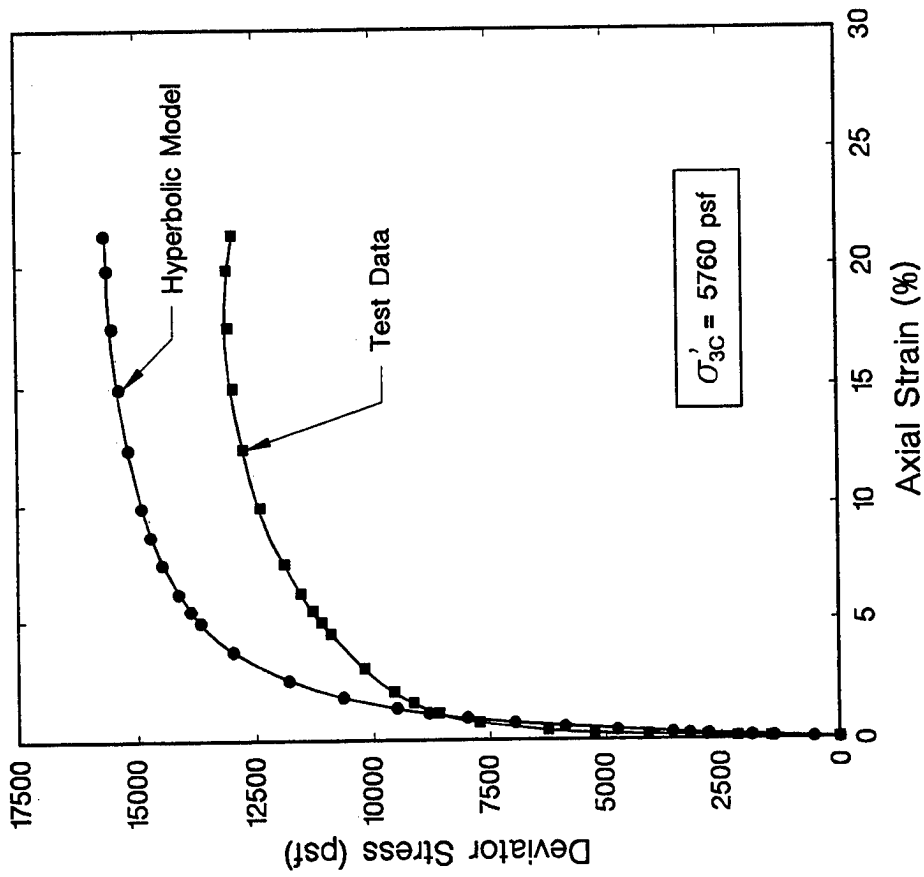


Figure 23. Comparison of measured and hyperbolic stress-strain relationships of partially saturated structured/cemented silt at an effective confining pressure of 5760 psf.

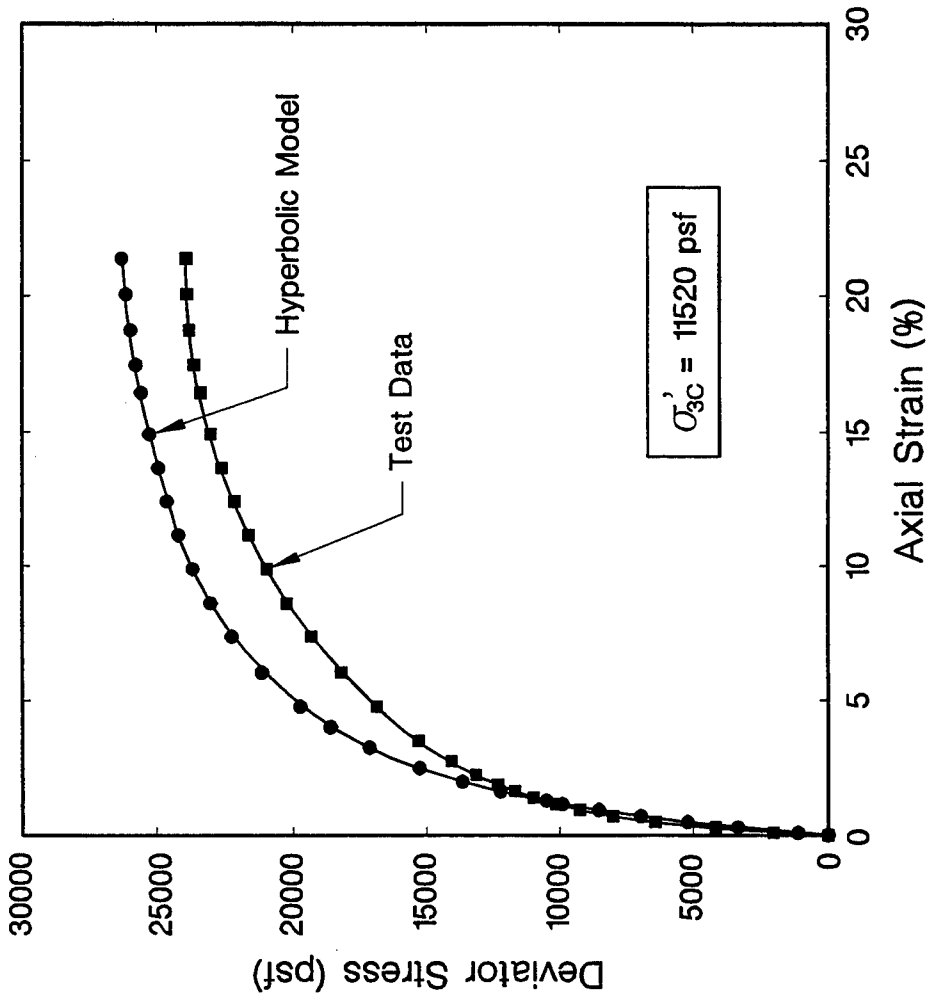


Figure 24. Comparison of measured and hyperbolic stress-strain relationships of partially saturated structured/cemented silt at an effective confining pressure of 11,520 psf.

Table 9
Effective Stress Mohr-Coulomb Shear Strength and Hyperbolic Stress-Strain Parameters for Partially Saturated Structured/Cemented and Reconstituted Silt

Type of Specimen	Average Initial Total Unit Weight (pcf)	Average Initial Water Content (%)	Range of Effective Confining Pressure (tsf)	Effective Stress Cohesion (psf)	Effective Stress Friction Angle (degrees)	Modulus Number K	Modulus Exponent n	Failure Ratio Rf
Structured/Cemented (Field Orientation)	106.4	17.2	0.5 - 5.8	950	28	1200	-0.4	0.85
Reconstituted	113.9	19.9	0.5 - 5.8	0	30	80	0.80	0.85
Structured/Cemented (90 Degrees from Field Orientation)	113.9	19.9	0.5 - 5.8	250	31	305	-0.10	0.95

shows that the modulus exponent is negative. Typically, the modulus exponent is positive, which reflects an increase in stiffness or tangent modulus with increasing effective confining pressure. However, the breaking or removal of the structure/cementation with increasing confining pressure causes a decrease in tangent modulus. This behavior is unique to structured/cemented soils and should be incorporated into design decisions.

Figures 25 through 28 present the geometric agreement between the measured and hyperbolic stress-strain relationships for the partially saturated reconstituted silt. The hyperbolic stress-strain model provides acceptable agreement with the measured deviator stress-axial strain data for the four effective confining stresses. This is attributed to the removal of the structure/cementation during the reconstitution process. Figures 25 through 28 show that the hyperbolic model also cannot represent the small decrease in deviator stress at large axial strains.

The hyperbolic parameters that provided the best geometric agreement for the triaxial compression data at effective confining pressures of 2160 and 5760 psf were initially estimated. These parameters were then varied to provide reasonable agreement with the test data at effective confining pressures of 1000 and 11,520 psf. Therefore, the resulting hyperbolic parameters provide an excellent representation at effective confining pressures between 1000 and 11,520 psf.

Table 9 presents the effective stress Mohr-Coulomb shear strength and hyperbolic stress-strain parameters for the partially saturated reconstituted silt. The hyperbolic stress-strain parameters for the reconstituted silt specimens differ significantly from the parameters for the structured/cemented silt. The modulus number, i.e., stiffness, of the structured/cemented silt is approximately fifteen times higher than that of the reconstituted silt. In addition, the modulus exponent is positive, which indicates that the tangent modulus increases with increasing effective confining pressure.

Anisotropy of Structured/Cemented Silt

Table 9 also presents the effective stress Mohr-Coulomb shear strength and hyperbolic stress-strain parameters for partially saturated, structured/cemented silt that was tested 90 degrees from the field orientation. It can be seen that the nonfield-oriented silt exhibits similar Mohr-Coulomb shear strength parameters as the field-oriented silt. However, the nonfield-oriented silt exhibits significantly lower values of modulus number and exponent. In fact, the modulus number of the field-oriented silt is approximately four times greater than that of the nonfield-oriented silt (Table 9).

The modulus exponent value for the nonfield-oriented silt is -0.10 or nearly zero. Therefore, the stiffness or tangent modulus does not decrease significantly with increasing confining pressure. This means there is a smaller collapse of the structure/cementation in the nonfield orientation. This reinforces the large difference in the modulus numbers, which implies that the structure/ cementation is anisotropic. The anisotropy results in a stiffer behavior in the vertical or field direction. Clearly this anisotropic behavior should be incorporated into design decisions involving structured/cemented silt.

Initial Stiffness from Hyperbolic Stress-Strain Model

Table 10 presents the initial tangent modulus and the tangent modulus at an axial strain of 0.5 percent for the structured/cemented silt tested in the field orientation. The initial tangent is calculated using Equation (1) of the hyperbolic stress-strain model, and the tangent modulus at an axial strain of 0.5 percent is estimated using Equation (4). To estimate the tangent modulus at an axial strain of 0.5 percent, the deviator stress at 0.5 percent axial strain was obtained from the hyperbolic stress-strain curve. The effective stress Mohr-Coulomb shear strength and hyperbolic stress-strain parameters in Table 9 were used in Equations (1) and (4) to estimate these tangent moduli. Table 11 presents the initial tangent modulus and the tangent modulus at an axial strain of 0.5 percent for the partially saturated, reconstituted silt.

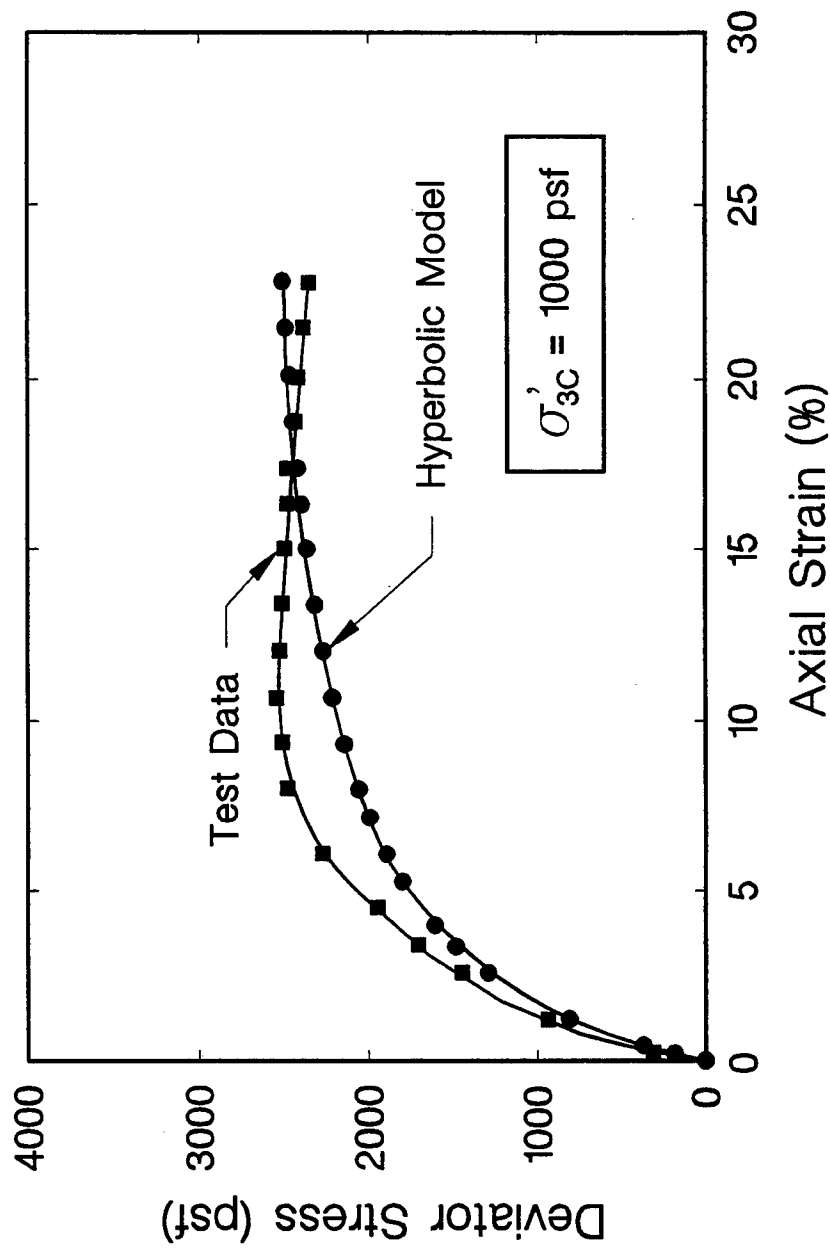


Figure 25. Comparison of measured and hyperbolic stress-strain relationships of partially saturated reconstituted silt at an effective confining pressure of 1000 psf.

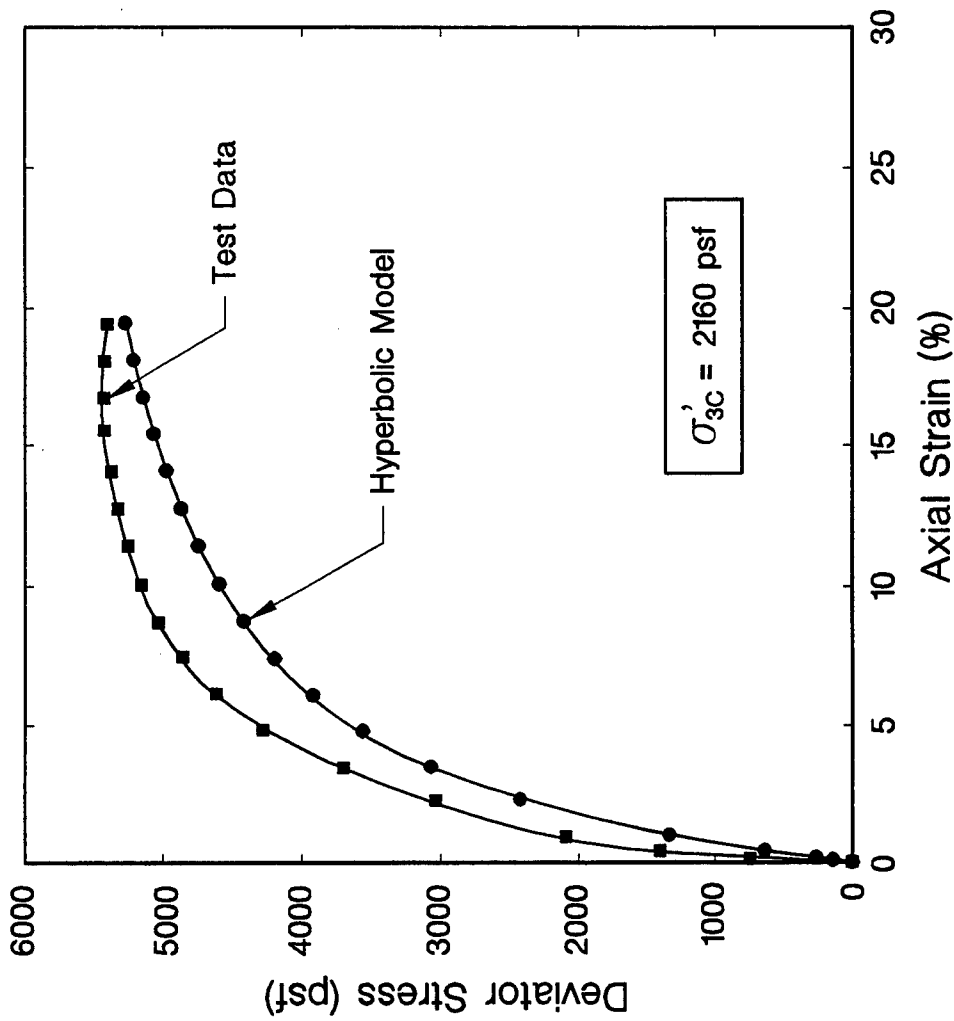


Figure 26. Comparison of measured and hyperbolic stress-strain relationships of partially saturated reconstituted silt at an effective confining pressure of 2160 psf.

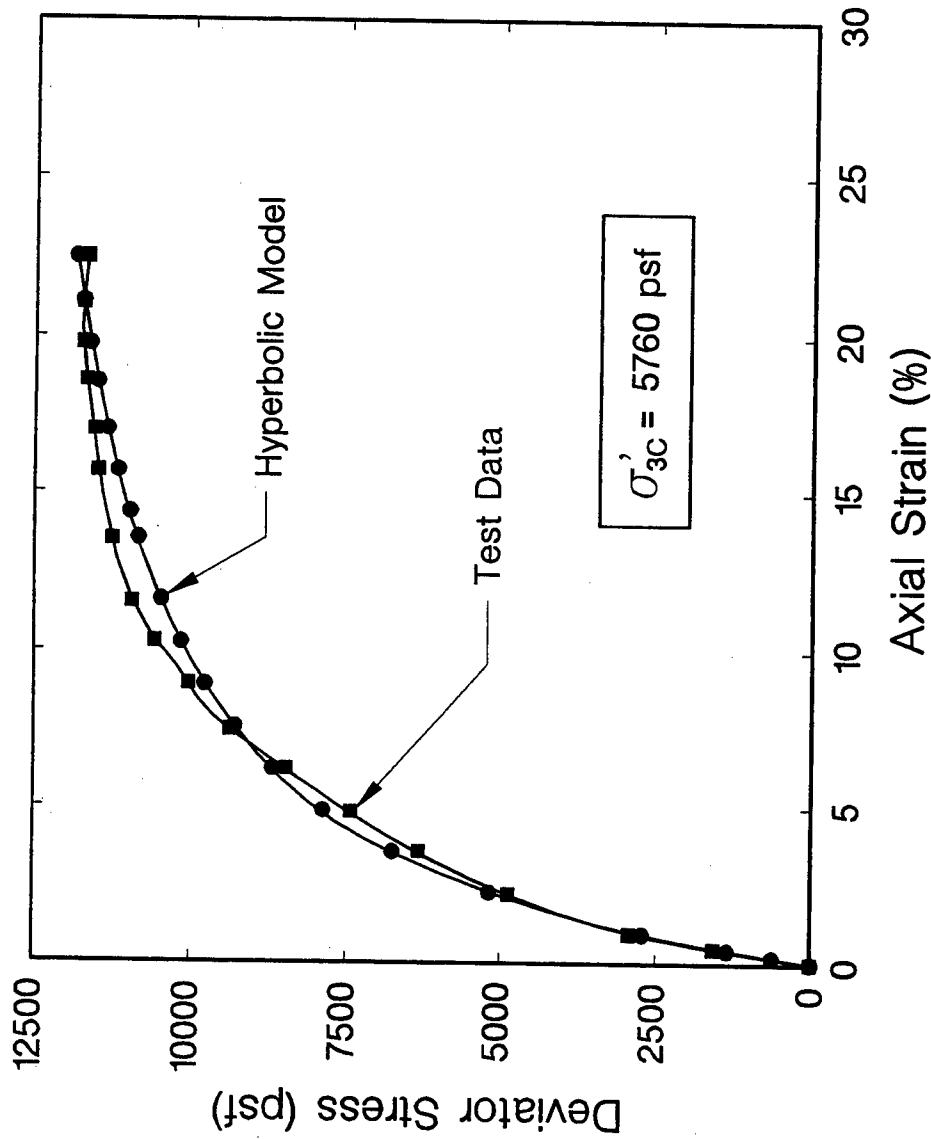


Figure 27. Comparison of measured and hyperbolic stress-strain relationships of partially saturated reconstituted silt at an effective confining pressure of 5760 psf.

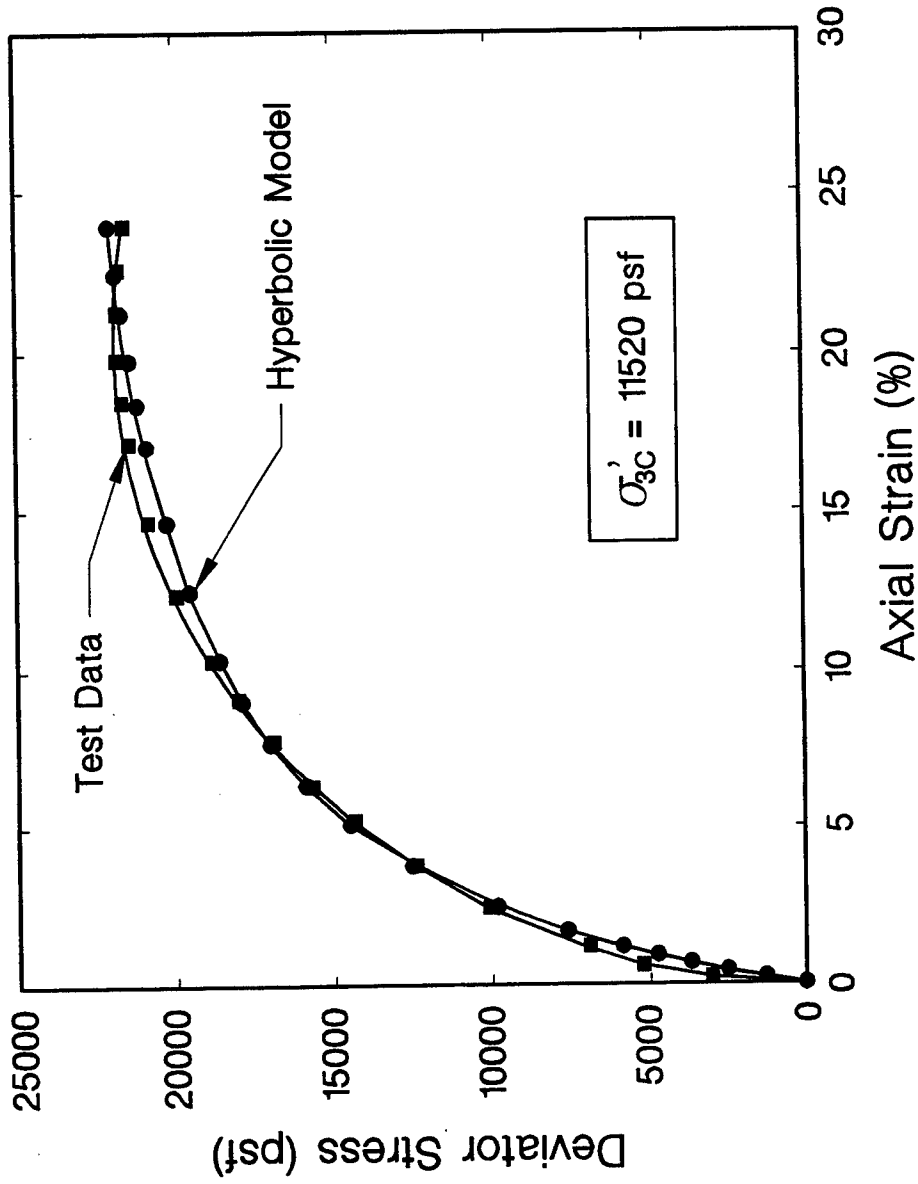


Figure 28. Comparison of measured and hyperbolic stress-strain relationships of partially saturated reconstituted silt at an effective confining pressure of 11,520 psf.

The data in Tables 10 and 11 are used in Figures 29 and 30 to quantify the variation in initial tangent modulus and tangent modulus at 0.5 percent axial strain, respectively, for structured/cemented and reconstituted silt. Figure 29 shows that the initial tangent modulus is significantly higher for the structured/cemented silt at low effective confining pressures. However, as the effective confining pressure increases, the difference in initial tangent modulus decreases. This indicates that at higher confining pressures, the effect of structure/cementation is removed and the soil behavior undergoes a transition towards that of a reconstituted material. Because the preconsolidation pressure of the structured/cemented silt is approximately 20,000 psf, the structured/cemented and reconstituted silt are expected to approach a similar value of initial modulus at confining pressures in excess of 20,000 psf.

The tangent modulus at an axial strain of 0.5 percent increases with increasing effective confining pressure for the structured/cemented and reconstituted silt (Figure 30). The tangent modulus for the structured/cemented silt remains higher than that for the reconstituted silt at confining pressures ranging from 1000 to 11,520 psf.

Appendixes A and B present the deviator stress-strain relationships for each axial test conducted on the partially saturated structured/cemented and reconstituted silt specimens, respectively.

Table 10
Initial Stiffness from Hyperbolic Stress-Strain Model for Structured/Cemented Silt
(Field Orientation)

Effective Confining Pressure (psf)	Range of Effective Preconsolidation Pressure (psf)	Normalized Effective Preconsolidation Pressure	Initial Tangent Modulus (tsf)	Tangent Modulus at Axial Strain of 0.50% (tsf)
1000	20000	20	1714.4	97.4
2160	20000	9.3	1259.9	81.5
5760	20000	3.5	851.0	269.9
11520	20000	1.7	644.9	377.8

Table 11
Initial Stiffness from Hyperbolic Stress-Strain Model for Reconstituted Silt

Effective Confining Pressure (psf)	Range of Effective Preconsolidation Pressure (psf)	Normalized Effective Preconsolidation Pressure	Initial Tangent Modulus (tsf)	Tangent Modulus at Axial Strain of 0.50% (tsf)
1000	8000	8.0	46.5	26.9
2160	8000	3.7	86.1	43.1
5760	8000	1.4	188.6	140.5
11520	8000	1.0*	328.4	224.8

NOTE:

* Normally consolidated at confining pressure of 11,520 psf

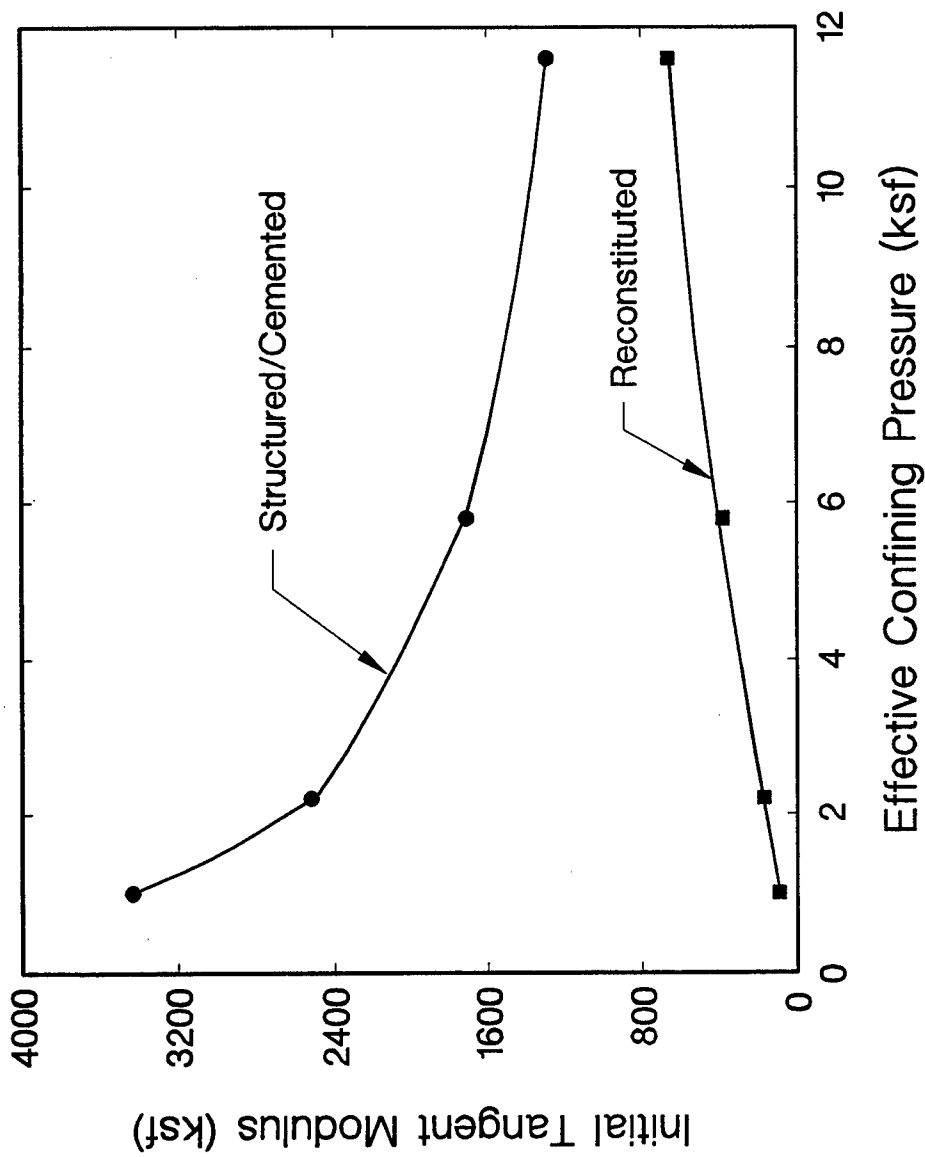


Figure 29. Variation in initial tangent modulus for partially saturated structured/cemented and reconstituted silt.

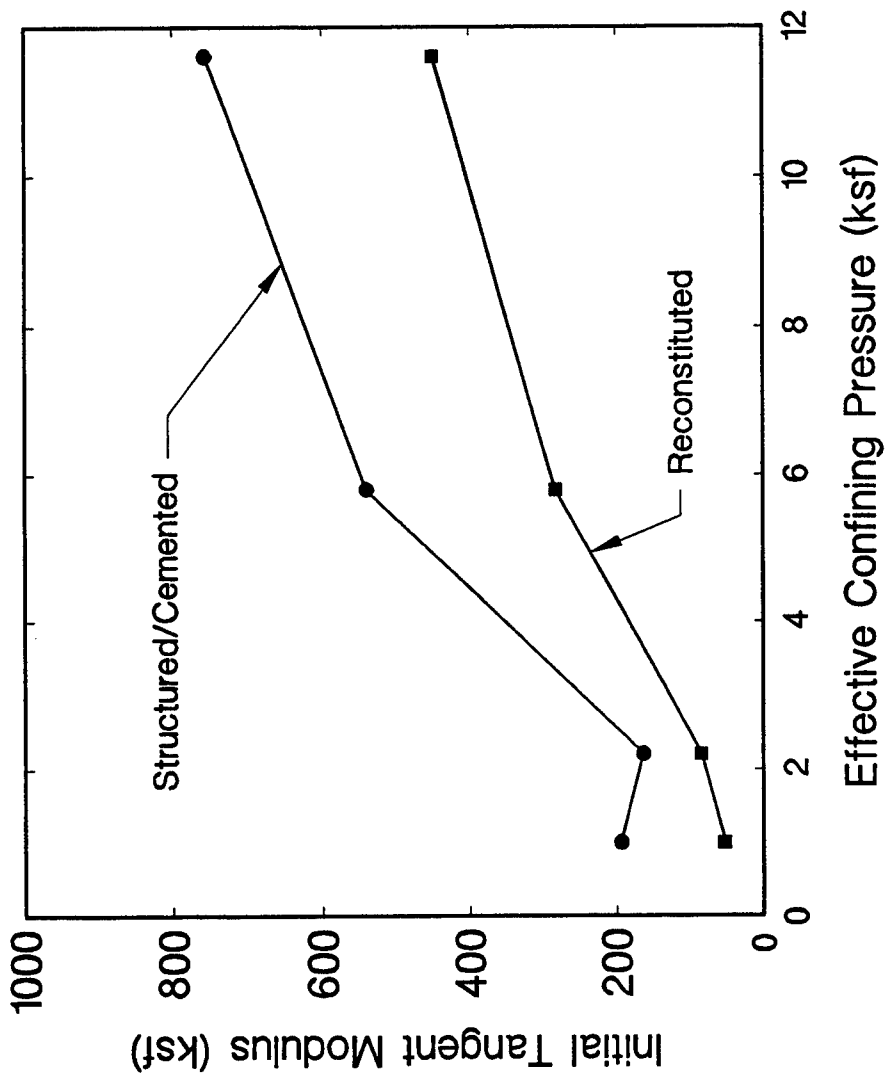


Figure 30. Variation in tangent modulus at an axial strain of 0.5 percent for partially saturated structured/cemented and reconstituted silt.

8 ICD Triaxial Compression Tests on Saturated Specimens

Laboratory Saturation of Silt Specimens

Silt specimens were saturated to investigate the effect of laboratory saturation on the stress-strain behavior of structured/cemented silt. In addition, saturation of the specimens allowed volume change information to be obtained. The laboratory saturation technique, referred to as hydrostatic saturation, involved percolating distilled-deaired water through the specimen under a hydraulic head of 1 ft, or 62.4 psf, for a period of 24 hr. A confining pressure of 500 psf was applied to the specimen prior to the percolation/saturation process.

Hydrostatic Saturation of Structured/Cemented Silt Specimens

Four and three isotropically consolidated-drained triaxial compression tests were conducted on structured/cemented and reconstituted silt specimens, respectively, after hydrostatic saturation. These test results illustrate the effect of hydrostatic saturation on the structure/cementation of naturally occurring silts. Figure 31 presents the deviator stress-axial strain relationships from the ICD triaxial compression tests on structured/cemented silt. The specimens were trimmed in such a manner that the tests were conducted in the same orientation as the field. The effective confining pressure ranged from 1000 to 11,520 psf. The deviator stress at an axial strain of approximately 20 percent increased with increasing effective confining pressure. The Mohr-Coulomb shear strength parameters were estimated using either the peak deviator stress or the deviator stress at an axial strain of 20 percent. The resulting effective stress cohesion and friction angle are 0 psf and 33 deg, respectively. These parameters result in a lower shear strength than the effective stress cohesion (950 psf) and friction angle (28 deg) measured using partially saturated structured/cemented silt (Table

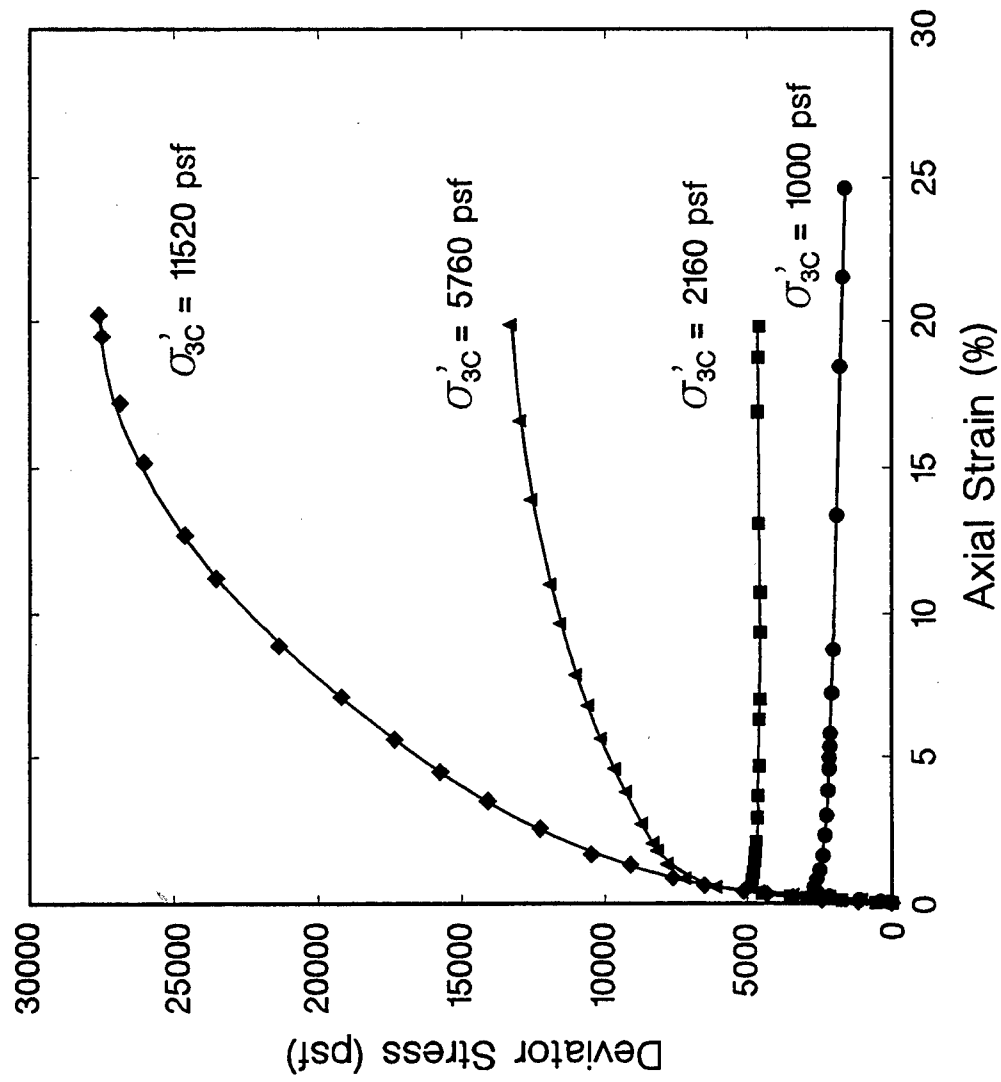


Figure 31. Stress-strain relationships from ICD triaxial compression tests on hydrostatically saturated structured/cemented silt.

9). For example, at a normal stress of 4000 psf, the partially saturated silt exhibited a shear strength of 3080 psf, while the saturated silt exhibited a shear strength of 2600 psf based on the reported Mohr-Coulomb shear strength parameters. Therefore, laboratory hydrostatic saturation using distilled-deaired water appears to reduce the drained shear strength of the structured/cemented silt by approximately 15 percent.

This finding provides insight to the importance of the various cementation mechanisms in Mississippi loess. The two major cementation mechanisms appear to be carbonate and clay/capillary effects. Since the partially saturated and saturated triaxial specimens generally yield similar shear strength and compressibility (Chapter 5) parameters, it was concluded that the carbonate cementation is resistant to distilled water and is a stronger cementing agent than the clay/capillary effects. The increase in moisture content from approximately 18 to 26 percent during laboratory saturation undoubtedly reduced the effect of the clay/capillary bonding. Since the shear strength after laboratory saturation is similar to the shear strength of the loess at the natural water content, the importance of the clay/capillary bonding is assumed to be small. Therefore, the difference between the shear strength of laboratory saturated reconstituted and structured/cemented specimens is attributed to carbonate cementation.

The Mississippi loess tested during this investigation contains 33 percent carbonates and 15 percent clay minerals. The large percentage of carbonate is expected because the block samples were obtained from a depth of approximately 25 ft in the exposed bluff. Krinitzsky and Turnbull (1967) showed that the Vicksburg loess is calcareous if the carbonate has not been removed by weathering. They concluded that weathering and moisture infiltration remove the carbonates in the upper 5 to 6 ft. It should be noted that natural precipitation is chemically different from distilled water and may adversely affect the structure/cementation.

In summary, the block samples obtained for this study were below the depth of weathering, and the weathered material on the exposed slope was removed prior to sampling. Therefore, a large percentage of carbonates was present in the block samples. The numerous concretions found in the loess during trimming of the specimens, the measured 33 percent of carbonate in the loess,

and scanning electron microscope analyses (Figures 4-7) confirm the presence of carbonate bonding.

Krinitzsky and Turnbull (1967) showed that infiltration of rainwater and weathering can remove the carbonate bonding. Therefore, site-specific testing of loess should be conducted to evaluate the permanence of the carbonate cementation under site-specific infiltration/inundation conditions. For example, the effect of reservoir inundation caused by construction of a lock and dam structure on the carbonate bonding should be investigated.

Hydrostatic Saturation of Reconstituted Specimens

Figure 32 presents the deviator stress-axial strain relationships from the three ICD triaxial compression tests on hydrostatically saturated, reconstituted specimens. This figure shows that the deviator stress at an axial strain of approximately 20 percent slightly increases with increasing effective confining pressure. The Mohr-Coulomb shear strength parameters were estimated using the deviator stress at an axial strain of 20 percent. The resulting effective stress cohesion and friction angle are 0 psf and 31 deg, respectively. These parameters are also similar to the effective stress cohesion (0 psf) and friction angle (30 deg) measured using partially saturated reconstituted silt (Table 9). As expected, the hydrostatic saturation does not appear to significantly alter the shear strength of reconstituted silt because the structure/cementation was removed during the reconstitution process.

It is also important to compare the Mohr-Coulomb shear strength parameters of the hydrostatically saturated, structured/cemented and reconstituted specimens. The saturated structured/cemented silt exhibited an effective stress cohesion and friction angle of 0 psf and 33 deg, respectively. The reconstituted silt yielded an effective stress cohesion and friction angle of 0 psf and 31 deg, respectively. Therefore, the structure/cementation was not significantly affected by the laboratory saturation with distilled water, and thus the structured/cemented silt exhibits higher shear strength parameters.

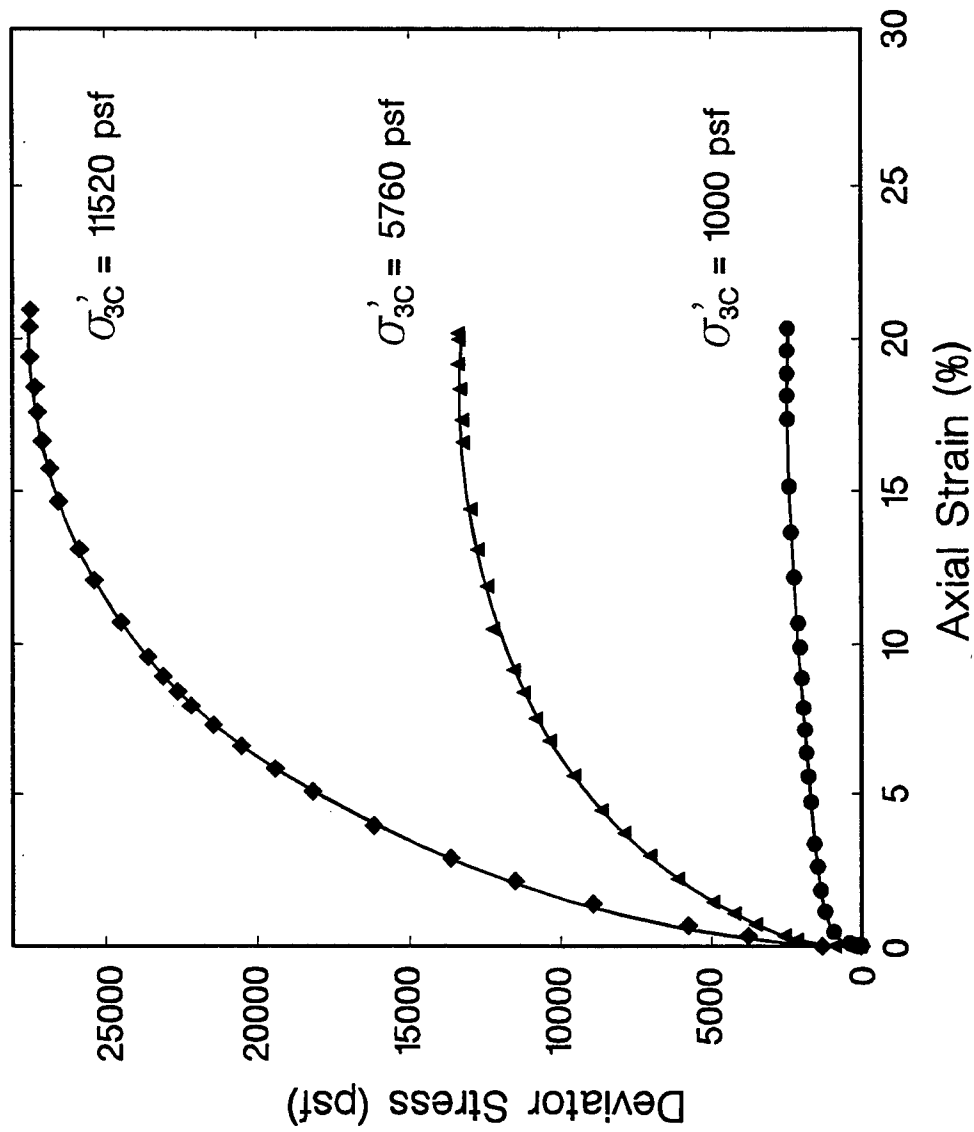


Figure 32. Stress-strain relationships from ICD triaxial compression tests on hydrostatically saturated reconstituted silt.

Table 12
Effective Stress Mohr-Coulomb Shear Strength and Hyperbolic Stress-Strain Parameters for Laboratory Saturated
Structured/Cemented and Reconstituted Silt

Type of Specimen	Type of Laboratory Saturation	Average Initial Total Weight (pcf)	Average Initial/Final Water Content (%)	Range of Effective Confining Pressure (tsf)	Effective Stress Cohesion (psf)	Effective Stress Friction Angle (degrees)	Modulus Number K	Modulus Exponent n	Failure Ratio Rf
Structured/Cemented (Field Orientation)	Hydrostatic	106.5	17.3/27.5	0.5-5.8	0	33	850	-0.55	0.85
Reconstituted	Hydrostatic	109.2	19.6/25.4	0.5 - 5.8	0	31	95	0.80	0.85
Structured/Cemented (90 Degrees from Field Orientation)	Hydrostatic	113.9	18.2/26.0	0.5 - 5.8	250	31	305	-0.10	0.95

In summary, the hydrostatic saturation in the laboratory did not significantly alter the Mohr-Coulomb shear strength parameters of the structured/cemented silt. Therefore, it appears that the naturally occurring structure/cementation, primarily carbonate bonding, is not soluble in the presence of distilled water. The oedometer test results discussed previously reinforce this conclusion.

Drained Hyperbolic Stress-Strain Parameters of Saturated Silt

The hyperbolic stress-strain parameters for the saturated structured/cemented and reconstituted silt specimens were obtained using the previously reported Mohr-Coulomb shear strengths parameters and the best geometric agreement between measured and hyperbolic stress-strain relationships. The geometric agreement was emphasized at axial strains of less than 5 percent to provide a reasonable estimate of the initial tangent modulus. The hyperbolic stress-strain model provides a reasonable representation of the measured deviator stress relationship for the saturated structured/cemented and reconstituted silt.

Table 12 presents the effective stress Mohr-Coulomb and hyperbolic stress-strain parameters for the hydrostatically-saturated, structured/cemented silt. Table 12 shows that the modulus exponent is negative. Typically, the exponent is positive, which reflects an increase in stiffness or tangent modulus with increasing effective confining pressure. However, the degradation of the structure/cementation with increasing confining pressure causes a decrease in tangent modulus. This behavior is unique to structured/cemented soils and should be incorporated into design decisions.

Table 12 also presents the Mohr-Coulomb and hyperbolic stress-strain parameters for the hydrostatically-saturated, reconstituted silt. The hyperbolic stress-strain parameters for the reconstituted silt specimens differ from the parameters for the structured/cemented silt. The modulus number of the structured/cemented silt is approximately nine times greater than the modulus number of the reconstituted silt. This indicates that the structured/cemented silt is significantly stiffer than the reconstituted silt. In addition, the modulus

exponent of the reconstituted silt is positive and approximately one and one-half times higher than the modulus exponent of the hydrostatically-saturated, structured/cemented silt specimens. This indicates that the tangent modulus increases with increasing effective confining pressure. Therefore, there is no degradation of the structure/cementation with increasing confining pressure in the reconstituted specimens. The observed trends in modulus number and modulus exponent between reconstituted and structured/cemented silt specimens are expected because the structure/cementation was destroyed during the reconstitution process.

Anisotropy of Saturated Structured/Cemented Silt

The effective stress Mohr-Coulomb shear strength and hyperbolic stress-strain parameters for laboratory saturated, structured/cemented silt that was tested 90 deg from the field orientation are presented in Table 12. The nonfield-oriented silt exhibits similar shear strength parameters as the field oriented silt. However, the nonfield-oriented silt again exhibits significantly lower values of modulus number and exponent. The modulus number of the field-oriented silt is approximately three times greater than the nonfield-oriented silt (Table 12).

The modulus exponent value for the nonfield-oriented silt is again -0.10 or near zero. This means there is a smaller collapse of the structure/cementation in the nonfield orientation than in the field orientation even after laboratory saturation. Therefore, the anisotropy observed in the partially saturated, structured/cemented silt appears to be not significantly changed by laboratory saturation.

Hyperbolic Volume Change Parameters

Table 13 presents the volume change parameters for the laboratory saturated, structured/cemented and reconstituted silt specimens. The hyperbolic stress-strain model did not provide an excellent representation of the volumetric strain relationship for the structured/cemented silt specimens. This is attributed to the

structured-cemented silt exhibiting dilation during shear and the inability of the hyperbolic model to represent specimen expansion. The volume change parameters shown in Table 13 were obtained using the best geometric agreement between measured and hyperbolic stress-strain relationships at low axial strains, i.e., before the specimen exhibited dilation. In contrast to the results of the structured/cemented specimens, the hyperbolic stress-strain model provided a reasonable representation of the volumetric strain relationship for the reconstituted specimens. The reconstituted specimens exhibited no dilation during shearing, which can be attributed to the absence of structure/cementation in the reconstituted specimens.

Table 13 also presents the hyperbolic volume change parameters for the nonfield-oriented, structured/cemented silt. The bulk modulus exponents are similar between the field- and nonfield-oriented specimens. However, the modulus number of the field-oriented silt is approximately six times greater than the nonfield-oriented silt (Table 13). This is a greater difference than observed between the modulus numbers (Table 12).

Figures in Appendixes C and D present the deviator stress and volumetric strain relationships for each test conducted on the laboratory saturated structured/cemented and reconstituted silt specimens, respectively. Also shown in these figures is the volumetric strain relationship predicted by the hyperbolic stress-strain model and the parameters presented in Table 13. As expected, the structured/cemented silt specimens exhibited a negative bulk modulus exponent, and the reconstituted specimens exhibited a positive exponent (Table 13). In addition, the bulk modulus number of the structured/cemented silt is approximately thirteen times greater than that for the reconstituted silt.

Table 13
Effective Stress Mohr-Coulomb Shear Strength and Hyperbolic Volume Change Parameters for Laboratory Saturated Structured/Cemented and Reconstituted Silt

Type of Specimen	Type of Laboratory Saturation	Average Initial Total Weight (pcf)	Average Initial/Final Water Content (%)	Range of Effective Confining Pressure (tsf)	Effective Stress Cohesion (psf)	Effective Stress Friction Angle (degrees)	Bulk Modulus Number K_b	Bulk Modulus Exponent m
Structured/Cemented (Field Orientation)	Hydrostatic	106.5	17.3/27.5	0.5 - 5.8	0	33	310	-0.60
	Reconstituted	109.2	19.6/25.4	0.5 - 5.8	0	31	24	0.57
Structured/Cemented (90 Degrees from Field Orientation)	Hydrostatic	113.9	18.2/26.0	0.5 - 5.8	250	31	50	-0.40

9 ICD UNLOAD/RELOAD TRIAxIAL TESTS ON PARTIALLY SATURATED SPECIMENS

Unload/Reload Parameters

As noted previously, the unload/reload modulus is related to the effective confining pressure by the unload/reload number and the modulus exponent (Equation 8). The stress-strain relationship followed during unloading is steeper than the relationship followed during primary loading, as shown in Figure 2. The resulting hysteretic behavior clearly illustrates the inelastic behavior of soils. The same value of unload/reload modulus is used for both unloading and reloading.

Four unload/reload triaxial compression tests were conducted to estimate the unload/reload modulus of structured/cemented silt and the effect of unloading/reloading on the degradation of the structure/cementation of silt. The tests were conducted on partially saturated structured/cemented silt, i.e., silt at the natural water content.

In the unload/reload triaxial tests, a partially saturated structured/cemented specimen was loaded to approximately 50 percent of the maximum deviator stress measured in a previous test at the same confining pressure (Figure 15). The specimen was loaded to 50 percent of the maximum deviator stress using the same axial displacement rate of 0.2 mm/minute or axial strain rate of 1.7 percent/minute. After reaching 50 percent of the maximum deviator stress, the specimen was unloaded to a deviator stress of zero using an axial displacement rate of 0.2 mm/minute. The specimen was then reloaded to 50 percent of the maximum deviator stress and unloaded. This was repeated until the specimen had been subjected to four unload/reload cycles. After the last unloading, the specimen was reloaded to failure or an axial strain of 20 percent. Figures 33

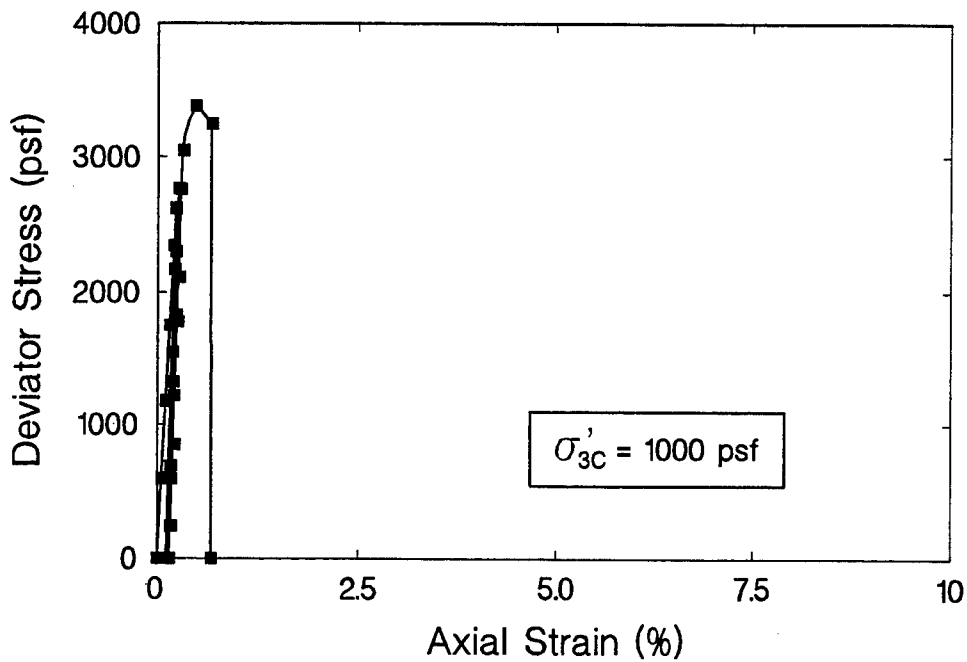
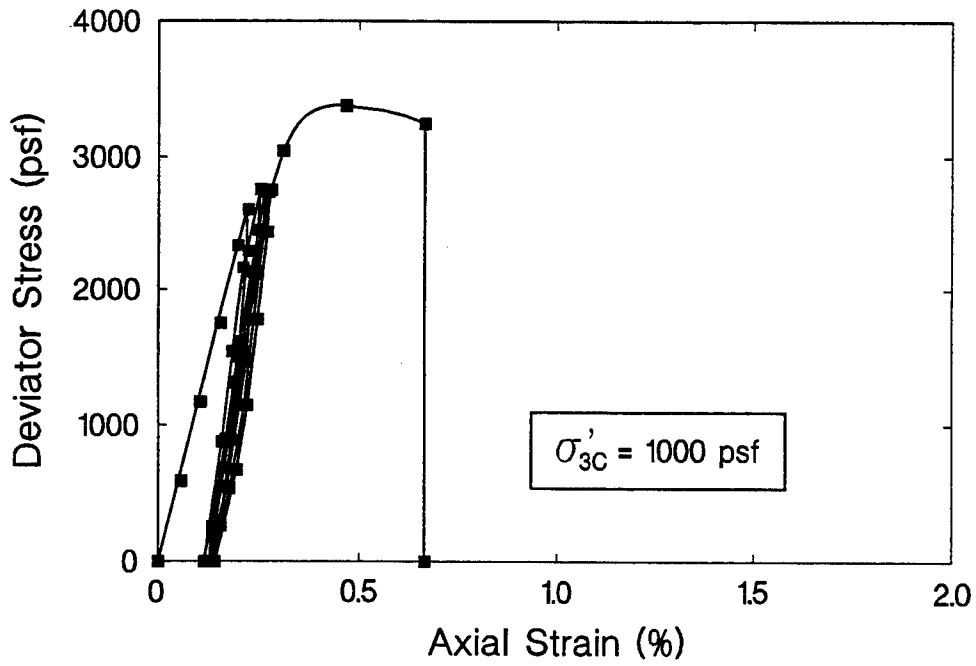


Figure 33. Results of ICD triaxial unload/reload test on partially saturated structured/cemented silt at an effective confining pressure of 1000 psf.

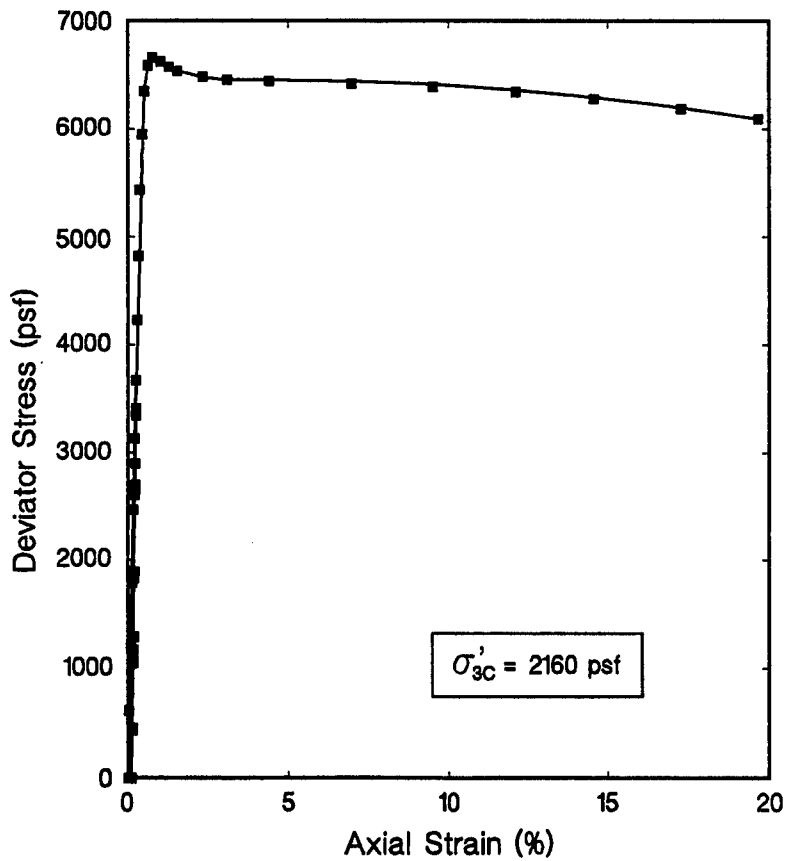
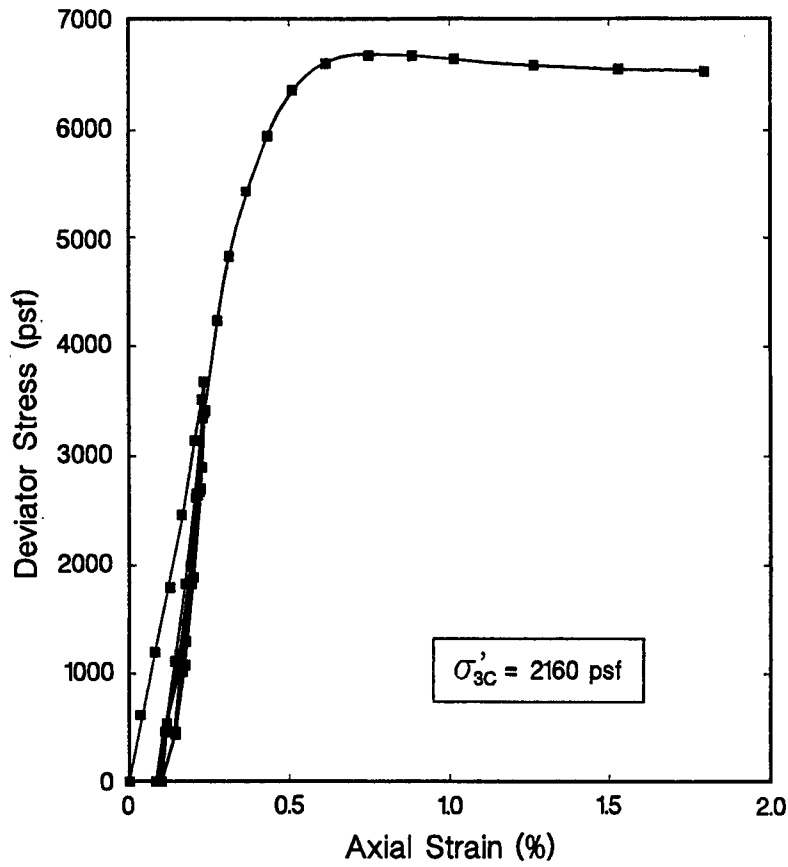


Figure 34. Results of ICD triaxial unload/reload test on partially saturated structures/cemented silt at an effective confining pressure of 2160 psf.

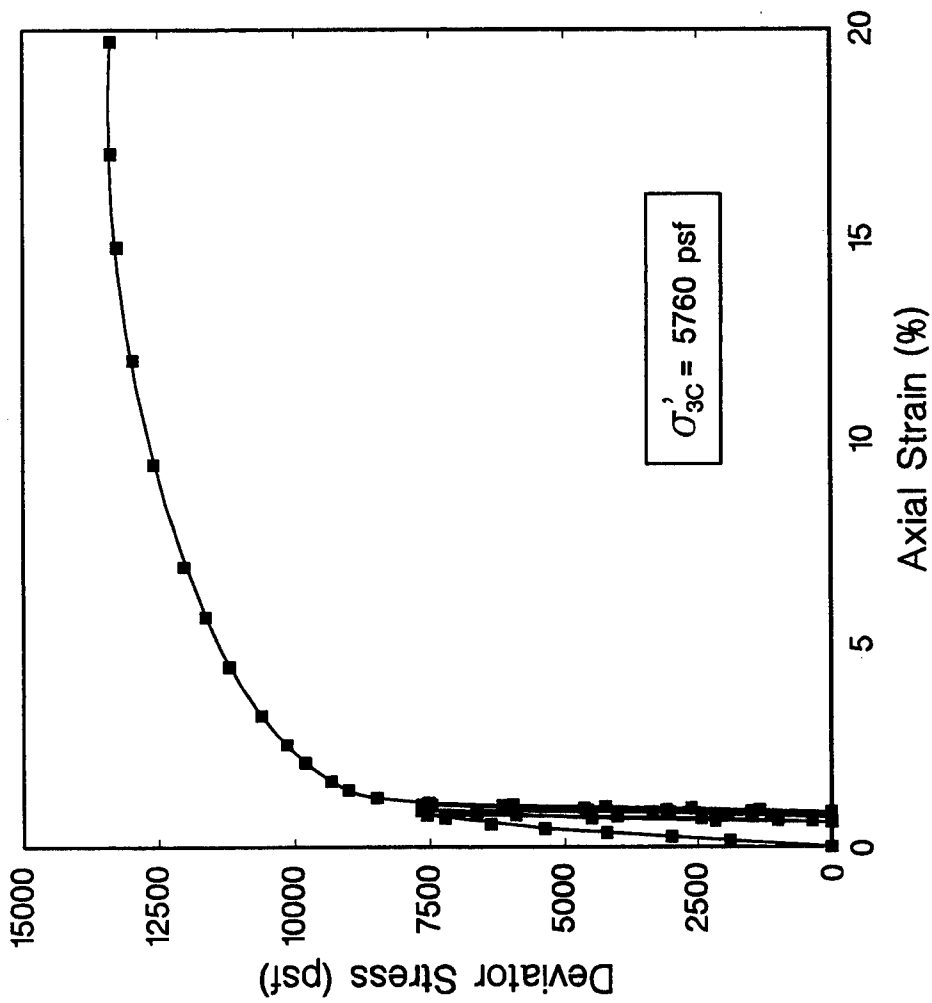


Figure 35. Results of ICD triaxial unload/reload test on partially saturated structured/cemented silt at an effective confining pressure 5760 psf.

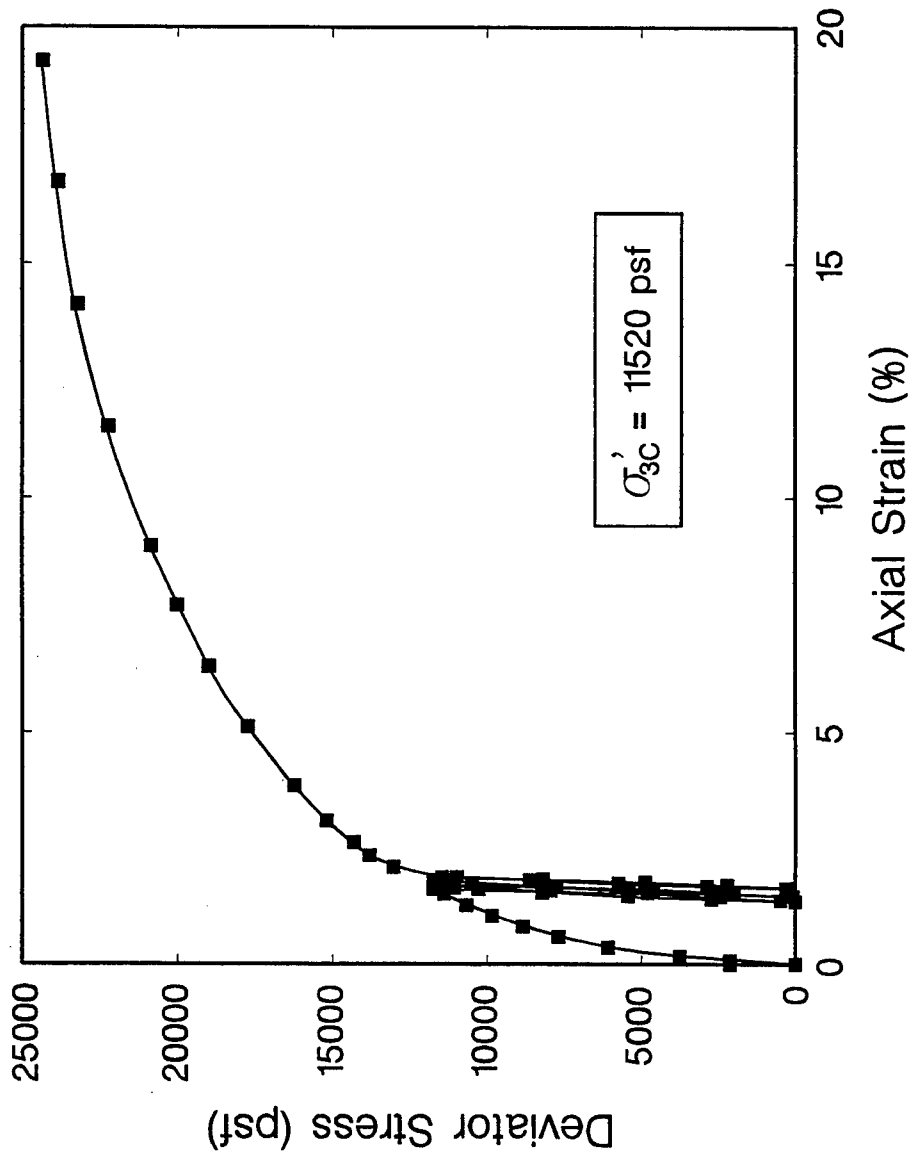


Figure 36. Results of ICD triaxial unload/reload test on partially saturated structured/cemented silt at an effective confining pressure of 11,520 psf.

through 36 present the deviator stress-axial strain relationships from the ICD unload/reload triaxial compression tests for effective confining pressures of 1000, 2160, 5760, and 11,520 psf, respectively. It should be noted that the upper graphs in Figures 33 and 34 represent an enlargement of the data during the unload/reload cycles. This enlargement was accomplished by plotting the data for only axial strain less than 2 percent.

Figure 33 presents results of the ICD unload/reload triaxial test at an effective confining pressure of 1000 psf. The specimen collapsed unexpectedly upon loading to failure after the unload/reload cycles. The specimen collapsed after application of a deviator stress of approximately 750 psf after the reload cycles. Figure 34 shows that the structured/cemented specimen at an effective confining pressure of 2160 psf was loaded to failure without collapsing. Therefore, it appears that the structure/cementation is more susceptible to collapse at low confining pressures. This may explain the shallow (low confining pressure) failures that occur rapidly in the natural loess bluffs near Vicksburg.

The Mohr-Coulomb shear strength parameters were estimated for effective confining pressures ranging from 1000 to 11,520 psf and either the maximum deviator stress or an axial strain of 20 percent. The resulting effective stress cohesion (c') and friction angle (ϕ') are 700 psf and 29 degrees, respectively. The corresponding effective stress cohesion (c') and friction angle (ϕ') measured in conventional ICD triaxial compression tests on partially saturated structured/cemented silt (Table 9) are 950 psf and 28 degrees, respectively. Though the friction angles are similar, the value of effective stress cohesion measured in unload/reload tests (700 psf) is slightly less than the cohesion (950 psf) measured in conventional ICD triaxial compression tests on partially saturated structured/cemented silt. Therefore, the unloading/reloading of the specimen may have broken or ruptured some of the structure/cementation in the silt. All of the structure/cementation was not removed during the four unload/reload cycles because the resulting effective stress cohesion is greater than the effective stress cohesion ($c' = 0$ psf) measured for the partially saturated reconstituted specimens (Table 9). However, more than four

unload/reload cycles and/or unload/reload cycles with a deviator stress greater than 50 percent of the maximum deviator stress may result in additional breakage or rupture of the structure/cementation in the loess.

Figures 37 and 38 present a comparison of the deviator stress-axial strain relationships for unload/reload and conventional ICD triaxial compression tests at effective confining stresses of 1000 and 2160 psf, respectively. At a confining stress of 1000 psf, the unload/reload cycles resulted in a peak deviator stress approximately 50 percent lower than that resulting from the ICD triaxial compression test (Figure 37). At a confining stress of 2160 psf, the unload/reload cycles did not significantly reduce the peak deviator stress (Figure 38). In summary, it appears that unload/reload cycles are more detrimental at lower confining stresses.

The unload/reload modulus number was estimated using the hysteresis loops in Figures 33 through 36. The value of E_{ur} was estimated from the unload/reload curves of each test, as in Figure 2. The variation of E_{ur} is linear when the logarithm of (E_{ur}/p_a) and the logarithm (σ'_3/p_a) are plotted against each other. The unload/reload modulus number equals (E_{ur}/p_a) when σ'_3/p_a equals unity and the unload/reload modulus exponent, n_{ur} , is the slope of the resulting line. Using this methodology, values of K_{ur} and n_{ur} of 1175 and 0.3, respectively, were estimated from the unload/reload data in Figures 33 through 36. The value of K_{ur} is approximately equal to the primary loading modulus number (1200) of the partially saturated structured/cemented silt (Table 9). This ratio of K_{ur}/K is slightly less than the recommended range of 1.2 to 3 times suggested by Duncan et al. (1980). The difference is attributed to different soil behavior during unload/reload cycles of structured/cemented soils.

Duncan et al. (1980) suggest that the value of n_{ur} is similar to n , which is the modulus exponent for primary loading for nonstructured soils. In fact, it is assumed in the hyperbolic model that n equals n_{ur} . If the unload/reload data in Figures 33 through 36 and n equal to -0.4 (Table 9) are used, the corresponding value of K_{ur} is 1180. In summary, the values of K_{ur} are similar, whereas the values of modulus exponent differ significantly. Because the difference is attributed to the structured/cemented nature of the silt, the conclusion that n equals n_{ur} appears unwarranted for structured/cemented soils. As a result, it is recommended that at least one unload/reload test be conducted to estimate the

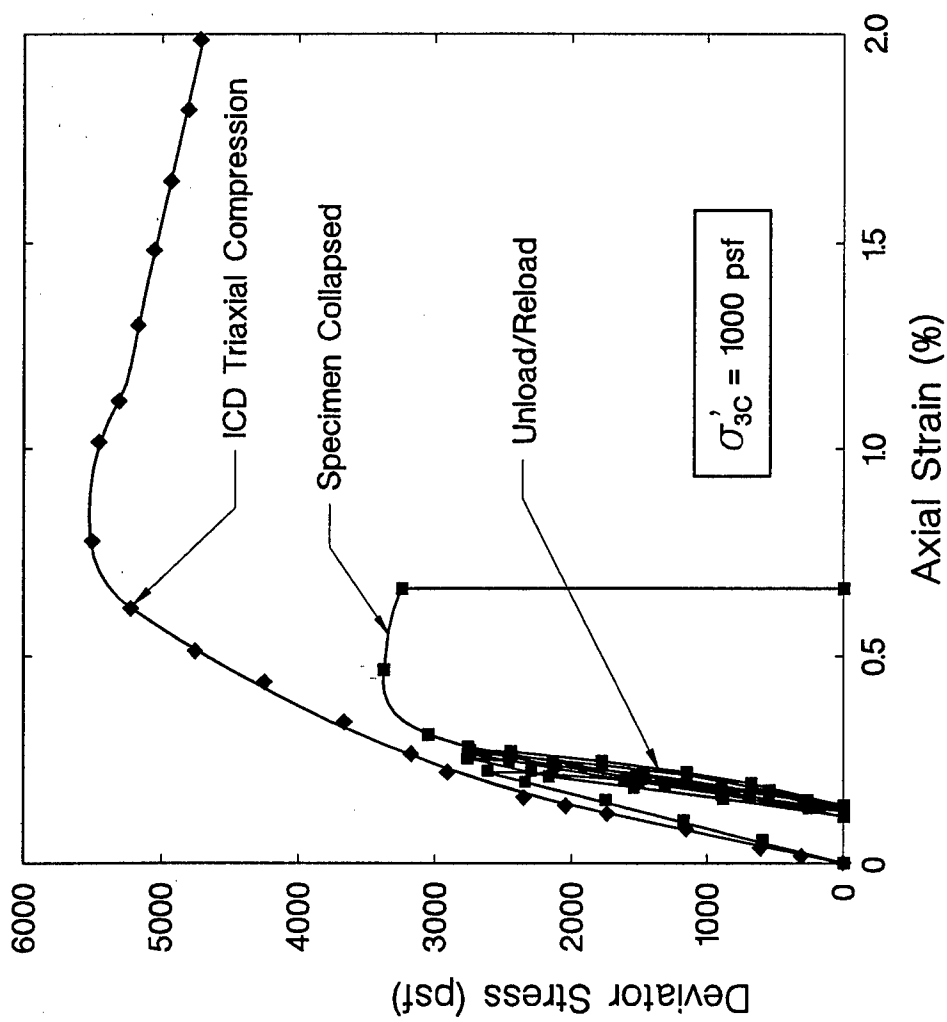


Figure 37. Comparison of results of partially saturated unload/reload and conventional ICD triaxial compression tests at an effective confining pressure of 1000 psf.

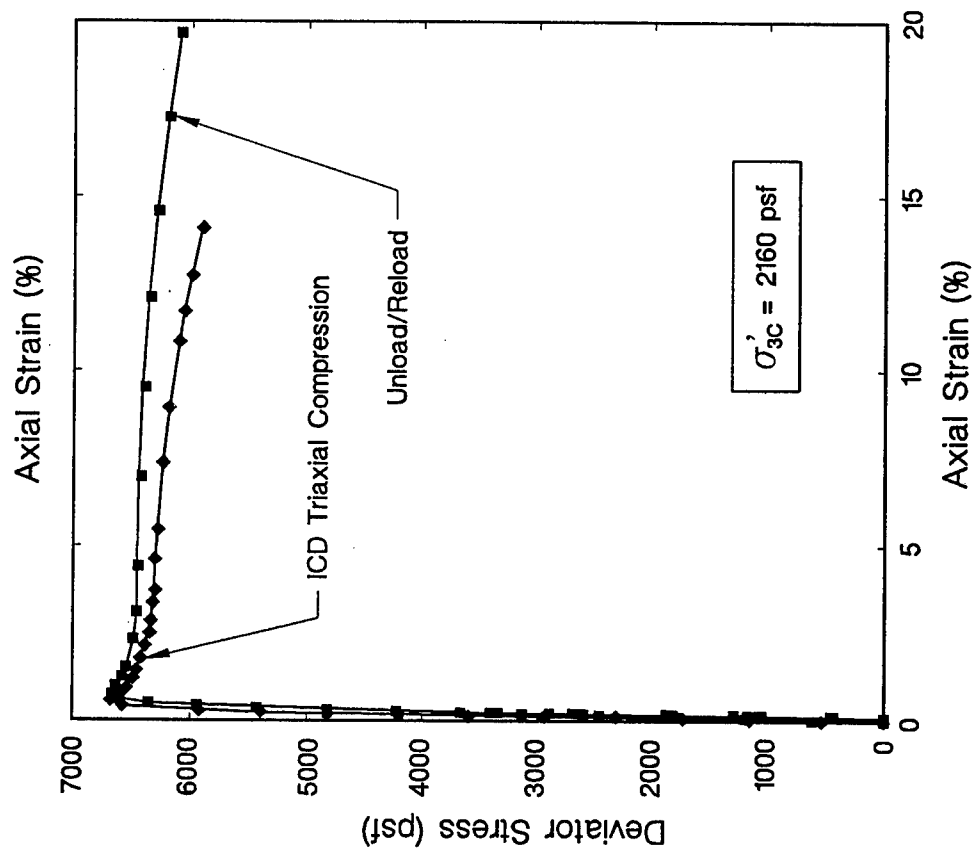


Figure 38. Comparison of results of partially saturated unload/reload and conventional ICD triaxial compression tests at an effective confining pressure of 2160 psf.

least one unload/reload test be conducted to estimate the appropriate values of K_{ur} and n_{ur} in structured/cemented materials instead of using K and n to estimate these values. For soil-structure interaction analysis involving the Vicksburg silt, values of K_{ur} and n_{ur} should be 1175 and 0.3, respectively.

10 SUMMARY

The main objective of the research reported herein was to characterize the drained stress-strain behavior of naturally occurring cemented/structured silts. To achieve this objective, extensive laboratory testing was conducted on reconstituted and structured/cemented silt specimens. The main conclusions regarding the behavior of naturally occurring structured/cemented silts are summarized below:

- 1.) The structure/cementation present in some naturally occurring silts results in high shear strength and stiffness characteristics. The structure/cementation frequently allows slopes to stand at vertical or nearly vertical angles. The two major cementation agents in Vicksburg loess appear to be carbonates and clay/capillarity. The carbonate cementation appears to provide the greatest contribution of the overall structure/cementation.
- 2.) The structure/cementation results in effective preconsolidation pressures that significantly exceed the effective overburden pressure and values measured for remolded or reconstituted silt specimens.
- 3.) The isotropically consolidated-drained triaxial compression tests revealed that the structure/cementation results in an effective stress cohesion that is two times greater than the reconstituted value. This difference in effective stress cohesion was observed for tests conducted on specimens at the natural water content, i.e., partially saturated, and after laboratory saturation with deionized water. The effective stress friction angle was measured to be 28 degrees for both structured/cemented and reconstituted silt specimens.
- 4.) If the effective confining pressure in a triaxial compression test exceeds the effective preconsolidation pressure, the effects of the structure/cementation are negated, and the silt exhibits a stress-strain behavior similar to that of a reconstituted silt. The pressure at which there is a transition from structured/cemented behavior to reconstituted behavior is an important

design parameter. At applied stresses greater than the transition pressure, settlement and/or stability problems may occur in structured/cemented silt.

- 5.) Inundation or saturation of the structured/cemented silt with deionized-deaired water did not significantly alter the compressibility, shear strength, or stress-strain behavior of the material. However, inundation in the virgin compression range in an oedometer test resulted in a small increase in axial strain, or a decrease in void ratio, without a change in vertical effective stress. Therefore, it is concluded that inundation with deionized water does not significantly damage or dissolve the carbonate cementation. Since the shear strength after laboratory saturation is similar to the shear strength of the loess at the natural water content, the importance of the clay/capillary cementation was assumed to be small.
- 6.) The hyperbolic stress-strain parameters for the partially saturated structured/cemented silt differ significantly from the reconstituted silt values. The modulus number for the structured/cemented silt is three times higher than the reconstituted value. This indicates a higher stiffness, and thus a higher initial tangent modulus. However, the structured/cemented modulus exponent is negative, which indicates that the tangent modulus decreases with increasing effective confining pressure. This is attributed to the breakage or removal of the structure/cementation at higher confining pressures. The laboratory saturated structured/cemented silt exhibited a similar modulus number as the laboratory saturated reconstituted silt, but the modulus exponent was negative and approximately one-third of the reconstituted value.
- 7.) Table 9 can be used to estimate the effective stress Mohr-Coulomb shear strength and hyperbolic stress-strain parameters of structured/cemented silts at their natural water content. Table 12 can be used to estimate the same parameters for structured/cemented silts saturated with deionized water.
- 8.) ICD triaxial compression tests were conducted on structured/cemented specimens oriented 90 degrees from the field orientation. The nonfield-oriented silt exhibited similar Mohr-Coulomb shear strength parameters as the field-oriented silt. However, the nonfield-oriented silt exhibited

significantly lower values of modulus number and exponent. Therefore, the stiffness of structured/cemented silts is anisotropic. This anisotropy should be considered in soil-structure interaction analysis.

- 9.) The average unload/reload modulus number of the partially saturated structured/cemented silt is 1175, which is similar to the modulus number of the partially saturated structured/cemented silt. However, the values of modulus exponent differ significantly. As a result, it is recommended that at least one unload/reload test be conducted on structured/cemented materials to estimate the unload/reload modulus number and exponent instead of assuming that the values are equal to the primary loading values.

- 10.) The four unload/reload cycles were initiated at a deviator stress corresponding to 50 percent of the maximum deviator stress in an ICD triaxial compression test. The effective stress cohesion and friction angle measured after the four unload/reload cycles were slightly lower than the values measured in conventional ICD triaxial compression tests. Therefore, the unload/reload cycles may have broken or ruptured some of the structure/cementation in the silt. If more than four unload/reload cycles and/or a deviator stress greater than 50 percent is used, the structure/cementation may undergo additional damage. As a result, site-specific testing of structured/cemented loess should be conducted to investigate the permanence of the structure/cementation under site infiltration/inundation and unload/reload conditions.

References

- American Society for Testing and Materials. (1993). "Soil and rock, building stones; Geotextiles." *Annual book of standards*. Philadelphia, Sec. 4, 04.08.
- Bishop, A.W., and Henkel, D.J. (1962). *The measurement of soil properties in the triaxial tests*. Edward Arnold Ltd., London.
- Black, D.K., and Lee, K.L. (1973). "Saturating laboratory samples by back pressure," *Journal of the Soil Mechanics and Foundations Division*, American Society of Civil Engineers, Vol 99, No.(SM1), pp. 75-93.
- Chang, C-Y. (1969). "Finite element analyses of soil movements caused by deep excavation and dewatering," Ph.D. diss., University of California, Berkeley.
- Clough, G.W., and Duncan, J.M. (1969). "Finite element analyses of Port Allen and Old River Locks," Report No. TE 69-3, University of California, Berkeley.
- Duncan, J.M., Byrne, P., Wong, K.S., and Mabry, P. (1978). "Strength, stress-strain and bulk modulus parameters for finite element analyses of stresses and movements in soil masses," Report No. UCB/GT/78-02, University of California, Berkeley.
- Duncan, J.M., Byrne, P., Wong, K.S., and Mabry, P. (1980). "Strength, stress-strain and bulk modulus parameters for finite element analyses of stresses and movements in soil masses," Report No. UCB/GT/80-01, University of California, Berkeley.
- Duncan, J.M., and Chang, C-Y. (1970). "Nonlinear analysis of stress and strain in soils," *Journal of the Soil Mechanics and Foundations Division*, ASCE 96(SM5),pp. 1629-1653.
- Duncan, J.M., Clough, G.W., and Ebeling, R.M. (1990). "Behavior and design of gravity earth retaining structures." *Proceedings, Design and performance of earth retaining structures*. ASCE Specialty Conference, Cornell University, Ithaca, New York, 18-21 June, ASCE, pp.251-277.
- Duncan, J.M., Lucia, P.C., and D'Orazio, T.B. (1982). "Finite element analyses of stresses and movements in Arcadia Dam," Geotechnical Engineering Report No. UCB/GT/82-07 to U.S. Army Corps of Engineers, Tulsa District, University of California, Berkeley.
- Ebeling, R.M. (1990). "Review of finite Element procedures for earth retaining structures," Miscellaneous Paper No. ITL-90-5, U.S. Army Engineer Waterways Experiment Station, Vicksburg, MS.

- Ebeling, R.M., Duncan, J.M., and Clough, G.W. (1990). "Methods of evaluating the stability and safety of gravity retaining structures founded on rock - Phase 2 Study," Technical Report No. ITL-90-7, U.S. Army Engineer Waterways Experiment Station, Vicksburg, MS.
- Ebeling, R.M., Clough, G.W., Duncan, J.M., and Brandon, T.L. (1992a). "Methods of evaluating the stability and safety of gravity retaining Structures founded on rock," Technical Safety Report REMR CS-29, U.S. Army Engineer Waterways Experiment Station, Vicksburg, MS.
- Ebeling, R.M., Peters, J., and Clough, G.W. (1992b). "User's guide for the incremental construction, soil-structure interaction program SOILSTRUCT," Technical Report No. ITL-90-6, U.S. Army Engineer Waterways Experiment Station, Vicksburg, MS.
- Ebeling, R.M., Mosher, R.M., Abraham, K., and Peters, J.F. (1993). "Soil-structure interaction study of Red River Lock and Dam No. 1 subjected to sediment loading," Technical Report ITL-93-3, U.S. Army Engineer Waterways Experiment Station, Vicksburg, MS.
- Gibson, R.E., and Henkel, D.J. (1954). "Influence of duration of tests at constant rate of strain on measured "Drained" Strength," *Geotechnique* 4(1), 6-15.
- Houston, W.N. and Chan, C.K., (1983). "Laboratory testing manual," Geotechnical Engineering Report, University of California, Berkeley.
- Janbu, N. (1963). "Soil compressibility as determined by oedometer and triaxial tests." *Proceedings, European Conference on Soil Mechanics and Foundation Engineering*. Wiesbaden, Germany, 1, 19-25.
- Krinitzky, E.L., and Turnbull, W.J. (1967). "Loess deposits of Mississippi," Special Paper Number 94, Geological Society of America, Boulder, Colorado.
- Kuppusamy, T., Zarco, M.A., and Ebeling, R.M. (1994). "User's guide for the incremental construction, soil-structure interaction program SOILSTRUCT with far-field boundary elements," Technical Report ITL-94-2, U.S. Army Engineer Waterways Experiment Station, Vicksburg, MS.
- Lutton, R.J. (1969). "Fractures and failure mechanisms in loess and applications to rock mechanics," Research Report S-69-1, U.S. Army Engineer Waterways Experiment Station, Vicksburg, MS.
- Mana, A.I., and Clough, G.W. (1981). "Prediction of movements for braced cuts in clays." *Journal of Geotechnical Engineering*, ASCE, 107(GT6), 759-777.
- Office (1970). *Engineer Manual: Laboratory Soils Testing*. Chief of Engineers, Department of the Army, EM 1110-2-1906, Washington, D.C.

- Seed, R.B., and Duncan, J.M. (1986). "FE analyses: Compaction-induced stresses and deformations," *Journal of Geotechnical Engineering*, ASCE 112(GT1), 23-43.
- Stark, T.D., Vettel, J.J., Fitzwilliam, S.M., and Ebeling, R.M. (1991). "Soil-structure interaction parameters for silts," Technical Report No. ITL-91-2, U.S. Army Engineer Waterways Experiment Station, Vicksburg, MS.
- Stark, T.D., Ebeling, R.M., and Vettel, J.J. (1994). "Hyperbolic stress-strain parameters for silts," *Journal of Geotechnical Engineering*, ASCE 120(4), 420-441.
- Stark, T.D., and Ebeling, R.M. (1995). "Soil-structure interaction parameters for structured/cemented silts," Technical Report No. ITL-95-5, U.S. Army Engineer Waterways Experiment Station, Vicksburg, MS.

Appendix A

Results of ICD Triaxial Compression Tests on Partially Saturated Structured/Cemented Silt

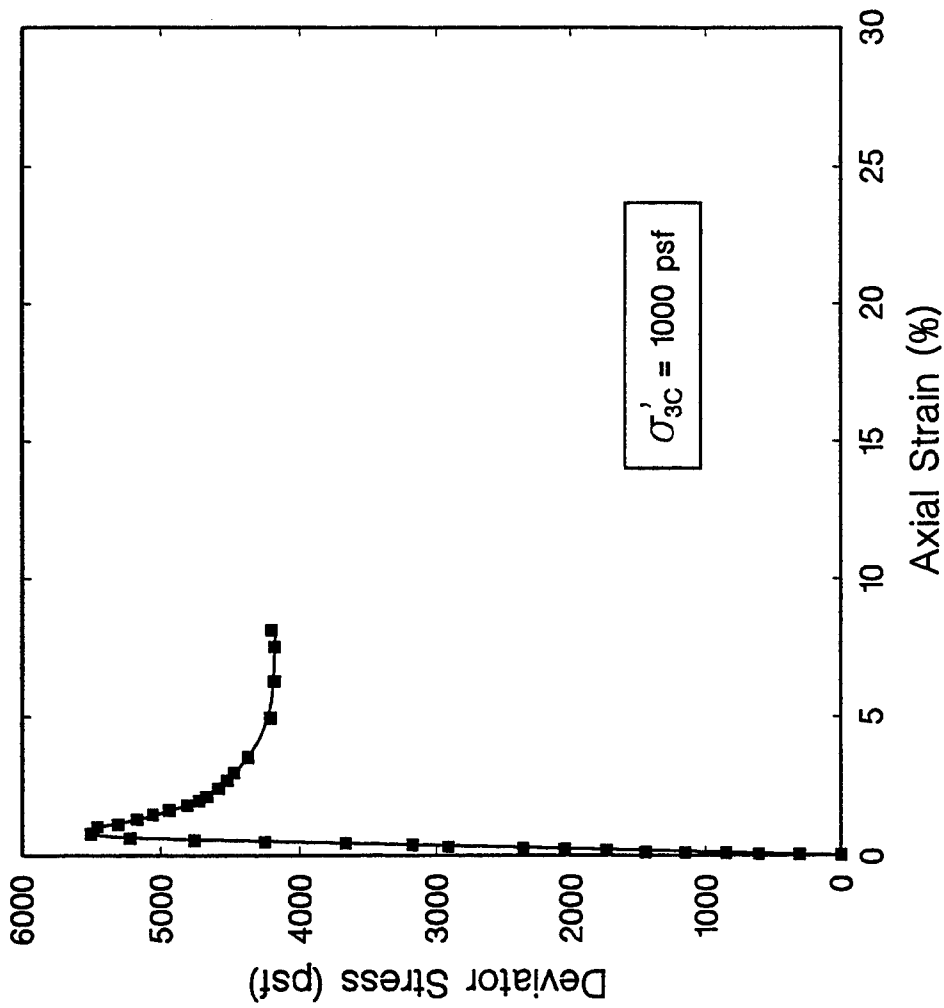


Figure A1. Results of ICD triaxial compression tests on partially saturated structured/cemented silt at an effective confining pressure of 1000 psf.

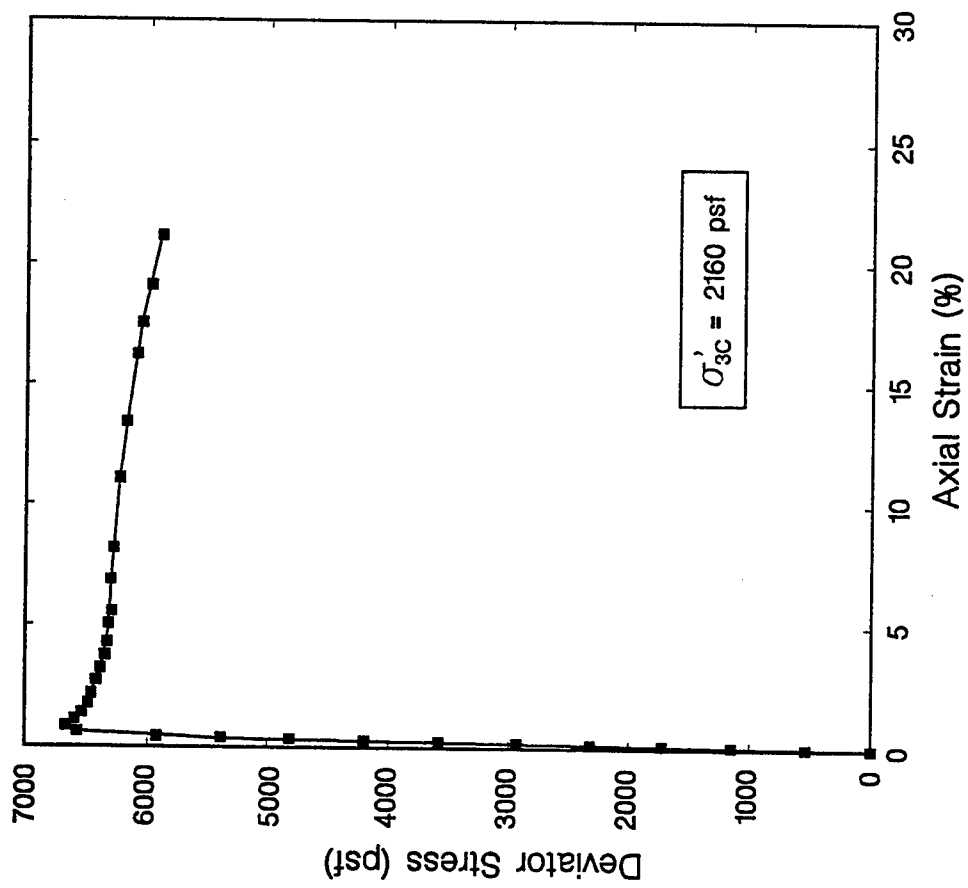


Figure A2. Results of ICD triaxial compression tests on partially saturated structured/cemented silt at an effective confining pressure of 2160 psf.

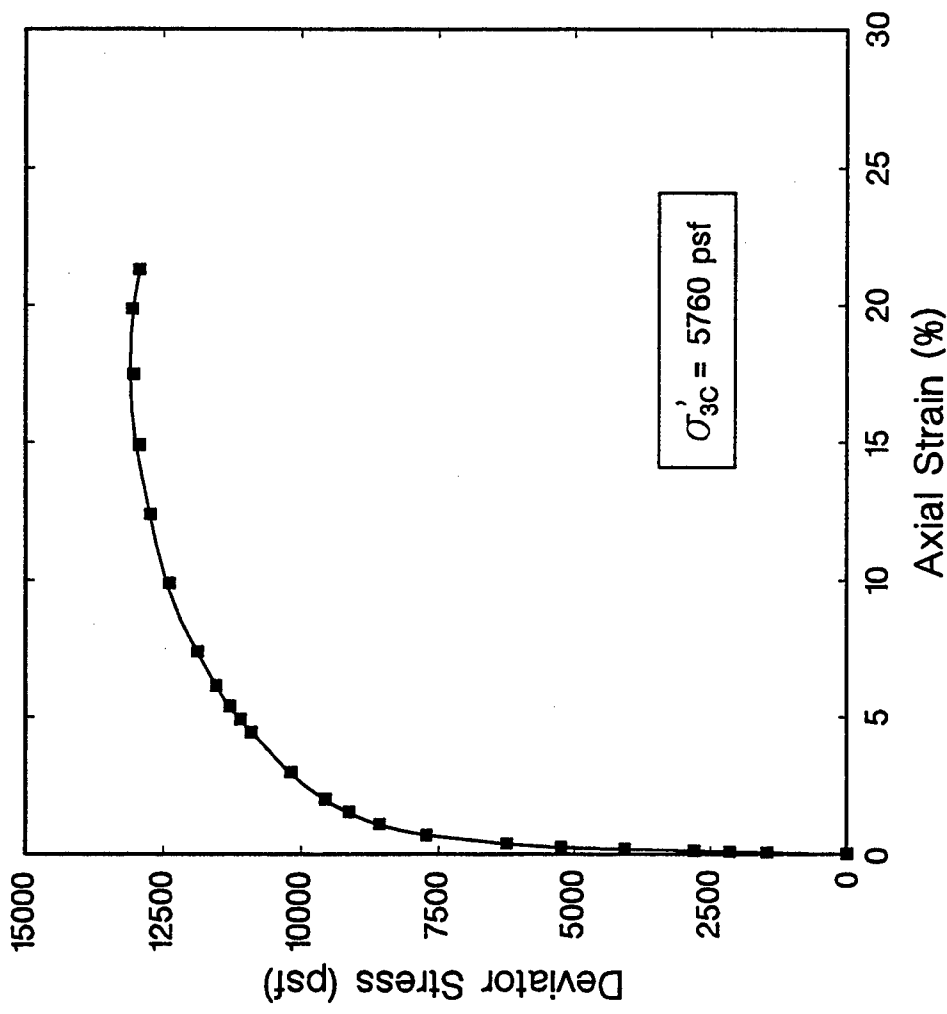


Figure A3. Results of ICD triaxial compression tests on partially saturated structured/cemented silt at an effective confining pressure of 5760 psf.

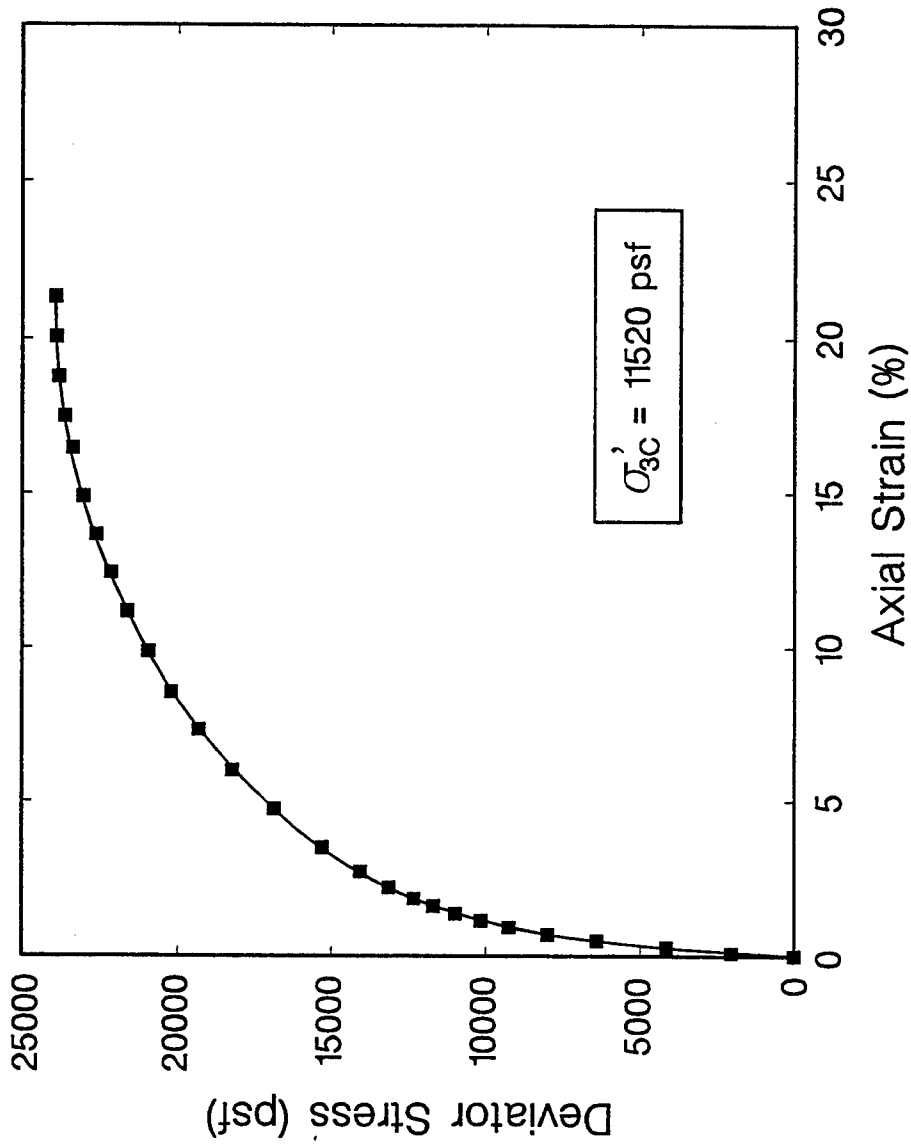


Figure A4. Results of ICD triaxial compression tests on partially saturated structured/cemented silt at an effective confining pressure of 11,520 psf.

Appendix B

Results of ICD Triaxial Compression Tests on Partially Saturated Reconstituted Silt

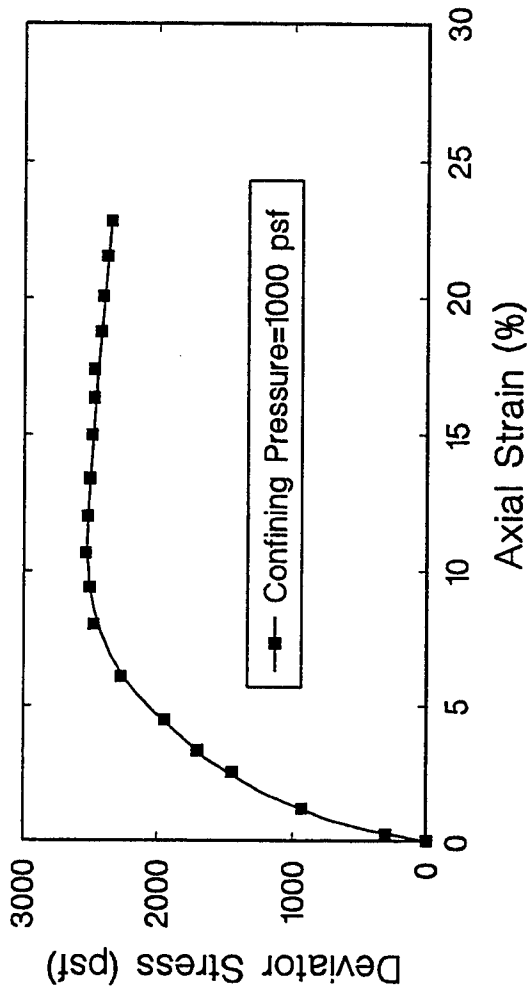


Figure B1. Results of ICD triaxial compression tests on partially saturated reconstituted silt at an effective confining pressure of 1000 psf.

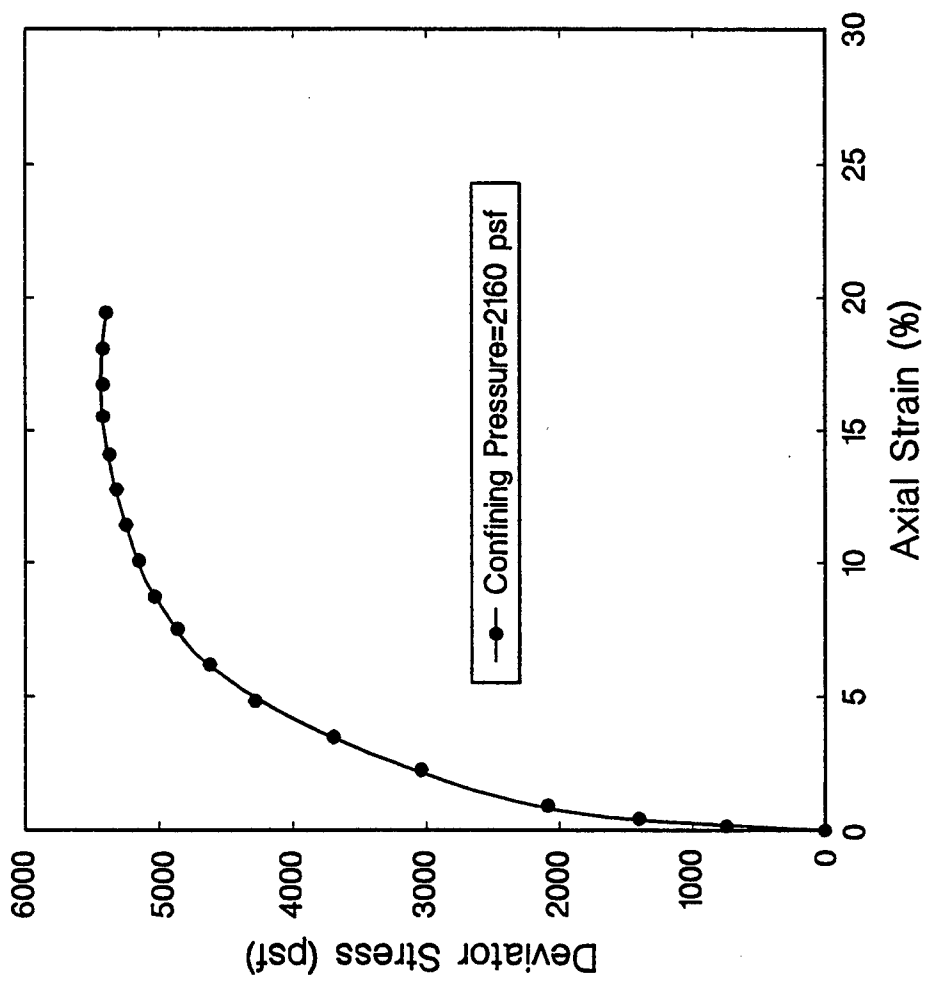


Figure B2. Results of ICD triaxial compression tests on partially saturated reconstituted silt at an effective confining pressure of 2160 psf.

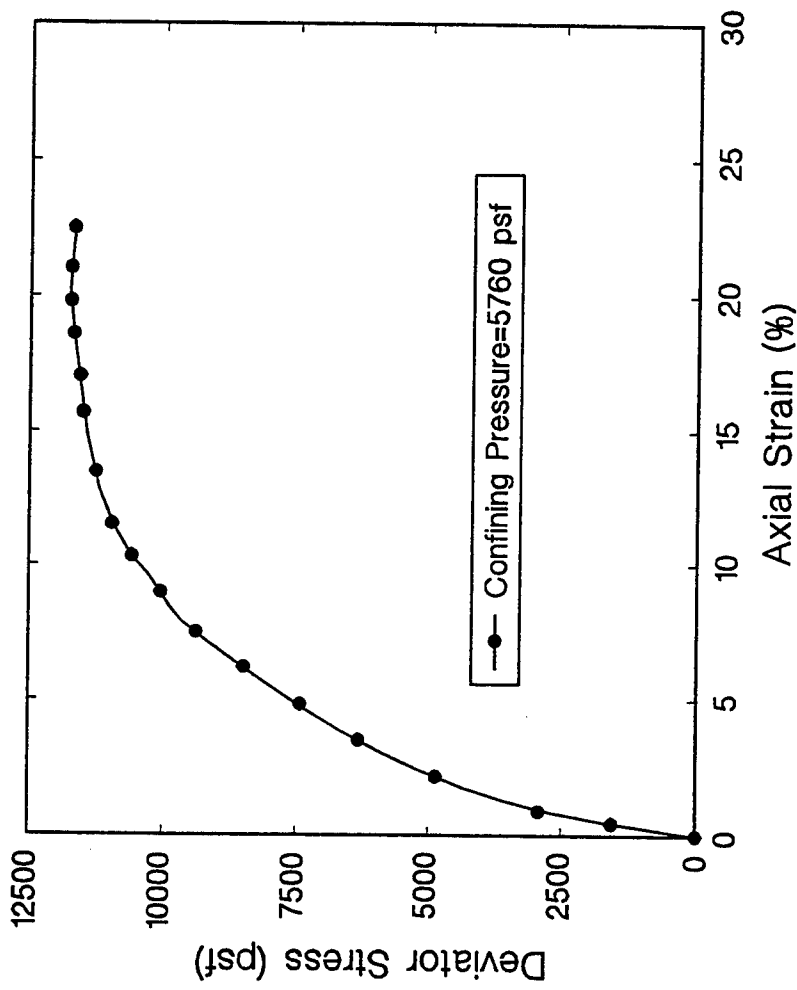


Figure B3. Results of ICD triaxial compression tests on partially saturated reconstituted silt at an effective confining pressure of 5760 psf.

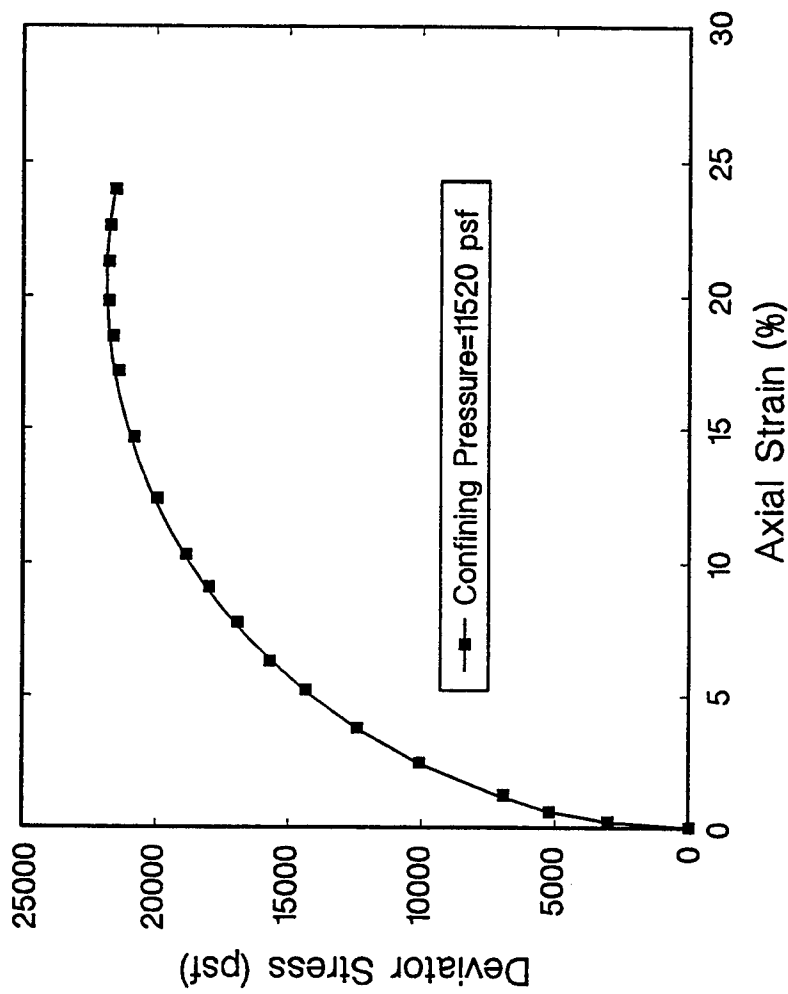


Figure B4. Results of ICD triaxial compression tests on partially saturated reconstituted silt at an effective confining pressure of 11,520 psf.

Appendix C
Results of ICD Triaxial Compression
Tests on Hydrostatically Saturated
Structured/Cemented Silt

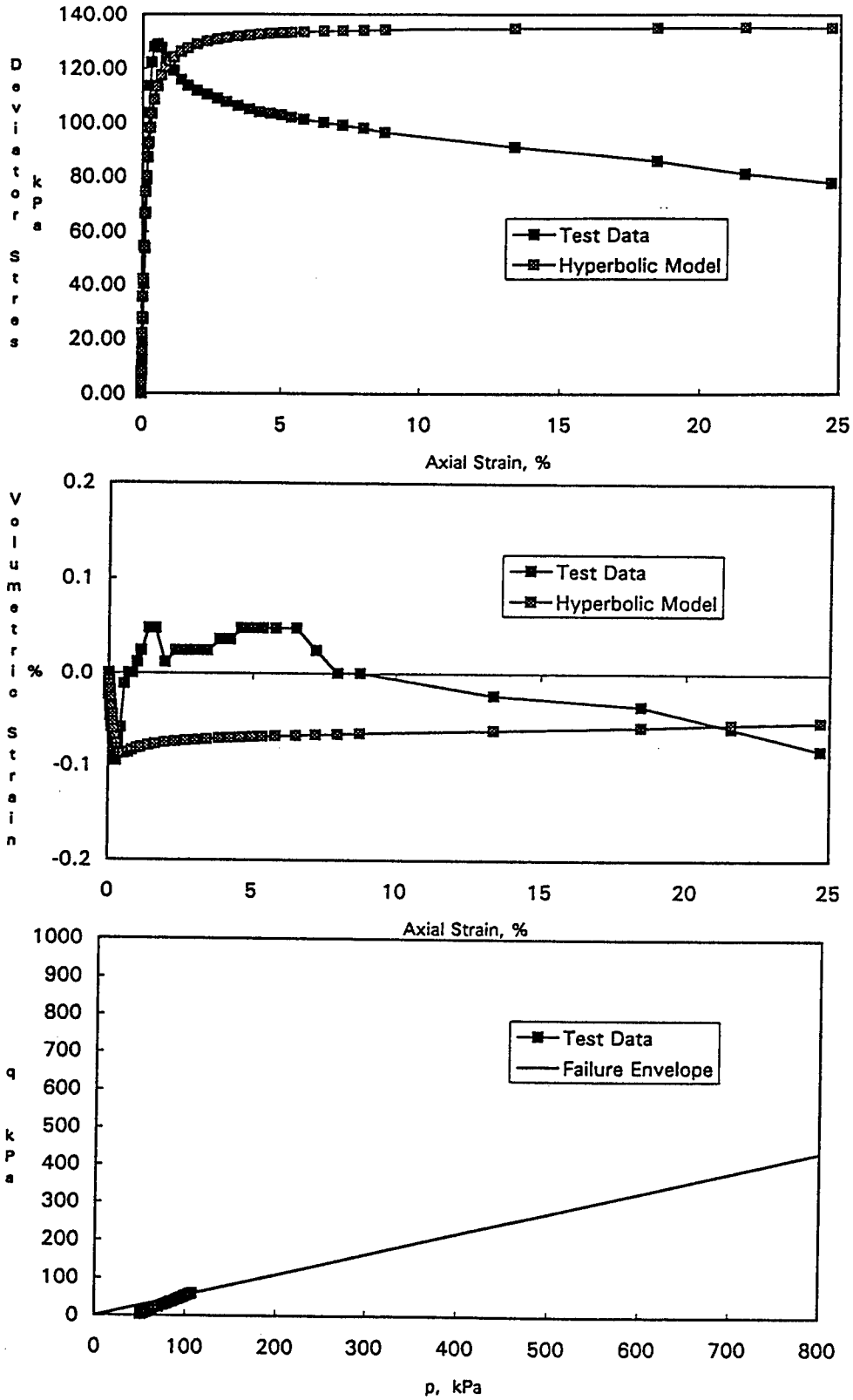


Figure C-1. Results of ICD triaxial compression tests on hydrostatically saturated structured/cemented silt at an effective confining pressure of 1000 psf.

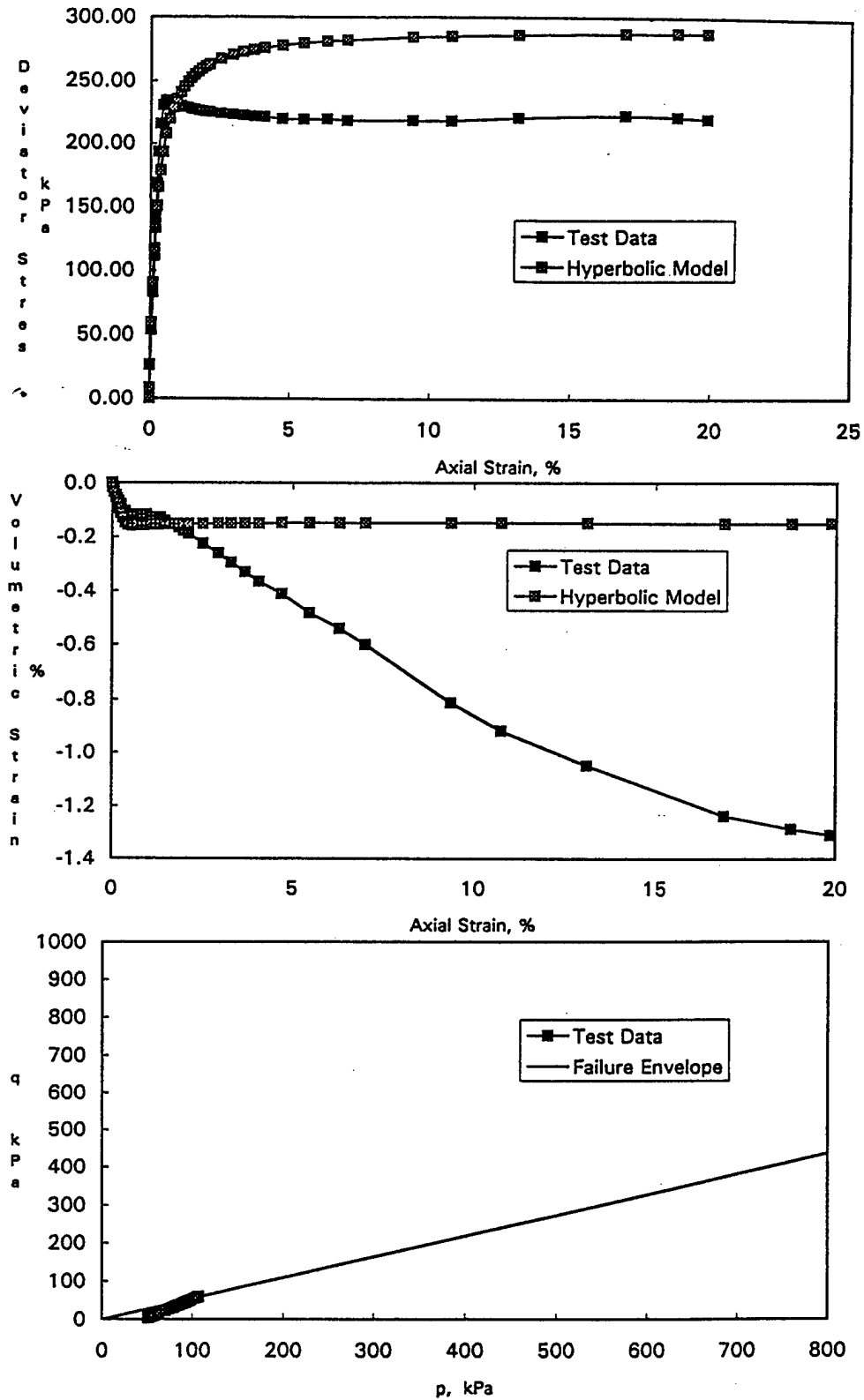


Figure C-2. Results of ICD triaxial compression tests on hydrostatically saturated structured/cemented silt at an effective confining pressure of 2160 psf.

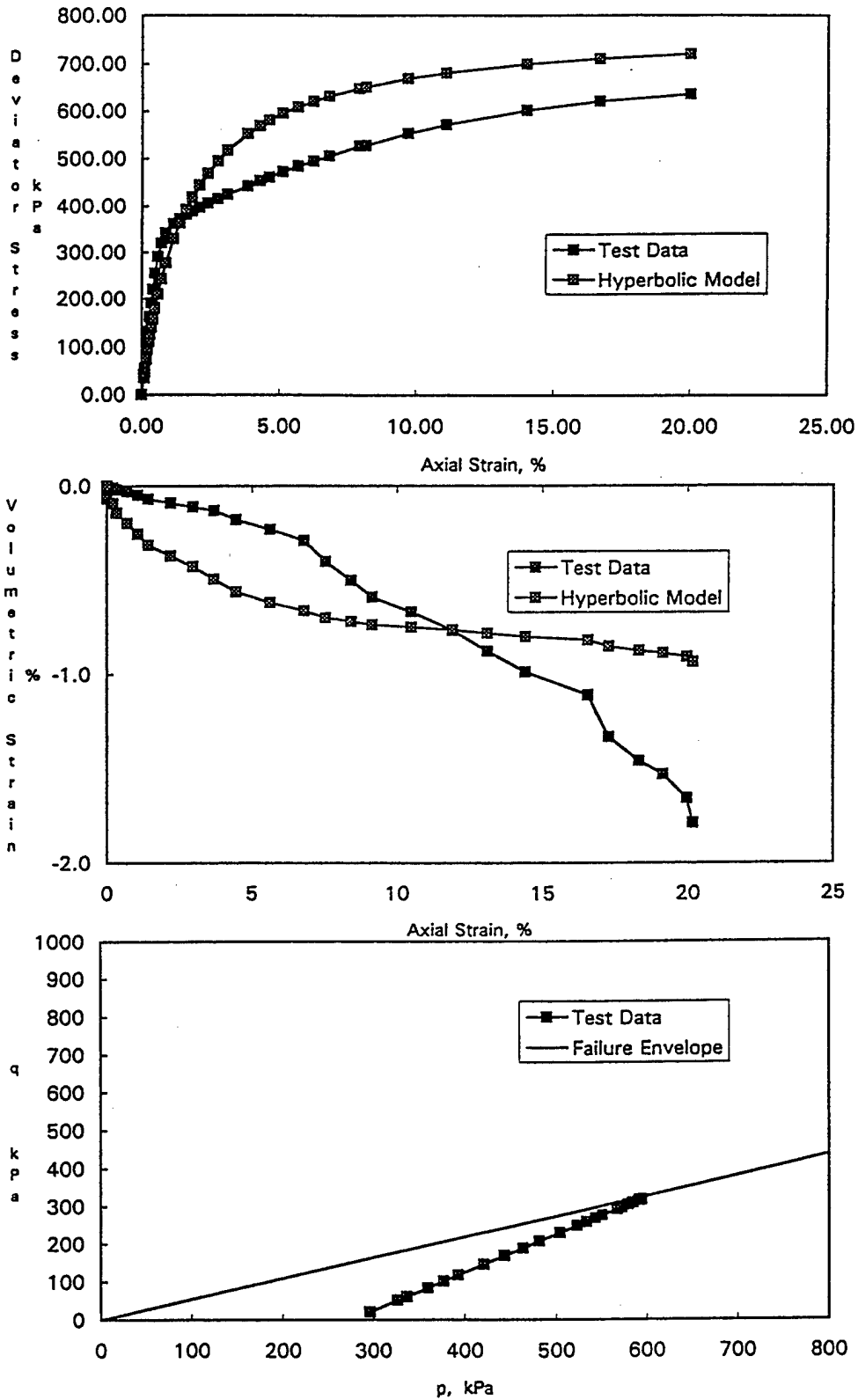


Figure C-3. Results of ICD triaxial compression tests on hydrostatically saturated structured/cemented silt at an effective confining pressure of 5760 psf.

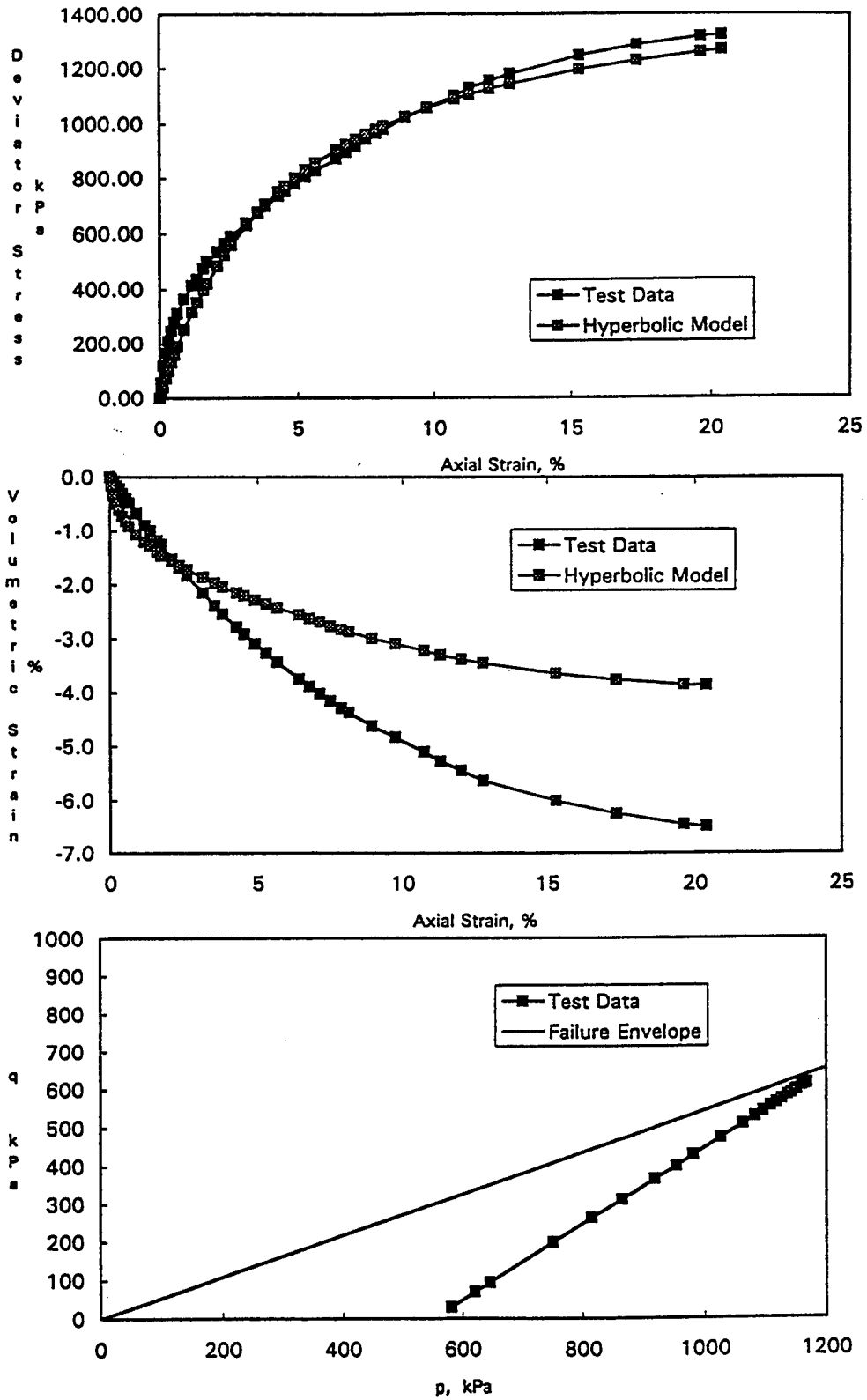


Figure C-4. Results of ICD triaxial compression tests on hydrostatically saturated structured/cemented silt at an effective confining pressure of 11,520 psf.

Appendix D
Results of ICD Triaxial Compression
Tests on Hydrostatically Saturated
Reconstituted Silt

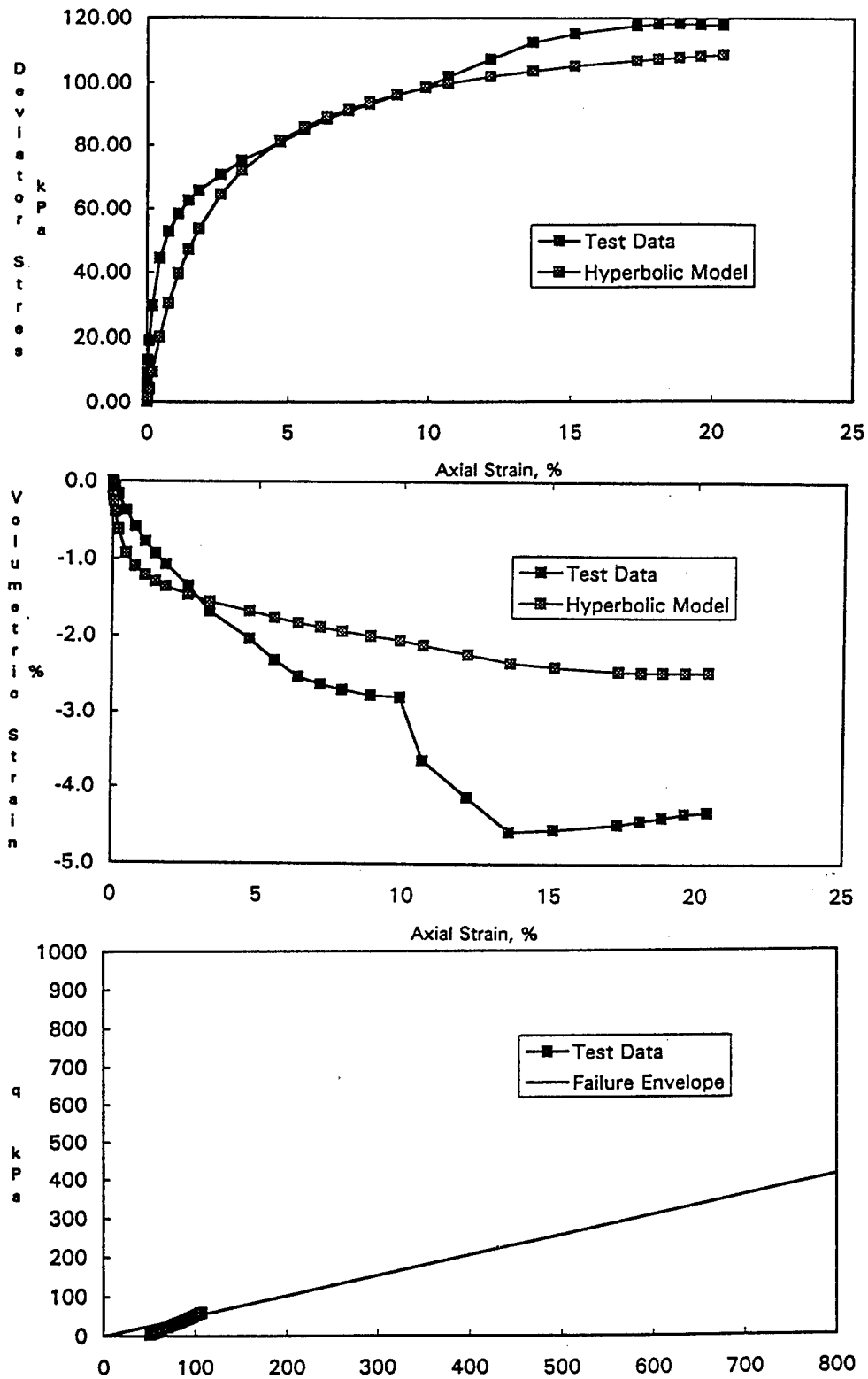


Figure D-1. Results of ICD triaxial compression tests on saturated reconstituted silt at an effective confining pressure of 1000 psf.

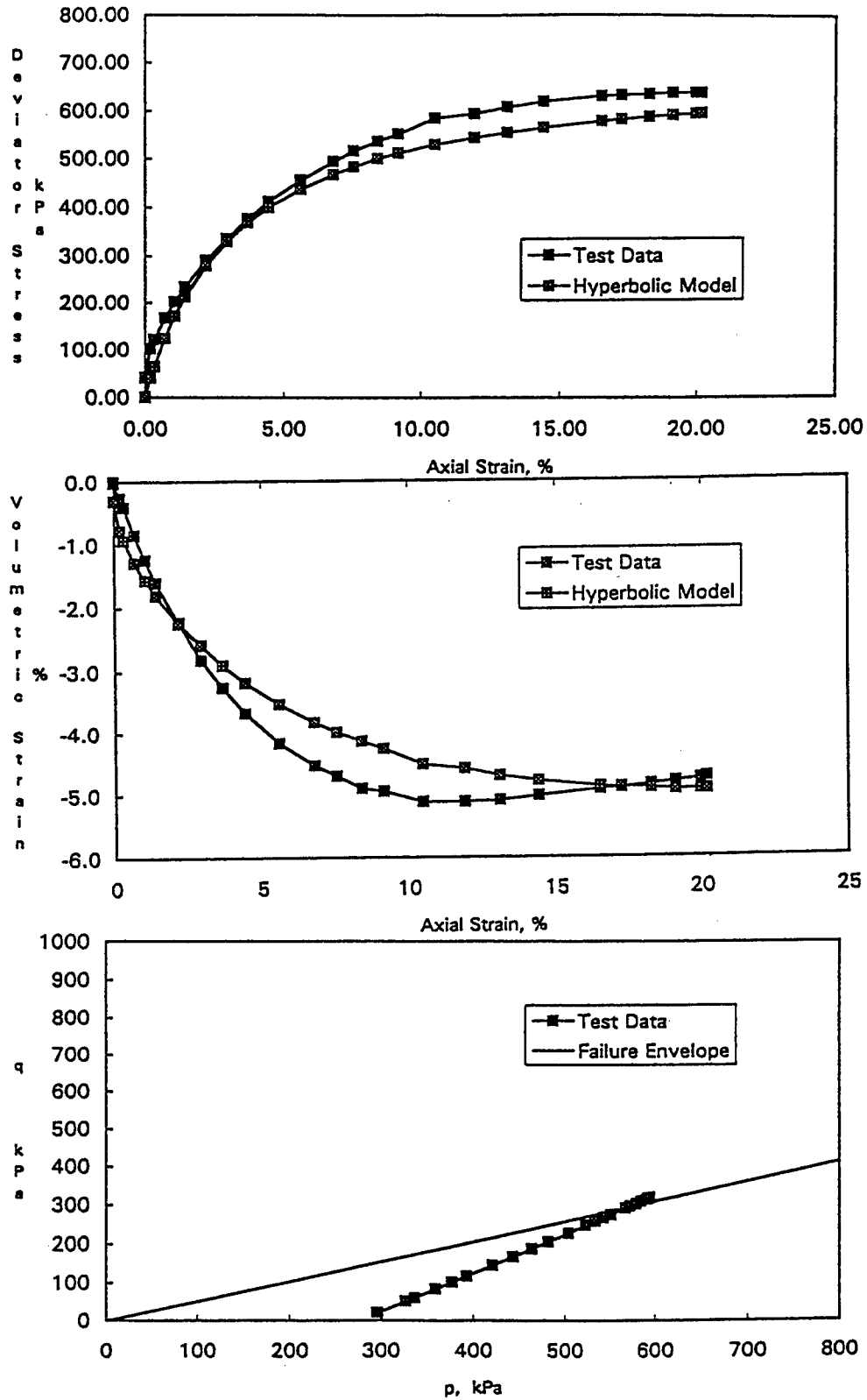


Figure D-2. Results of ICD triaxial compression tests on saturated reconstituted silt at an effective confining pressure of 5760 psf.

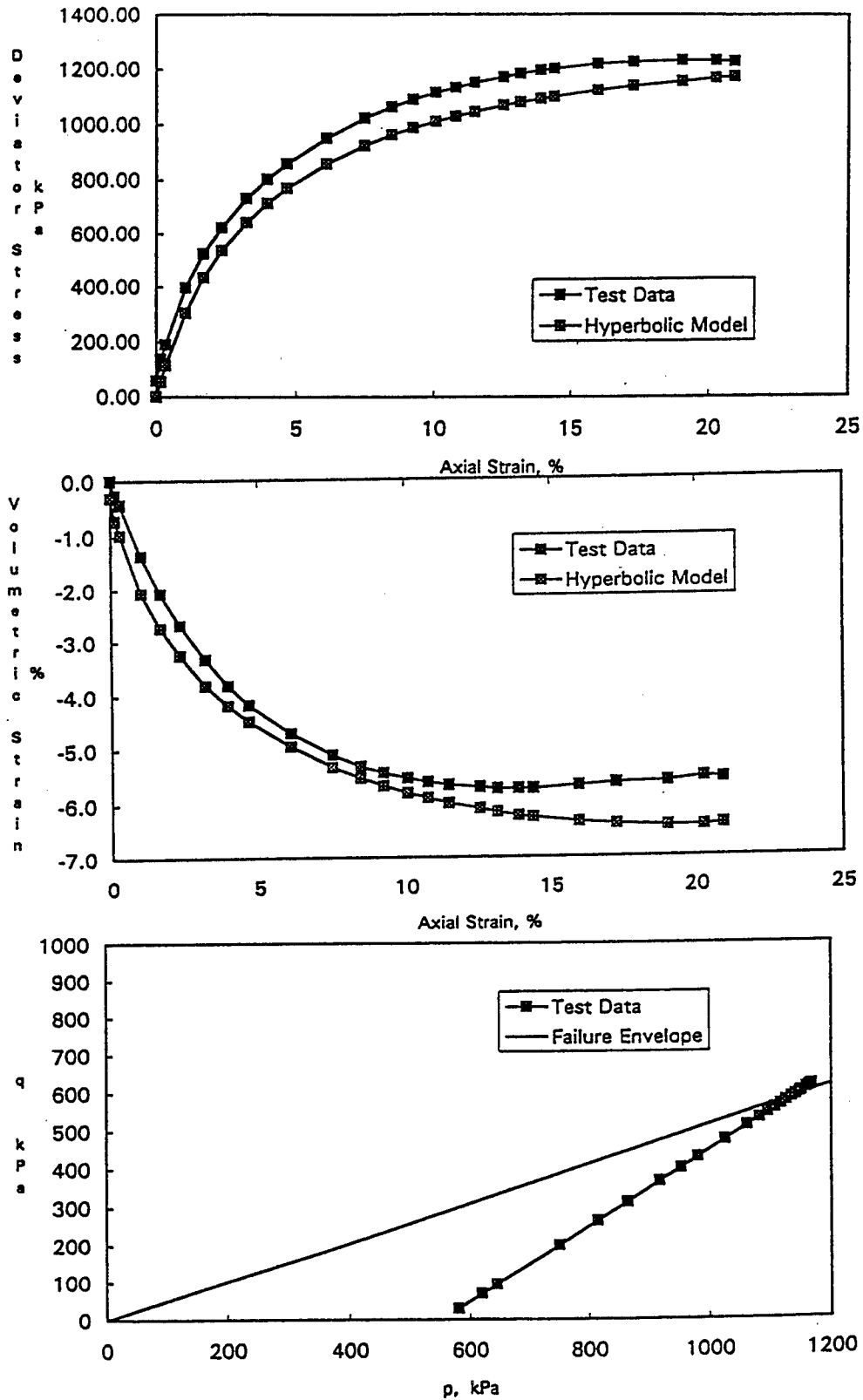


Figure D-3. Results of ICD triaxial compression tests on saturated reconstituted silt at an effective confining pressure of 11,520 psf.

REPORT DOCUMENTATION PAGE

Form Approved
OMB No. 0704-0188

Public reporting burden for this collection of information is estimated to average 1 hour per response, including the time for reviewing instructions, searching existing data sources, gathering and maintaining the data needed, and completing and reviewing the collection of information. Send comments regarding this burden estimate or any other aspect of this collection of information, including suggestions for reducing this burden, to Washington Headquarters Services, Directorate for Information Operations and Reports, 1215 Jefferson Davis Highway, Suite 1204, Arlington, VA 22202-4302, and to the Office of Management and Budget, Paperwork Reduction Project (0704-0188), Washington, DC 20503.

1.AGENCY USE ONLY (Leave blank)		2.REPORT DATE August 1996	3.REPORT TYPE AND DATES COVERED Final report	
4.TITLE AND SUBTITLE Hyperbolic Stress-Strain Parameters for Structured/Cemented Silts			5.FUNDING NUMBERS DACW39-94-M-6534	
6.AUTHOR(S) Timothy D. Stark, Kenneth R. Daly, Robert M. Ebeling				
7.PERFORMING ORGANIZATION NAME(S) AND ADDRESS(ES) Department of Civil Engineering, University of Illinois at Urbana-Champaign, Urbana, IL 61801; U.S. Army Engineer Waterways Experiment Station, 3909 Halls Ferry Road, Vicksburg, MS 39180-6199			8.PERFORMING ORGANIZATION REPORT NUMBER Technical Report ITL-96-8	
9.SPONSORING/MONITORING AGENCY NAME(S) AND ADDRESS(ES) U.S. Army Corps of Engineers Washington, DC 20314-1000			10.SPONSORING/MONITORING AGENCY REPORT NUMBER	
11.SUPPLEMENTARY NOTES Available from the National Technical Information Service, 5285 Port Royal Road, Springfield, VA 22161.				
12a.DISTRIBUTION/AVAILABILITY STATEMENT Approved for public release; distribution is unlimited.			12b.DISTRIBUTION CODE	
13.ABSTRACT (Maximum 200 words) <p>This report describes the research completed under the project titled "Soil-Structure Interaction Parameters for Structured Silts." The main objective of this research was to characterize the drained stress-strain behavior of naturally occurring structured/cemented silts. The results of this research were used to develop recommendations for hyperbolic stress-strain and Mohr-Coulomb shear strength parameters for use in soil-structure interaction analyses involving structured/cemented silts. This research utilized extensive oedometer and isotropically consolidated-drained triaxial compression tests on structured/cemented and reconstituted specimens to evaluate the importance of the structure/cementation on the stress-strain behavior and anisotropy of silts. Triaxial compression tests were also conducted on structured/cemented and reconstituted specimens at the natural degree of saturation and after laboratory saturation to investigate the effect of inundation on the drained stress-strain behavior of silts. In addition, unload/reload triaxial compression tests were conducted to estimate the unload/reload modulus and the effect of unloading/reloading on the degradation of the structure/cementation of silt. This report summarizes the test procedures, test results, and the resulting hyperbolic stress-strain and Mohr-Coulomb shear strength parameters for structured/cemented and reconstituted silt.</p>				
14.SUBJECT TERMS Elasticity modulus Finite element method Soil-structure interaction			15.NUMBER OF PAGES 136	
			16.PRICE CODE	
17.SECURITY CLASSIFICATION OF REPORT UNCLASSIFIED		18.SECURITY CLASSIFICATION OF THIS PAGE UNCLASSIFIED	19.SECURITY CLASSIFICATION OF ABSTRACT	
20.LIMITATION OF ABSTRACT				

**WATERWAYS EXPERIMENT STATION REPORTS
PUBLISHED UNDER THE COMPUTER-AIDED
STRUCTURAL ENGINEERING (CASE) PROJECT**

	Title	Date
Technical Report K-78-1	List of Computer Programs for Computer-Aided Structural Engineering	Feb 1978
Instruction Report O-79-2	User's Guide: Computer Program with Interactive Graphics for Analysis of Plane Frame Structures (CFRAME)	Mar 1979
Technical Report K-80-1	Survey of Bridge-Oriented Design Software	Jan 1980
Technical Report K-80-2	Evaluation of Computer Programs for the Design/Analysis of Highway and Railway Bridges	Jan 1980
Instruction Report K-80-1	User's Guide: Computer Program for Design/Review of Curvilinear Conduits/Culverts (CURCON)	Feb 1980
Instruction Report K-80-3	A Three-Dimensional Finite Element Data Edit Program	Mar 1980
Instruction Report K-80-4	A Three-Dimensional Stability Analysis/Design Program (3DSAD) Report 1: General Geometry Module Report 3: General Analysis Module (CGAM) Report 4: Special-Purpose Modules for Dams (CDAMS)	Jun 1980 Jun 1982 Aug 1983
Instruction Report K-80-6	Basic User's Guide: Computer Program for Design and Analysis of Inverted-T Retaining Walls and Floodwalls (TWDA)	Dec 1980
Instruction Report K-80-7	User's Reference Manual: Computer Program for Design and Analysis of Inverted-T Retaining Walls and Floodwalls (TWDA)	Dec 1980
Technical Report K-80-4	Documentation of Finite Element Analyses Report 1: Longview Outlet Works Conduit Report 2: Anchored Wall Monolith, Bay Springs Lock	Dec 1980 Dec 1980
Technical Report K-80-5	Basic Pile Group Behavior	Dec 1980
Instruction Report K-81-2	User's Guide: Computer Program for Design and Analysis of Sheet Pile Walls by Classical Methods (CSHTWAL) Report 1: Computational Processes Report 2: Interactive Graphics Options	Feb 1981 Mar 1981
Instruction Report K-81-3	Validation Report: Computer Program for Design and Analysis of Inverted-T Retaining Walls and Floodwalls (TWDA)	Feb 1981
Instruction Report K-81-4	User's Guide: Computer Program for Design and Analysis of Cast-in-Place Tunnel Linings (NEWTUN)	Mar 1981
Instruction Report K-81-6	User's Guide: Computer Program for Optimum Nonlinear Dynamic Design of Reinforced Concrete Slabs Under Blast Loading (CBARCS)	Mar 1981
Instruction Report K-81-7	User's Guide: Computer Program for Design or Investigation of Orthogonal Culverts (CORTCUL)	Mar 1981
Instruction Report K-81-9	User's Guide: Computer Program for Three-Dimensional Analysis of Building Systems (CTABS80)	Aug 1981
Technical Report K-81-2	Theoretical Basis for CTABS80: A Computer Program for Three-Dimensional Analysis of Building Systems	Sep 1981
Instruction Report K-82-6	User's Guide: Computer Program for Analysis of Beam-Column Structures with Nonlinear Supports (CBEAMC)	Jun 1982

(Continued)

**WATERWAYS EXPERIMENT STATION REPORTS
PUBLISHED UNDER THE COMPUTER-AIDED
STRUCTURAL ENGINEERING (CASE) PROJECT**

(Continued)

	Title	Date
Instruction Report K-82-7	User's Guide: Computer Program for Bearing Capacity Analysis of Shallow Foundations (CBEAR)	Jun 1982
Instruction Report K-83-1	User's Guide: Computer Program with Interactive Graphics for Analysis of Plane Frame Structures (CFRAME)	Jan 1983
Instruction Report K-83-2	User's Guide: Computer Program for Generation of Engineering Geometry (SKETCH)	Jun 1983
Instruction Report K-83-5	User's Guide: Computer Program to Calculate Shear, Moment, and Thrust (CSMT) from Stress Results of a Two-Dimensional Finite Element Analysis	Jul 1983
Technical Report K-83-1	Basic Pile Group Behavior	Sep 1983
Technical Report K-83-3	Reference Manual: Computer Graphics Program for Generation of Engineering Geometry (SKETCH)	Sep 1983
Technical Report K-83-4	Case Study of Six Major General-Purpose Finite Element Programs	Oct 1983
Instruction Report K-84-2	User's Guide: Computer Program for Optimum Dynamic Design of Nonlinear Metal Plates Under Blast Loading (CSDOOR)	Jan 1984
Instruction Report K-84-7	User's Guide: Computer Program for Determining Induced Stresses and Consolidation Settlements (CSETT)	Aug 1984
Instruction Report K-84-8	Seepage Analysis of Confined Flow Problems by the Method of Fragments (CFRAG)	Sep 1984
Instruction Report K-84-11	User's Guide for Computer Program CGFAG, Concrete General Flexure Analysis with Graphics	Sep 1984
Technical Report K-84-3	Computer-Aided Drafting and Design for Corps Structural Engineers	Oct 1984
Technical Report ATC-86-5	Decision Logic Table Formulation of ACI 318-77, Building Code Requirements for Reinforced Concrete for Automated Constraint Processing, Volumes I and II	Jun 1986
Technical Report ITL-87-2	A Case Committee Study of Finite Element Analysis of Concrete Flat Slabs	Jan 1987
Instruction Report ITL-87-1	User's Guide: Computer Program for Two-Dimensional Analysis of U-Frame Structures (CUFRAM)	Apr 1987
Instruction Report ITL-87-2	User's Guide: For Concrete Strength Investigation and Design (CASTR) in Accordance with ACI 318-83	May 1987
Technical Report ITL-87-6	Finite-Element Method Package for Solving Steady-State Seepage Problems	May 1987
Instruction Report ITL-87-3	User's Guide: A Three-Dimensional Stability Analysis/Design Program (3DSAD) Module	Jun 1987
	Report 1: Revision 1: General Geometry	Jun 1987
	Report 2: General Loads Module	Sep 1989
	Report 6: Free-Body Module	Sep 1989

(Continued)

**WATERWAYS EXPERIMENT STATION REPORTS
PUBLISHED UNDER THE COMPUTER-AIDED
STRUCTURAL ENGINEERING (CASE) PROJECT**

(Continued)

	Title	Date
Instruction Report ITL-87-4	User's Guide: 2-D Frame Analysis Link Program (LINK2D)	Jun 1987
Technical Report ITL-87-4	Finite Element Studies of a Horizontally Framed Miter Gate Report 1: Initial and Refined Finite Element Models (Phases A, B, and C), Volumes I and II Report 2: Simplified Frame Model (Phase D) Report 3: Alternate Configuration Miter Gate Finite Element Studies—Open Section Report 4: Alternate Configuration Miter Gate Finite Element Studies—Closed Sections Report 5: Alternate Configuration Miter Gate Finite Element Studies—Additional Closed Sections Report 6: Elastic Buckling of Girders in Horizontally Framed Miter Gates Report 7: Application and Summary	Aug 1987
Instruction Report GL-87-1	User's Guide: UTEXAS2 Slope-Stability Package; Volume I, User's Manual	Aug 1987
Instruction Report ITL-87-5	Sliding Stability of Concrete Structures (CSLIDE)	Oct 1987
Instruction Report ITL-87-6	Criteria Specifications for and Validation of a Computer Program for the Design or Investigation of Horizontally Framed Miter Gates (CMITER)	Dec 1987
Technical Report ITL-87-8	Procedure for Static Analysis of Gravity Dams Using the Finite Element Method – Phase 1a	Jan 1988
Instruction Report ITL-88-1	User's Guide: Computer Program for Analysis of Planar Grid Structures (CGRID)	Feb 1988
Technical Report ITL-88-1	Development of Design Formulas for Ribbed Mat Foundations on Expansive Soils	Apr 1988
Technical Report ITL-88-2	User's Guide: Pile Group Graphics Display (CPGG) Post-processor to CPGA Program	Apr 1988
Instruction Report ITL-88-2	User's Guide for Design and Investigation of Horizontally Framed Miter Gates (CMITER)	Jun 1988
Instruction Report ITL-88-4	User's Guide for Revised Computer Program to Calculate Shear, Moment, and Thrust (CSMT)	Sep 1988
Instruction Report GL-87-1	User's Guide: UTEXAS2 Slope-Stability Package; Volume II, Theory	Feb 1989
Technical Report ITL-89-3	User's Guide: Pile Group Analysis (CPGA) Computer Group	Jul 1989
Technical Report ITL-89-4	CBASIN—Structural Design of Saint Anthony Falls Stilling Basins According to Corps of Engineers Criteria for Hydraulic Structures; Computer Program X0098	Aug 1989

(Continued)

**WATERWAYS EXPERIMENT STATION REPORTS
PUBLISHED UNDER THE COMPUTER-AIDED
STRUCTURAL ENGINEERING (CASE) PROJECT**

(Continued)

	Title	Date
Technical Report ITL-89-5	CCHAN—Structural Design of Rectangular Channels According to Corps of Engineers Criteria for Hydraulic Structures; Computer Program X0097	Aug 1989
Technical Report ITL-89-6	The Response-Spectrum Dynamic Analysis of Gravity Dams Using the Finite Element Method; Phase II	Aug 1989
Contract Report ITL-89-1	State of the Art on Expert Systems Applications in Design, Construction, and Maintenance of Structures	Sep 1989
Instruction Report ITL-90-1	User's Guide: Computer Program for Design and Analysis of Sheet Pile Walls by Classical Methods (CWALSHT)	Feb 1990
Technical Report ITL-90-3	Investigation and Design of U-Frame Structures Using Program CUFRC Volume A: Program Criteria and Documentation Volume B: User's Guide for Basins Volume C: User's Guide for Channels	May 1990
Instruction Report ITL-90-6	User's Guide: Computer Program for Two-Dimensional Analysis of U-Frame or W-Frame Structures (CWFRAM)	Sep 1990
Instruction Report ITL-90-2	User's Guide: Pile Group—Concrete Pile Analysis Program (CPGC) Preprocessor to CPGA Program	Jun 1990
Technical Report ITL-91-3	Application of Finite Element, Grid Generation, and Scientific Visualization Techniques to 2-D and 3-D Seepage and Groundwater Modeling	Sep 1990
Instruction Report ITL-91-1	User's Guide: Computer Program for Design and Analysis of Sheet-Pile Walls by Classical Methods (CWALSHT) Including Rowe's Moment Reduction	Oct 1991
Instruction Report ITL-87-2 (Revised)	User's Guide for Concrete Strength Investigation and Design (CASTR) in Accordance with ACI 318-89	Mar 1992
Technical Report ITL-92-2	Finite Element Modeling of Welded Thick Plates for Bonneville Navigation Lock	May 1992
Technical Report ITL-92-4	Introduction to the Computation of Response Spectrum for Earthquake Loading	Jun 1992
Instruction Report ITL-92-3	Concept Design Example, Computer-Aided Structural Modeling (CASM) Report 1: Scheme A Report 2: Scheme B Report 3: Scheme C	Jun 1992 Jun 1992 Jun 1992
Instruction Report ITL-92-4	User's Guide: Computer-Aided Structural Modeling (CASM) -Version 3.00	Apr 1992
Instruction Report ITL-92-5	Tutorial Guide: Computer-Aided Structural Modeling (CASM) -Version 3.00	Apr 1992

(Continued)

**WATERWAYS EXPERIMENT STATION REPORTS
PUBLISHED UNDER THE COMPUTER-AIDED
STRUCTURAL ENGINEERING (CASE) PROJECT**

(Continued)

	Title	Date
Contract Report ITL-92-1	Optimization of Steel Pile Foundations Using Optimality Criteria	Jun 1992
Technical Report ITL-92-7	Refined Stress Analysis of Melvin Price Locks and Dam	Sep 1992
Contract Report ITL-92-2	Knowledge-Based Expert System for Selection and Design of Retaining Structures	Sep 1992
Contract Report ITL-92-3	Evaluation of Thermal and Incremental Construction Effects for Monoliths AL-3 and AL-5 of the Melvin Price Locks and Dam	Sep 1992
Instruction Report GL-87-1	User's Guide: UTEXAS3 Slope-Stability Package; Volume IV, User's Manual	Nov 1992
Technical Report ITL-92-11	The Seismic Design of Waterfront Retaining Structures	Nov 1992
Technical Report ITL-92-12	Computer-Aided, Field-Verified Structural Evaluation Report 1: Development of Computer Modeling Techniques for Miter Lock Gates Report 2: Field Test and Analysis Correlation at John Hollis Bankhead Lock and Dam Report 3: Field Test and Analysis Correlation of a Vertically Framed Miter Gate at Emsworth Lock and Dam	Nov 1992 Dec 1992 Dec 1993
Instruction Report GL-87-1	User's Guide: UTEXAS3 Slope-Stability Package; Volume III, Example Problems	Dec 1992
Technical Report ITL-93-1	Theoretical Manual for Analysis of Arch Dams	Jul 1993
Technical Report ITL-93-2	Steel Structures for Civil Works, General Considerations for Design and Rehabilitation	Aug 1993
Technical Report ITL-93-3	Soil-Structure Interaction Study of Red River Lock and Dam No. 1 Subjected to Sediment Loading	Sep 1993
Instruction Report ITL-93-3	User's Manual—ADAP, Graphics-Based Dam Analysis Program	Aug 1993
Instruction Report ITL-93-4	Load and Resistance Factor Design for Steel Miter Gates	Oct 1993
Technical Report ITL-94-2	User's Guide for the Incremental Construction, Soil-Structure Interaction Program SOILSTRUCT with Far-Field Boundary Elements	Mar 1994
Instruction Report ITL-94-1	Tutorial Guide: Computer-Aided Structural Modeling (CASM); Version 5.00	Apr 1994
Instruction Report ITL-94-2	User's Guide: Computer-Aided Structural Modeling (CASM); Version 5.00	Apr 1994
Technical Report ITL-94-4	Dynamics of Intake Towers and Other MDOF Structures Under Earthquake Loads: A Computer-Aided Approach	Jul 1994
Technical Report ITL-94-5	Procedure for Static Analysis of Gravity Dams Including Foundation Effects Using the Finite Element Method – Phase 1B	Jul 1994

(Continued)

**WATERWAYS EXPERIMENT STATION REPORTS
PUBLISHED UNDER THE COMPUTER-AIDED
STRUCTURAL ENGINEERING (CASE) PROJECT**

(Concluded)

	Title	Date
Instruction Report ITL-94-5	User's Guide: Computer Program for Winkler Soil-Structure Interaction Analysis of Sheet-Pile Walls (CWALSSI)	Nov 1994
Instruction Report ITL-94-6	User's Guide: Computer Program for Analysis of Beam-Column Structures with Nonlinear Supports (CBEAMC)	Nov 1994
Instruction Report ITL-94-7	User's Guide to CTWALL – A Microcomputer Program for the Analysis of Retaining and Flood Walls	Dec 1994
Contract Report ITL-95-1	Comparison of Barge Impact Experimental and Finite Element Results for the Lower Miter Gate of Lock and Dam 26	Jun 1995
Technical Report ITL-95-5	Soil-Structure Interaction Parameters for Structured/Cemented Silts	Aug 1995
Instruction Report ITL-95-1	User's Guide: Computer Program for the Design and Investigation of Horizontally Framed Miter Gates Using the Load and Resistance Factor Criteria (CMITER-LRFD)	Aug 1995
Technical Report ITL-95-8	Constitutive Modeling of Concrete for Massive Concrete Structures, A Simplified Overview	Sep 1995
Instruction Report ITL-96-1	User's Guide: Computer Program for Two-Dimensional Dynamic Analysis of U-Frame or W-Frame Structures (CDWFRM)	Jun 1996
Instruction Report ITL-96-2	Computer-Aided Structural Modeling (CASM), Version 6.00 Report 1: Tutorial Guide Report 2: User's Guide Report 3: Scheme A Report 4: Scheme B Report 5: Scheme C	Jun 1996
Technical Report ITL-96-8	Hyperbolic Stress-Strain Parameters for Structured/Cemented Silts	Aug 1996
Instruction Report ITL-96-3	User's Guide: Computer Program for the Design and Investigation of Horizontally Framed Miter Gates Using the Load and Resistance Factor Criteria (CMITERW-LRFD) Windows Version	Sep 1996